

THE JAHN-TELLER EFFECT IN HEXAUREAMANGANESE(III)PERCHLORATE  
AND  
MOLECULAR STRUCTURE OF HIGH COORDINATION COMPLEXES

BY

HOSSEIN AGHABOZORG

A DISSERTATION PRESENTED TO THE GRADUATE COUNCIL OF  
THE UNIVERSITY OF FLORIDA  
IN PARTIAL FULFILLMENT OF THE REQUIREMENTS FOR THE  
DEGREE OF DOCTOR OF PHILOSOPHY

UNIVERSITY OF FLORIDA

1982

To my parents  
and  
my wife

#### ACKNOWLEDGEMENTS

The author would like to take this opportunity to express his appreciation to Dr. R.C. Stoufer, research director, for his guidance; to Dr. G.J. Palenik for his encouragement and assistance in solving the crystal structures; to Mrs. R.C. Palenik for preparation of the Co, Pb and Th complexes.

Special appreciation is due to Dr. W. Weltner for his helpful discussions on interpretation of the EPR spectra. Thanks are due to Dr. J.H. Hall for obtaining the DSC spectra; to the remaining members of the supervisory committee, Dr. E.V. Dose and Dr. J.G. Fiskell, for reviewing this work and attending its defense.

Furthermore, the author wishes to thank his wife, Fereshteh, for her sacrifice and devotion. Thanks are due to the Center for Instructional and Research Computing Activities, University of Florida, for a grant of computer time. Finally, appreciation is due to Ms. Patty Hickerson for her skill and patience in the preparation of this manuscript.

## TABLE OF CONTENTS

	<u>Page</u>
ACKNOWLEDGEMENTS . . . . .	iii
LIST OF TABLES . . . . .	vi
LIST OF FIGURES. . . . .	ix
ABSTRACT . . . . .	xi
CHAPTER	
I. INTRODUCTION . . . . .	1
A. The Jahn-Teller Effect in Hexaureamanganese(III) Perchlorate. . . . .	1
B. Molecular Structure of High Coordination Complexes . .	21
II. GENERAL DIFFRACTION EXPERIMENTAL . . . . .	29
III. PREPARATION AND CRYSTAL STRUCTURE OF HEXAUREAMANGANESE (III)PERCHLORATE . . . . .	36
A. Experimental Section . . . . .	37
B. Results and Discussion . . . . .	39
IV. ELECTRON PARAMAGNETIC RESONANCE AND DIFFERENTIAL SCANNING CALORIMETRY OF THE HEXAUREAMANGANESE(III)PERCHLORATE . . .	59
A. Experimental Section . . . . .	60
B. Results and Discussion . . . . .	62
V. THE CRYSTAL STRUCTURE OF DIAQUA[2,9-DIFORMYL-1,10-PHEN- ANTHROLINE BIS(SEMICARBAZONE)] COBALT(II) NITRATE, [Co(PHENS)(H <sub>2</sub> O) <sub>2</sub> ](NO <sub>3</sub> ) <sub>2</sub> . . . . .	74
A. Experimental Section . . . . .	75
B. Results and Discussion . . . . .	77

	<u>Page</u>
VI. THE CRYSTAL STRUCTURE OF DINITRATO[2,9-DIFORMYL-1,10-PHENANTHROLINE BIS(SEMICARBAZONE)]LEAD(II), [Pb(PHENSC)(NO <sub>3</sub> ) <sub>2</sub> ] . . . . .	94
A. Experimental Section. . . . .	94
B. Results and Discussion. . . . .	95
VII. THE CRYSTAL STRUCTURE OF $\mu$ -OXO-BIS NITRATO[2,9-DIFORMYL-1,10-PHENANTHROLINE BIS(SEMICARBAZONE)]AQUA THORIUM(IV) NITRATE MONOHYDRATE, {[Th(PHENSC)(H <sub>2</sub> O)(NO <sub>3</sub> ) <sub>2</sub> ](NO <sub>3</sub> ) <sub>4</sub> ·H <sub>2</sub> O} . . . . .	117
A. Experimental Section. . . . .	118
B. Results and Discussion. . . . .	119
APPENDIX. . . . .	148
REFERENCES. . . . .	149
BIOGRAPHICAL SKETCH . . . . .	158

# LIST OF TABLES

Table	Page
1 Crystal Data for $\text{Mn}[\text{OC}(\text{NH}_2)_2]_6(\text{ClO}_4)_3$ . . . . .	32
2 Crystal Data for $[\text{Co}(\text{PHENSC})(\text{H}_2\text{O})_2](\text{NO}_3)_2$ . . . . .	33
3 Crystal Data for $[\text{Pb}(\text{PHENSC})(\text{NO}_3)_2]$ . . . . .	34
4 Crystal Data for $[(\text{Th}[\text{PHENSC}])_2\text{O}(\text{NO}_3)_2(\text{H}_2\text{O})_2](\text{NO}_3)_4 \cdot \text{H}_2\text{O}$ . . . . .	35
5 Final Positional Parameters ( $\times 10^4$ ) for $\text{Mn}[\text{OC}(\text{NH}_2)_2]_6(\text{ClO}_4)_3$ . . . . .	52
6 Final Thermal Parameters ( $\times 10^4$ ) for $\text{Mn}[\text{OC}(\text{NH}_2)_2]_6(\text{ClO}_4)_3$ . . . . .	53
7 Bond Distances (in Å) for $\text{Mn}[\text{OC}(\text{NH}_2)_2]_6(\text{ClO}_4)_3$ with Estimated Standard Deviations . . . . .	54
8 Bond Angles (in deg) in $\text{Mn}[\text{OC}(\text{NH}_2)_2]_6(\text{ClO}_4)_3$ . . . . .	55
9 Hydrogen Atom Position ( $\times 10^3$ ) and Isotropic Thermal Parameter in $\text{Mn}[\text{OC}(\text{NH}_2)_2]_6(\text{ClO}_4)_3$ . . . . .	56
10 Hydrogen Bonds in $\text{Mn}[\text{OC}(\text{NH}_2)_2]_6(\text{ClO}_4)_3$ . . . . .	57
11 $\text{M}[\text{OC}(\text{NH}_2)_2]_6(\text{ClO}_4)_3$ Mean Square Displacements . . . . .	58
12 Final Positional Parameters ( $\times 10^4$ except for Co which is $\times 10^5$ ) for $[\text{Co}(\text{PHENSC})(\text{H}_2\text{O})_2](\text{NO}_3)_2$ . . . . .	82
13 Final Thermal Parameters ( $\times 10^4$ except for Co which is $\times 10^5$ ) for $[\text{Co}(\text{PHENSC})(\text{H}_2\text{O})_2](\text{NO}_3)_2$ . . . . .	83
14 Bond Distances (in Å) in $[\text{Co}(\text{PHENSC})(\text{H}_2\text{O})_2](\text{NO}_3)_2$ With Estimated Standard Deviations . . . . .	84
15 Bond Angles (in deg) in $[\text{Co}(\text{PHENSC})(\text{H}_2\text{O})_2](\text{NO}_3)_2$ With Estimated Standard Deviations . . . . .	85
16 Final Hydrogen Atom Parameters for $[\text{Co}(\text{PHENSC})(\text{H}_2\text{O})_2](\text{NO}_3)_2$ . . . . .	88

<u>Table</u>	<u>Page</u>
17 Bond Distances (in Å) for Hydrogens of [Co(PHENSC)(H <sub>2</sub> O) <sub>2</sub> ](NO <sub>3</sub> ) <sub>2</sub> With Estimated Standard Deviations . . . . .	89
18 Hydrogen Bonds in [Co(PHENSC)(H <sub>2</sub> O) <sub>2</sub> ](NO <sub>3</sub> ) <sub>2</sub> . . . . .	90
19 Least-Squares Planes for [Co(PHENSC)(H <sub>2</sub> O) <sub>2</sub> ](NO <sub>3</sub> ) <sub>2</sub> . . . . .	91
20 Dihedral Angles for Various Planes in [Co(PHENSC)(H <sub>2</sub> O) <sub>2</sub> ](NO <sub>3</sub> ) <sub>2</sub> . . . . .	93
21 Final Positional Parameters (x 10 <sup>+4</sup> except for Pb which is x 10 <sup>+5</sup> ) for [Pb(PHENSC)(NO <sub>3</sub> ) <sub>2</sub> ] . . . . .	105
22 Final Thermal Parameters (x 10 <sup>+4</sup> except for Pb which is x 10 <sup>+5</sup> ) for [Pb(PHENSC)(NO <sub>3</sub> ) <sub>2</sub> ] . . . . .	106
23 Bond Distances (in Å) in [Pb(PHENSC)(NO <sub>3</sub> ) <sub>2</sub> ] . . . . .	107
24 Bond Angles (in deg) in [Pb(PHENSC)(NO <sub>3</sub> ) <sub>2</sub> ] With Estimated Standard Deviations . . . . .	108
25 Dimensions of Symmetrically Bidentate Nitrato-Groups in Å and Degrees . . . . .	110
26 Least-Squares Planes for [Pb(PHENSC)(NO <sub>3</sub> ) <sub>2</sub> ] . . . . .	112
27 A Comparison of the Interplanar Angles for the Coordination Polyhedron in [Pb(PHENSC)(NO <sub>3</sub> ) <sub>2</sub> ] Complex . . . . .	113
28 A Comparison of the Interplanar Angles for the Coordination Polyhedron in [Pb(PHENSC)(NO <sub>3</sub> ) <sub>2</sub> ] Complex . . . . .	115
29 Final Parameters for [(Th[PHENSC]) <sub>2</sub> O(NO <sub>3</sub> ) <sub>2</sub> (H <sub>2</sub> O) <sub>2</sub> ](NO <sub>3</sub> ) <sub>4</sub> ·H <sub>2</sub> O . . . . .	126
30 Bond Distances (in Å) for [(Th[PHENSC]) <sub>2</sub> O(NO <sub>3</sub> ) <sub>2</sub> (H <sub>2</sub> O) <sub>2</sub> ](NO <sub>3</sub> ) <sub>4</sub> ·H <sub>2</sub> O . . . . .	128
31 Bond Angles (in deg) in [(Th[PHENSC]) <sub>2</sub> O(NO <sub>3</sub> ) <sub>2</sub> (H <sub>2</sub> O) <sub>2</sub> ](NO <sub>3</sub> ) <sub>4</sub> ·H <sub>2</sub> O . . . . .	131
32 Least-Squares Planes for Th(1)-PHENSC in [(Th[PHENSC]) <sub>2</sub> O(NO <sub>3</sub> ) <sub>2</sub> (H <sub>2</sub> O) <sub>2</sub> ](NO <sub>3</sub> ) <sub>4</sub> ·H <sub>2</sub> O . . . . .	135
33 Least-Squares Planes for Th(2)-PHENSC in [(Th[PHENSC]) <sub>2</sub> O(NO <sub>3</sub> ) <sub>2</sub> (H <sub>2</sub> O) <sub>2</sub> ](NO <sub>3</sub> ) <sub>4</sub> ·H <sub>2</sub> O . . . . .	137

<u>Table</u>	<u>Page</u>
34 Dihedral Angles for Various Planes In $[(\text{Th}[\text{PHENSC}])_2\text{O}(\text{NO}_3)_2(\text{H}_2\text{O})_2](\text{NO}_3)_4 \cdot \text{H}_2\text{O}$ . . . . .	139
35 A Comparison of the Interplanar Angles for the Coordination Polyhedron in $\{[\text{Th}(\text{PHENSC})(\text{H}_2\text{O})(\text{NO}_3)]_2\text{O}\}(\text{NO}_3)_4 \cdot \text{H}_2\text{O}$ Around Th(1) . . . . .	140
36 A Comparison of the Interplanar Angles for the Coordination Polyhedron in $\{[\text{Th}(\text{PHENSC})(\text{H}_2\text{O})(\text{NO}_3)]_2\text{O}\}(\text{NO}_3)_4 \cdot \text{H}_2\text{O}$ Around Th(2) . . . . .	142
37 A Comparison of the Interplanar Angles for the Coordination Polyhedron in $\{[\text{Th}(\text{PHENSC})(\text{H}_2\text{O})(\text{NO}_3)]_2\text{O}\}(\text{NO}_3)_4 \cdot \text{H}_2\text{O}$ Around Th(1) . . . . .	144
38 A Comparison of the Interplanar Angles for the Coordination Polyhedron in $\{[\text{Th}(\text{PHENSC})(\text{H}_2\text{O})(\text{NO}_3)]_2\text{O}\}(\text{NO}_3)_4 \cdot \text{H}_2\text{O}$ Around Th(2) . . . . .	146



# LIST OF FIGURES

<u>Figure</u>		<u>Page</u>
1	Trigonal and tetragonal distortion of an octahedral complex. . . . .	3
2	Orbital energy diagram for a tetragonal field. . . . .	6
3	The two components of internal motion of $e_g$ symmetry in an octahedral complex. . . . .	7
4	The Jahn-Teller Effect. The simplest forms of Jahn-Teller distortion for an octahedron. . . . .	8
5	The potential energy surfaces "Mexican Hat". . . . .	12
6	Patterns available for hexadentate chelating agents. . . . .	22
7	Hexadentate chelating agents . . . . .	24
8	2,9-Diformyl-1,10-phenanthroline bis(semicarbazone). . . . .	28
9	Stereoscopic view of the $[\text{Mn}(\text{urea})_6](\text{ClO}_4)_3$ . . . . .	45
10	An ORTEP view of $[\text{Mn}(\text{urea})_6](\text{ClO}_4)_3$ showing the atomic numbering and the thermal ellipsoids . . . . .	47
11	An ORTEP view of perchlorate ion in $[\text{Mn}(\text{urea})_6](\text{ClO}_4)_3$ showing the atomic numbering and the thermal ellipsoids. . . . .	48
12	An ORTEP view of the coordinated urea molecule in $[\text{Mn}(\text{urea})_6](\text{ClO}_4)_3$ showing the atomic number and thermal ellipsoids, and bond distances (Å) with estimated standard deviations in parenthesis . . . . .	50
13	Term level diagram for a $d^4$ ion in three fields. . . . .	51
14	A typical Differential Scanning Calorimetry curve. . . . .	66
15	Differential scanning calorimetry of $[\text{Mn}(\text{urea})_6](\text{ClO}_4)_3$ . . . . .	67

<u>Figure</u>	<u>Page</u>
16 EPR spectra of microcrystalline $[\text{Mn}(\text{urea})_6](\text{ClO}_4)_3$ . . .	69
17 EPR spectrum of microcrystalline manganese(III)-doped $[\text{Al}(\text{urea})_6](\text{ClO}_4)_3$ at room temperature. . . . .	70
18 EPR spectra of manganese(III)-doped $[\text{Al}(\text{urea})_6](\text{ClO}_4)_3$ at liquid nitrogen temperature. . . . .	72
19 EPR spectrum of $[\text{Mn}(\text{urea})_6](\text{ClO}_4)_3$ in perchloric acid (60%) saturated with urea at liquid nitrogen temperature. . . . .	73
20 Stereoscopic view of $[\text{Co}(\text{PHENSC})(\text{H}_2\text{O})_2](\text{NO}_3)_2$ . . . . .	79
21 An ORTEP view of $[\text{Co}(\text{PHENSC})(\text{H}_2\text{O})_2](\text{NO}_3)_2$ showing the atomic numbering and the thermal ellipsoids . . . . .	81
22 Stereoscopic view of $[\text{Pb}(\text{PHENSC})(\text{NO}_3)_2]$ . . . . .	100
23 An ORTEP view of $[\text{Pb}(\text{PHENSC})(\text{NO}_3)_2]$ showing the atomic numbering and the thermal ellipsoids. . . . .	102
24 Six possible polyhedra for a coordination number of ten .	103
25 Six possible polyhedra represented as points on a sphere for a coordination number of ten. . . . .	104
26 Stereoscopic view of $\{[\text{Th}(\text{PHENSC})(\text{H}_2\text{O})(\text{NO}_3)]_2\text{O}\}(\text{NO}_3)_4 \cdot \text{H}_2\text{O}$ . . . . .	123
27 An ORTEP view of $\{[\text{Th}(\text{PHENSC})(\text{H}_2\text{O})(\text{NO}_3)]_2\text{O}\}(\text{NO}_3)_4 \cdot \text{H}_2\text{O}$ showing the atomic numbering and the thermal ellipsoids .	125

Abstract of Dissertation Presented to the Graduate Council  
of the University of Florida in Partial Fulfillment of the  
Requirements for the Degree of Doctor of Philosophy

THE JAHN-TELLER EFFECT IN HEXAUREAMANGANESE(III)PERCHLORATE  
AND  
MOLECULAR STRUCTURE OF HIGH COORDINATION COMPLEXES

By

Hossein Aghabozorg

May, 1982

Chairman: Dr. Robert C. Stoufer  
Major Department: Chemistry

The high-spin complex hexaureamanganese(III)perchlorate,  $[\text{Mn}(\text{urea})_6](\text{ClO}_4)_3$ , crystallizes in the space group  $R\bar{3}c$  with  $a = 18.124(4)$ ,  $c = 14.042(3)$  Å and six molecules per unit cell. The cation was found to have site symmetry  $\bar{3}$  requiring that the six Mn-O bonds be equivalent in apparent violation of the Jahn-Teller theorem. Analyses of the mean-square displacements and the visible absorption spectra data are in accord with the existence of a dynamic Jahn-Teller effect in the cation.

Detailed ESR measurements made predominantly at liquid nitrogen temperatures on the microcrystalline pure complex, the microcrystalline, manganese(III)-doped aluminum(III) complex, and the glassy sample were presented and discussed.

Complexes of the planar hexadentate ligand 2,9-diformyl-1,10-phenanthroline bis(semicarbazone), PHENSC, were studied.

In  $[\text{Co}(\text{PHENSC})(\text{H}_2\text{O})_2](\text{NO}_3)_2$ , the complex crystallizes in the monoclinic system (space group  $P2_1/c$ ) with  $a = 8.012(3)$ ,  $b = 10.257(9)$ ,  $c = 26.260(15)$  Å,  $\beta = 92.71(4)^\circ$ , and four molecules per unit cell. The cobalt atom is in the center of a pentagonal bipyramidal arrangement consisting of five of the six donor atoms of the planar ligand in the equatorial plane and two axial water molecules. The  $\text{NO}_3^-$  anions are joined by hydrogen bonds.

In  $[\text{Pb}(\text{PHENSC})(\text{NO}_3)_2]$ , the complex crystallizes in the monoclinic system (space group  $C2/c$ ) with  $a = 14.831(4)$ ,  $b = 16.722(4)$ ,  $c = 8.399(2)$  Å,  $\beta = 95.27(2)^\circ$ , and four molecules per unit cell. The lead atom has an unusual coordination number of ten involving six donor atoms of the planar in the equatorial plane and four oxygen atoms from two axial symmetric bidentate nitrate groups.

In  $\{[\text{Th}(\text{PHENSC})(\text{H}_2\text{O})(\text{NO}_3)]_2\text{O}\}(\text{NO}_3)_4 \cdot \text{H}_2\text{O}$ , the complex crystallizes in the monoclinic system (space group  $P2_1/c$ ) with  $a = 14.423(3)$ ,  $b = 25.833(10)$ ,  $c = 13.140(3)$  Å,  $\beta = 93.52(2)^\circ$ , and four molecules per unit cell. The two thorium atoms in the binuclear, oxo-bridged complex both have coordination numbers of ten involving six donor atoms of the planar ligand, two oxygen atoms from one bidentate nitrate group, one oxygen from water, and one oxygen from the unusual oxo bridge.

## CHAPTER I

### INTRODUCTION

#### A. The Jahn-Teller Effect in Hexaureamanganese(III)Perchlorate

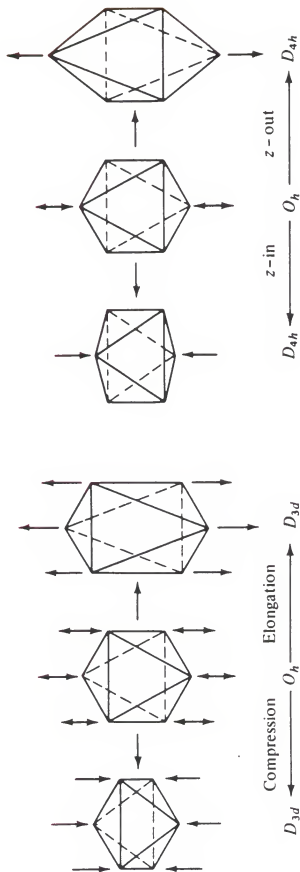
In 1937 Jahn and Teller<sup>1</sup> proved that, for a nonlinear molecule in an electronically degenerate term, distortion must occur which will lower the symmetry and split the degenerate term.<sup>2</sup> In fact,

a configuration of a polyatomic molecule for an electronic state having orbital degeneracy cannot be stable with respect to all displacements of the nuclei unless in the original configuration the nuclei all lie on a straight line. An extension of the theorem to cover additional degeneracy arising from the spin is established, which shows that if the total electronic state of orbital and spin motion is degenerate, then a non-linear configuration of the molecule will be unstable unless the degeneracy is the special twofold one (discussed by Kramers 1930) which can occur only when the molecule contains an odd number of electrons. The additional instability caused by the spin degeneracy alone, however, is shown to be very small and its effect for all practical purposes negligible (p. 117).<sup>2</sup>

Let us consider the influence of the metal d electrons upon structure.<sup>3</sup> For  $d^0, d^5$  (high spin) or  $d^{10}$  configurations, the d electrons cause no distortion, i.e., the central metal has spherical electrical symmetry. Thus the sites occupied by equivalent ligands are

identical. For  $d^1$  configuration, if the electron occupies a  $d_{xy}$  orbital, the electron will repel electron-rich ligands which are near it; the four ligands bonding in the  $xy$  plane should move away from the central metal atom. Therefore, in this case, the four equatorial bonds should be longer than the two axial bonds. Also, a small distortion is expected for octahedral  $d^2$  systems. For  $d^3$  ( $t_{2g}^3$ ),  $d^6$  low-spin ( $t_{2g}^6$ ) and  $d^8$  ( $t_{2g}^6 e_g^2$ ) systems, the repulsion between the  $d$  electrons and all six donor atoms should be identical; thus no distortion is expected. For  $d^4$  high-spin ( $t_{2g}^3 e_g^1$ ) systems, the first three electrons occupy  $t_{2g}$  orbitals; but the fourth electron occupies an  $e_g$  orbital. If that electron occupies the  $d_{z^2}$  orbital, the ligands on the  $z$  axis will be repelled ( $z$ -out); if the electron occupies the  $d_{x^2-y^2}$  orbital, the four ligands on  $xy$  plane will be repelled ( $z$ -in). We expect the same result for the  $d^9$  configuration, and experimental evidence has been published showing distortions from octahedral symmetry. Similar arguments may be made for  $d^7$  low-spin ( $t_{2g}^6 e_g^1$ ) systems. Trigonal and tetragonal distortion are two important departures from cubic symmetry. The distortion can appear either as an elongation or a compression along the  $C_3$  or  $C_4$  rotation axes of the octahedron (Figure 1).<sup>4</sup>

According to the group theory, two  $e_g$  orbitals have the same energy, and all three  $t_{2g}$  orbitals have identical energy under  $O_h$  symmetry. The  $t_{2g}$  and  $e_g$  orbitals will split under  $D_{4h}$  tetragonal symmetry containing the irreducible representations  $a_{1g}$ ,  $b_{1g}$ ,  $b_{2g}$ , and  $e_g$ .<sup>5</sup>



### Tetragonal distortion

### Trigonal distortion

Figure 1. Trigonal and tetragonal distortion of an octahedral complex.  
Either may occur via elongation or compression.

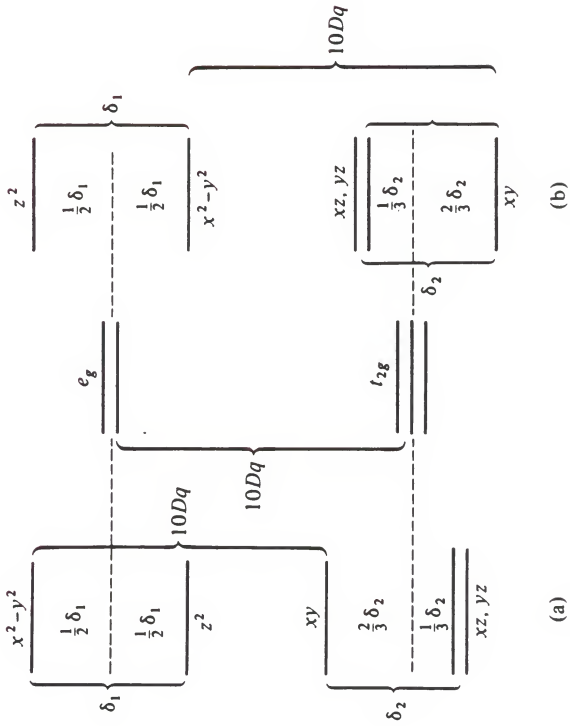


The orbital energy diagram for a tetragonal field for both elongation (z-out) and compression (z-in) are shown in Figure 2.<sup>4</sup> As we can see, the splittings obey a center-of-gravity rule. The two  $e_g$  orbitals separate so that one goes up as much as the other goes down; the  $t_{2g}$  orbitals separate so that the doubly degenerate pair goes down or up only half as far as the single orbital goes up or down. Therefore, for  $d^4$  and  $d^9$  configurations, there is no net energy change for the  $t_{2g}$  electrons; for the  $e_g$  electrons, however, a net stabilization occurs. Accordingly for the configurations  $t_{2g}^6 e_g^1$ ,  $t_{2g}^6 e_g^3$  and  $t_{2g}^3 e_g^1$  tetragonal distortions of the octahedron will cause stabilization. Thus, we predict, as could also be done by blind application of the Jahn-Teller theorem, that distortions from octahedral symmetry are to be expected for six-coordinate metal complexes with the configurations noted above.<sup>4,6</sup>

In a regular octahedron, one of the normal vibrational modes [ $S_{2a}(e_g)$  in Figure 3] is the movement of two opposite ligand atoms outwards or inwards (axial position) and the simultaneous movement of four ligand atoms (in the plane) inwards or outwards.<sup>7,8</sup> These motions are shown in Figure 4 as the simplest forms of Jahn-Teller distortion for an octahedron.<sup>7</sup> In both cases, those displacements lead to a reduced energy for the system. The Static Jahn-Teller Effect can explain a permanent distortion of the molecule. In fact, it occurs whenever the displacement of the ligand atoms takes place into



Figure 2. Orbital energy diagram for a tetragonal field:  
(a) Z ligands out; (b) Z ligands in.



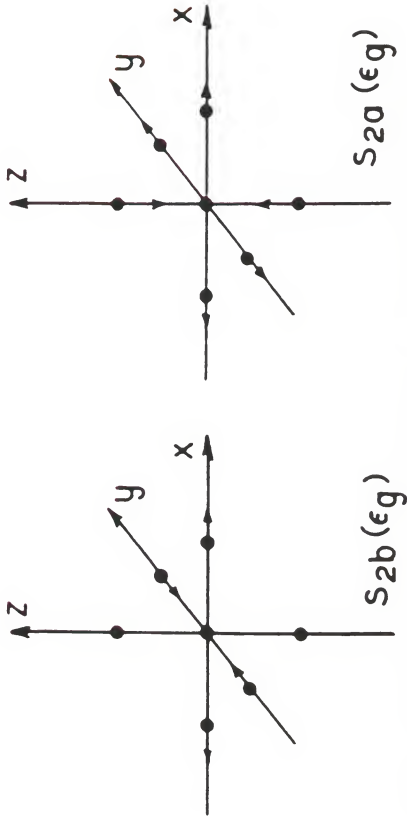


Figure 3. The two components of internal motion of  $e_g$  symmetry in an octahedral complex.

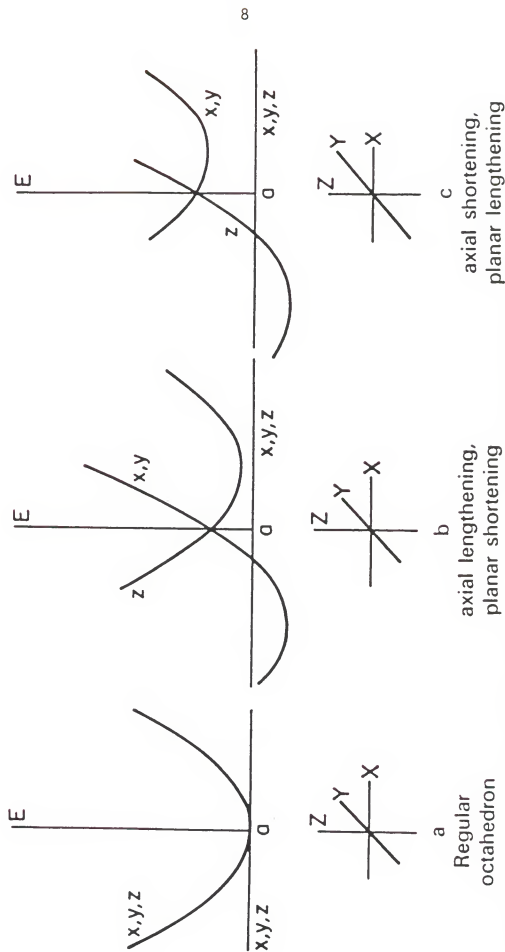


Figure 4. The Jahn-Teller Effect. The simplest forms of Jahn-Teller distortion for an octahedron.

one of the arrangements represented in Figure 4b or 4c. The Dynamic Jahn-Teller Effect occurs whenever both distorted forms are of lower energy than the undistorted octahedron, and the potential barrier for interconversion between two forms is small. In this case, the molecule can convert from one form to another, and the time average position of the ligand atoms around the center of metal atom in complex may be close to the regular octahedral positions.<sup>7</sup>

A wide range of physical and chemical properties can be measured in studying the Jahn-Teller effect. The measurements may be <sup>9</sup>

(a) resonance investigations (i.e., in the whole range of spectroscopy),

(b) non-resonance investigations (i.e., stereochemistry, crystal chemistry, chemical reactivity, magnetic and electric polarizability, and so on).

Therefore, several techniques such as structural analysis by X-ray, neutron or electron diffraction, EPR spectroscopy at different temperatures, vibrational analysis, optical absorption spectroscopy, and Mössbauer spectroscopy can be considered.<sup>9,10,11</sup> Electron paramagnetic resonance proves to be the most powerful method for analyzing the symmetry aspects and static-to-dynamic phase transitions of Jahn-Teller-unstable solid compounds, and gives information about the electronic and magnetic properties. Structural analysis by X-ray, neutron or electron diffraction gives information on the Jahn-Teller radius  $R_{JT}$ . In the case of a permanent static distortion in low symmetry sites,  $R_{JT}$  is given by the equation<sup>11</sup>

$$R_{JT}^2 = S_{2a}^2 + S_{2b}^2 = \sum_{i=1}^6 \Delta d_i^2$$

where  $S_{2a}$  and  $S_{2b}$  denote the two components of the degenerate  $e_g$  distortion (Figure 3) and six  $\Delta d_i$ 's show the deviations of individual Metal-Ligand bond lengths from the average Metal-Ligand bond distance  $d_0$ . In cases of purely dynamic or disordered static distortion,  $R_{JT}$  is given by the equation<sup>11</sup>

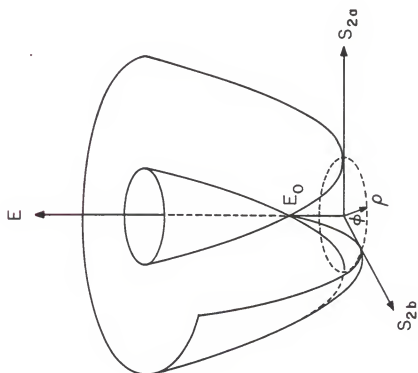
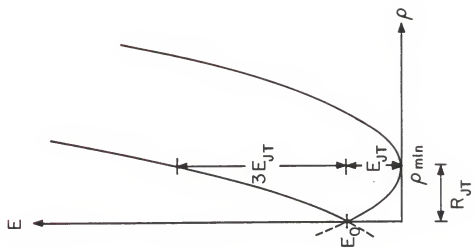
$$R_{JT}^2 = \sum_{i=1}^6 \langle \Delta d_i^2 \rangle_{JT} = \sum_{i=1}^6 \langle \Delta d_i^2 \rangle_{\text{obsd}} - \sum_{i=1}^6 \langle \Delta d_i^2 \rangle_{\text{res}}$$

The linear coupling between electronic and vibrational motions lead to potential surface which is called the "Mexican Hat" (Figure 5).<sup>12,13</sup> The energy surfaces which arise from this coupling (upper and lower potential surfaces),  $E_{\pm}$ , given below<sup>12</sup>

$$E_{\pm} = E_0 \pm V\rho + \frac{M\omega^2}{2}\rho^2$$

The electronic energy in the absence of the Jahn-Teller effect is  $E_0$ . The second and third terms represent the strength of the linear Jahn-Teller coupling and the potential energy associated with the  $E_g$  vibrations, respectively. The radial coordinate measuring the extent of distortion is  $\rho$ ,  $M$  is the mass of one of the six ligands, and  $\omega$  is the frequency of the radial vibration. The circular valley (dotted line at bottom of potential) with radius  $R_{JT}$  is stabilized by the Jahn-Teller energy  $E_{JT}$  relative to the energy  $E_0$  at  $S_{2a} = S_{2b} = 0$ .<sup>11</sup> The Jahn-Teller stabilization energy with respect to  $E_0$  is<sup>12</sup>

Figure 5. The potential energy surfaces "Mexican Hat". The circular valley (dotted line at bottom of potential) with radius  $R_{JT}$  is stabilized by the Jahn-Teller energy  $E_{JT}$  relative to the energy  $E_0$  at  $S_{2a} = S_{2b} = 0$ .

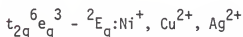
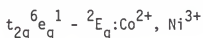
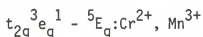




$$E_{JT} \equiv E_{\min} - E_0 = \frac{M\omega^2}{2} \rho_{\min}^2 = \frac{V^2}{2M\omega^2}; \quad \rho_{\min} = \frac{|V|}{M\omega^2}$$

The distance between the minimum positions and the upper potential surface gives  $4E_{JT}$  value.<sup>11,12</sup> Optical absorption spectroscopy gives approximate information on the cubic ligand field splitting  $\Delta$  and also indirectly on the Jahn-Teller energy  $E_{JT}$ .<sup>11</sup>

The best candidates for consideration of Jahn-Teller effect are the following:<sup>12</sup>



but more examples are available for the  $Cu^{2+}$  and  $Mn^{3+}$  ions than for the others. However, the crystal structure of chromium(II)fluoride,  $CrF_2$  shows the two axial Cr-F distances are significantly longer (2.43 Å) than the other four Cr-F distances (2.00 Å)<sup>4</sup>. The structure of the low-spin complex,  $K_2BaCo(NO_2)_6$ , has been determined by three-dimensional X-ray diffraction at room temperature, and all of the Co-N bonds are equivalent (1.98 Å).<sup>14</sup> But, at 233 K,<sup>15</sup> this complex shows three independent Co-N bond lengths of 1.94 Å, 2.10 Å, and 1.90 Å along the x, y, and z axes, respectively. The results indicate a dynamic Jahn-Teller distortion at 233 K.<sup>14,15</sup> Silver(II) Bis(pyridine-2,6-dicarboxylate) monohydrate,  $Ag(C_7H_4NO_4)_2 \cdot H_2O$ , shows a very distorted octahedral structure.<sup>16</sup> However, the two ligands coordinated

are different, i.e., one is anionic and the other is molecular. In the anionic ligand the Ag-N bond length is  $2.09 \text{ \AA}$ , and the two negatively-charged oxygen atoms are  $2.20 \text{ \AA}$ . In the neutral ligand, the Ag(II) is bonded less strongly to the nitrogen ( $2.21 \text{ \AA}$ ) and to the "Ketonic" oxygen atoms at  $2.53 \text{ \AA}$ .

An excellent example of a species undergoing a Jahn-Teller distortion is the  $d^9$  Copper(II) ion. Many articles have been published concerning the Jahn-Teller effect in Cu(II) systems. A series of compounds containing the hexanitrocuprate(II) ion,  $[\text{Cu}(\text{NO}_2)_6]^{4-}$ , have been reported.<sup>17-26</sup> The most accurate determination of the structure of potassium lead hexanitrocuprate(II),  $\text{K}_2\text{PbCu}(\text{NO}_2)_6$ , shows the Cu-N<sub>6</sub> configuration is octahedral, an apparent violation of the Jahn-Teller theorem. However, the thermal parameters of the nitrogen atoms are in accord with the assumption of a dynamic Jahn-Teller effect. The Cu-N bond distance in this complex is  $2.111 \text{ \AA}$ ; the space group is Fm3.<sup>17</sup> The structure of potassium lead hexanitrocuprate(II) at 276 K shows a compressed tetragonal Jahn-Teller distortion with two short Cu-N bond distances  $2.058 \text{ \AA}$  and four long Cu-N bonds with an average distance  $2.160 \text{ \AA}$ ; the space group is Fmmm.<sup>18</sup> In fact, by decreasing the temperature a few degrees, the dynamic Jahn-Teller effect is "frozen" out and the structure becomes distorted. The single crystal EPR of  $\text{K}_2\text{PbCu}(\text{NO}_2)_6$  has been interpreted in terms of a tetragonally compressed environment for Cu(II).<sup>19</sup> The compound  $\text{Tl}_2\text{PbCu}(\text{NO}_2)_6$ , cubic, Fm3, is isomorphous with  $\text{K}_2\text{PbCu}(\text{NO}_2)_6$  at 295 K; the Cu-N bond distance is  $2.118 \text{ \AA}$ .<sup>20</sup> The EPR results indicate both compounds undergo phase transitions to lower symmetry

lattices when the temperature is decreased.<sup>19,21</sup> The root-mean-square nitrogen atom displacements for both complexes at 295 K indicate that the nitrogen atoms show greater thermal motion along the Cu-N bond than at right angle to it.<sup>20,22</sup> This feature of the thermal motion is consistent with the presence of a dynamic Jahn-Teller effect.<sup>17</sup>

The isomorphous compounds  $K_2PbNi(NO_2)_6$ , cubic (Fm3) and  $K_2PbCu(NO_2)_6$  have been compared to each other.<sup>22</sup> In  $K_2PbNi(NO_2)_6$ , the thermal parameters suggest less motion along the Ni-N bond and greater motion at right angles.<sup>22</sup> In contrast to the salts discussed above, the structures of the isomorphous series of compounds  $K_2CaCu(NO_2)_6$ ,<sup>23</sup>  $K_2BaCu(NO_2)_6$ ,<sup>24</sup>  $K_2SrCu(NO_2)_6$ ,<sup>25</sup> and  $Rb_2PbCu(NO_2)_6$ <sup>26</sup> are distorted at room temperature (Fmmm space group).

Redetermination of the crystal structure of tris(ethylenediamine) Copper(II) sulfate,  $Cu(NH_2CH_2CH_2NH_2)_3SO_4$ , indicates the copper and sulfur atoms are located at positions of 32 ( $D_3$ ) symmetry. This compound is isostructural with  $Ni(NH_2CH_2CH_2NH_2)_3SO_4$ . The compound crystallizes in the trigonal space group  $P\bar{3}1c$ , with a Cu-N bond length of 2.150 Å. The site symmetry of copper is in violation of the Jahn-Teller theorem.<sup>27</sup> The thermal parameters for the copper(II) compound are somewhat larger than those in  $Ni(en)_3SO_4$ ; but the difference is small. Therefore, it is difficult to draw conclusions about the existence of such an effect based upon these data above. It is significant that the crystal structure of  $Cu(NH_2CH_2CH_2NH_2)_3SO_4$  at 120 K indicates the triclinic space group  $P\bar{1}$ . The two shortest Cu-N distances are 2.05 and 2.06, but the average of the four long Cu-N lengths is 2.22 Å.<sup>28</sup> The single-crystal polarized and ESR spectra of

$\text{Cu(en)}_3\text{SO}_4$  at room and low temperatures were considered in terms of dynamic distortions. The ESR spectra between room and liquid helium temperature of this complex have been interpreted on the basis of dynamic-static Jahn-Teller distortions. Since vibronic coupling determines distortions along the bond directions, the systems can be better described as tetragonally distorted.<sup>29</sup> On the other hand, the structure of  $\text{Cu(en)}_3\text{Cl}_2 \cdot 0.75\text{en}$  is best described as a tetragonally elongated octahedra.<sup>28</sup>

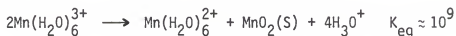
Another example of a Cu(II) complex exhibiting no static Jahn-Teller distortion is tris(octamethylpyrophosphoramide) copper(II) perchlorate,  $\text{Cu(OMPA)}_3(\text{ClO}_4)_2$ , with trigonal space group  $\bar{P}3c1$ . The Cu-O bond length is 2.065 Å, and the site symmetry of the copper ion is  $D_3$ . According to the Jahn-Teller theorem, this symmetry should be unstable. This complex is isomorphous with Mg(II) and Co(II) complexes. The anisotropic thermal parameters of the three complexes were considered for the dynamic Jahn-Teller distortions. The root-mean-square amplitudes for O-Cu and O-Mg [Jahn-Teller distortions are absent for Mg(II)] are almost the same. Therefore, the thermal parameters fail to show any oscillation which can be interpreted in terms of a dynamic Jahn-Teller effect.<sup>30</sup> Single crystal EPR spectra of this compound have been obtained at 90 K, and the results are correlated with X-ray structural data.<sup>31</sup>

The crystal and molecular structure of tris-(2,2'-bipyridyl) copper(II) perchlorate,  $\text{Cu(bipy)}_3(\text{ClO}_4)_2$ , indicates unequal distortions of the axial Cu-N bonds. The average Cu-N(eq) is 2.031 Å, Cu-N(ax) 2.226 and 2.450 Å,<sup>32</sup> but the crystal and molecular structure

of tris(1,10-phenanthroline)copper(II) perchlorate,  $\text{Cu}(\text{phen})_3(\text{ClO}_4)_2$ , shows equal distortion of the axial Cu-N bonds. The average Cu-N(eq) is  $2.04 \text{ \AA}$ , and the average Cu-N(ax) is  $2.33 \text{ \AA}$ .<sup>33</sup>

The crystal structure of  $\text{Cu}(\text{tach})_2(\text{NO}_3)_2$  and  $\text{Cu}(\text{tach})_2(\text{ClO}_4)_2$  (tach cis,cis-1,3,5-triaminocyclohexane) were investigated by X-ray crystallography at room temperature and by ESR spectroscopy between 4 and 300 K.<sup>11</sup> The complex  $\text{Ni}(\text{tach})_2(\text{NO}_3)_2$ , in which the Jahn-Teller effect is absent, was also studied for comparison. "Both  $R_{JT}$  and the average Cu-N distance,  $d_0$ , were found to be equal within experimental error for dynamically distorted  $\text{Cu}(\text{tach})_2(\text{NO}_3)_2$  and statically distorted  $\text{Cu}(\text{tach})_2(\text{ClO}_4)_2$ " (p. 749).<sup>11</sup>

An excellent example of a  $d^4$  species undergoing Jahn-Teller distortion is Mn(III). The Mn(III) has a strong tendency to disproportionate. The equilibrium constant for the reaction represented below is  $10^9$ .<sup>34</sup>



The standard electrode potential for Mn(III)/Mn(II) in acid media is +1.51 V. Therefore, Mn(III) is a strongly oxidizing species comparable to permanganate ion in acid media ( $\text{MnO}_4^-/\text{Mn}^{2+} = +1.51 \text{ V}$ ).<sup>35,36</sup> The Mn(III) stability can be increased either by increasing the acidity or by complex formation.<sup>36</sup> Almost all Mn(III) complexes -- except those containing cyanide ion -- are high spin ( $t_{2g}^3 e_g^1$ ).<sup>6</sup>

The  $d^4$ , manganese(III) ion has a  $^5D$  field-free ground term level which, in an octahedral field, splits into a  $^5E_g$  ground term and a  $^5T_{2g}$  excited term. However, the Jahn-Teller theorem predicts that an

octahedral complex will distort in order to remove the orbital degeneracy of the ground term. Because the orbital degeneracy lies in the  $e_g$  orbitals, the ground term splitting is expected to be larger than that of the excited term. Therefore, the ground electronic term anticipated in octahedral complexes,  ${}^5E_g$ , is subject to strong Jahn-Teller forces.<sup>37</sup> In general, the three absorption bands observed in the visible region of the electronic spectra have been satisfactorily assigned in terms of  $D_{4h}$  symmetry.<sup>37,38</sup> A few crystal structures for Mn(III) complexes containing six chemically equivalent donor atoms are available for consideration of Jahn-Teller effects.

It is interesting to consider  $\beta$ -manganese(III)acetylacetonate,  $Mn(acac)_3$ , which crystallizes with the space group  $P2_1/c$ . The structure reported by Morosin and Brathovde (MB) was believed to show no Jahn-Teller distortion.<sup>39</sup> However, the structure of  $Co(acac)_3$  determined by Hon and Pfluger was found to be nearly identical to that reported by MB for  $Mn(acac)_3$ .<sup>40</sup> Since the possibility was strong that  $Mn(acac)_3$  and  $Co(acac)_3$  compounds were mis-labeled, Fackler and Avdeef reexamined the structure of  $Mn(acac)_3$  and suggested that the  $Mn(acac)_3$  structure reported previously by MB was actually that of  $Co(acac)_3$ .<sup>41</sup> Fackler and Avdeef found two short Mn-O average bond distances of 1.95 Å and four long Mn-O bond distances averaging 2.00 Å. The  $\beta$  form of  $Mn(acac)_3$  was reexamined by Stults et al., and their results are somewhat more precise.<sup>42</sup>

The crystal and molecular structure of a  $\gamma$  form of  $Mn(acac)_3$  with space group  $P2_1/n$  was determined by Stults et al.<sup>42</sup> The structure of the  $\gamma$  form indicates a tetragonal elongation with an average of the two

long trans Mn-O bond lengths of 2.111 Å and the four short Mn-O bond lengths of 1.935 Å. This distortion is presumably the result of the Jahn-Teller effects for the high-spin  $d^4$  Mn(III).

The structure of tris(tropolonato)manganese(III),  $\text{Mn}(\text{trop})_3$ , space group  $P2_1/c$ , has been determined.<sup>43</sup> The unit cell contains two crystallographically independent molecules. Molecule I is tetragonally elongated  $\text{MnO}_6$  geometry with average bond lengths of 1.94 and 2.13 Å and with an average trigonal twist angle of 48.9°. Molecule II is orthorhombic  $\text{MnO}_6$  distortion with average bond distances of 1.94, 1.99 and 2.05 Å with an average trigonal twist angle of 49.9°. It is obvious that in a regular  $D_3$  symmetry encountered in tris chelate complexes, the degeneracy of the  $^5E$  ground term is not lifted; further reduction in symmetry is required. Accordingly, both asymmetric molecules show distortion from a regular  $D_3$  conformation.<sup>43</sup> For comparison, the average twist angle for  $\text{Mn}(\text{acac})_3$  is 60.2°, indicating very little distortion from regular  $D_3$  symmetry.<sup>41</sup> The average twist angle for  $\text{Mn}(\text{acac})_3$  is larger than for  $\text{Mn}(\text{trop})_3$ , because of the larger "bite" distance for acac.

The crystal structure of tripotassium tris(malonato) manganese (III) dihydrate,  $\text{K}_3[\text{Mn}(\text{mal})_3] \cdot 2\text{H}_2\text{O}$  has also been reported, space group  $C2/c$ . "The  $[\text{Mn}(\text{mal})_3]^{3-}$  ion is approximately a trigonally distorted octahedron with small deviations from  $D_3$  symmetry, arising from lattice forces which vary as a result of the packing of the complex, from Jahn-Teller distortion in Mn(III) complexes, and from crystallographic symmetry which imposes a  $C_2$  axis on the  $D_3$  geometry"(p. 1945).<sup>44</sup> The Mn-O bond distances for this complex are 1.92, 2.00 and 2.04 Å. These values indicate the distortion from octahedral symmetry.

The crystal structure of tris-(NN-diethyldithiocarbamate) manganese(III),  $\text{Mn}(\text{S}_2\text{CNET}_2)_3$ , space group  $\text{P2}_1/\text{a}$ , was determined using single-crystal X-ray photographic data. The compound shows large distortions from regular  $\text{D}_3$  point-symmetry.<sup>45</sup> The complex contains approximately three opposing and equivalent pairs of Mn-S bond distances of 2.38, 2.43 and 2.55 Å.

The crystal and molecular structure of the dichloromethane-solvated tris[morpholinocarbodithioate of manganese(III)],  $\text{Mn} \cdot \text{M} \cdot \text{CH}_2\text{Cl}_2$ , shows space group  $\text{P}\bar{1}$  with a tetragonal distortion. This distortion arises from the Jahn-Teller effect.<sup>46</sup> The  $\text{Mn} \cdot \text{M} \cdot \text{CHCl}_3$  has been determined by single-crystal X-ray diffraction. The compound has space group  $\text{P}\bar{1}$  and shows strong tetragonal distortion in addition to the trigonal distortion. The solvent interaction in this complex, as well as the Jahn-Teller effect, is responsible for the strong distortion.<sup>47</sup>

Indeed, there are a significant number of structures reported for manganese(III) complexes which purport to demonstrate the existence of an axial distortion. However, in the majority of instances, the complexes investigated contain multifunctional ligands, in which case there are inherent constraints imposed upon the nature and extent of the distortion permitted. No X-ray data are reported for mononuclear manganese(III) complexes containing only identical, monofunctional ligands. Only in such a system can one expect to observe the full extent of a structural distortion and the attendant large spectral splitting. A suitable candidate for this study was found in the complex  $\text{Mn}(\text{urea})_6(\text{ClO}_4)_3$ , which has been used over a period of



years as a reagent in the synthesis of a variety of manganese(III) complexes.<sup>48</sup> The hexaureamanganese(III) complex is reasonably stable in the absence of moisture, it does not seem to be subject to photo-decomposition, and it is easily prepared. On the basis of solution, diffuse reflectance, and mull spectra data, this complex seems to be typically distorted.<sup>48</sup> These considerations and the absence of reported structure data for the hexaureamanganese(III) complex have prompted the preparation and study of this interesting ion.

### B. Molecular Structure of High Coordination Complexes

Metal complexes of Schiff bases have been considered in the development of coordination chemistry. Some possible patterns available for hexadentate chelating agents are shown in Figure 6, excluding cyclic structures with fewer than six donor atoms in the ring.<sup>49</sup>

The most important hexadentate chelating agent is probably ethylenediaminetetraacetic acid (EDTA or  $H_4Y$ ), Figure 7a. The capacity of this ligand with different metal ions has been studied. Three-dimensional X-ray analyses of those complexes are available.<sup>50-55</sup> Hoard and coworkers have determined the geometry of the type  $[M(EDTA)(H_2O)]^{n-}$ , seven-coordinate aquo complexes with different metal ions  $[M = Fe(III), Mn(II), Mg(II)]$ . They have noted that two kinds of geometries can be obtained, viz., pentagonal bipyramid and capped trigonal prism. The coordination numbers in  $K[La(H_2O)_3EDTA] \cdot 5H_2O$  and  $H[La(H_2O)_4 \cdot EDTA] \cdot 3H_2O$  are nine and ten, respectively, and both structures have been determined by X-ray diffraction.<sup>54,55</sup> Trans-1,2-diaminocyclohexane-N,N'-tetraacetic acid (DCTA) also functions as

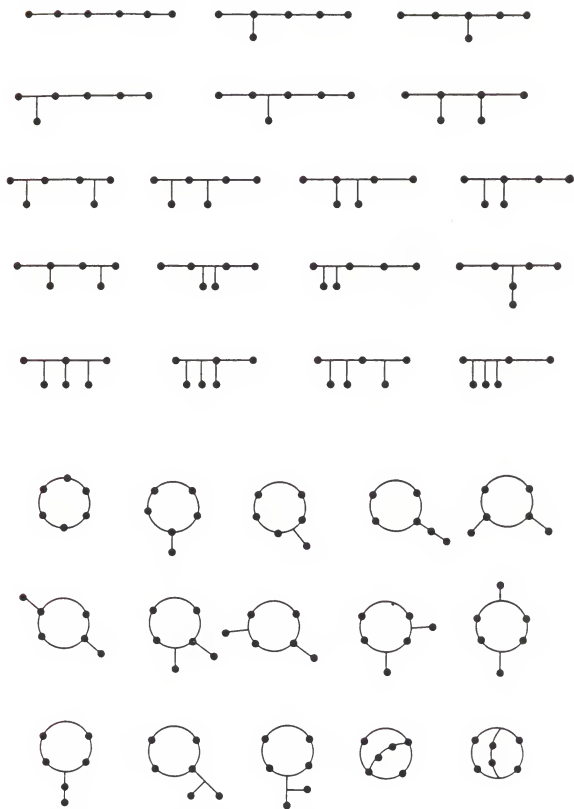
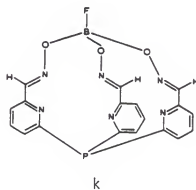
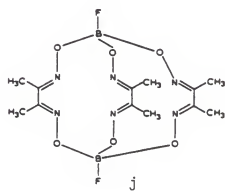
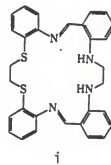
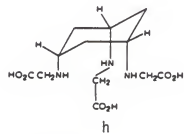
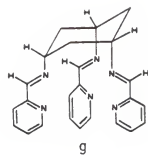
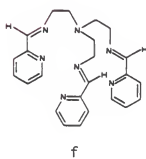
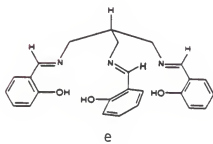
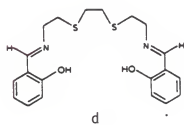
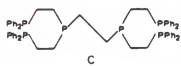
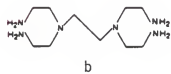
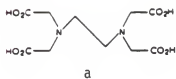


Figure 6. Patterns available for hexadentate chelating agents.

Figure 7: Hexadentate chelating agents.

- (a) Ethylenediamine tetraacetic acid
- (b) N,N,N',N'-tetrakis (2'-aminoethyl)-1,2-diaminoethane
- (c) Hexatertiaryphosphine 1,1,4,4-tetrakis(2-diphenyl phosphinoethyl)-1,4-diphosphabutane
- (d) 1,8-Bis-(salicylidenamino)-3,6-dithiaoctane
- (e) Tris-(salicylidene)derivative of 2-aminomethyl-1,3-diaminopropane
- (f) Tris[1-(2-pyridyl)-2-azabuten-4-yl]amine
- (g) cis,cis-1,3,5-tris(pyridine-2-aldimino)cyclohexane
- (h) cis,cis-1,3,5-Triaminocyclohexane-N,N',N''-triacetic acid
- (i) 15,18-Dithia-1,5,8,12-tetraaza-3,4:9,10:13,14:19,20-tetra-benzocycloeicosane-1,11-diene
- (j) 1,8-Bis(fluoroboro)-2,7,9,14,15,20-hexaoxa-3,6,10,13,16,19-hexaaza-4,5,11,12,17,18-hexamethylbicyclo[6.6.6]eicosa-3,5,10,12,16,18-hexaene
- (k) Fluoroborotris-(2-carboxaldimino-6-pyridyl)phosphine



a hexadentate ligand in  $\text{Ca}[\text{Fe}(\text{H}_2\text{O})\text{DCTA}]_2 \cdot 8\text{H}_2\text{O}$ . The  $[\text{Fe}(\text{H}_2\text{O})\text{DCTA}]^-$  ion is a seven-coordinate aquo complex; the crystal structure was studied by three-dimensional X-ray analysis.<sup>56</sup> Figure 7b and Figure 7c show two analogous hexadentate ligands with nitrogen<sup>57</sup> and phosphorus<sup>58</sup> donors, respectively. The X-ray structure of the first one is available.<sup>57</sup>

The first linear hexadentate chelating agent, 1,8-bis-(salicylidenamino)-3,6-dithiaoctane, was made by Dwyer and Lions<sup>59</sup> (Figure 7d). There are many articles published on hexadentate ligands;<sup>60-69</sup> Dwyer and Lions contributed to many of these. The sulphur donor atoms can be replaced by oxygen<sup>64</sup> or nitrogen,<sup>70</sup> and the o-hydroxyphenyl fragment can be replaced by the  $\alpha$ -pyridyl group.<sup>67,71</sup>

The tris(salicylidene) derivative of 2-aminomethyl-1,3-diaminopropane has been prepared and forms the hexadentate chelate agent (Figure 7e); the o-hydroxyphenyl fragment can be replaced by the  $\alpha$ -pyridyl group.<sup>67</sup>

Figure 7f shows a flexible ligand with seven nitrogen donors. The nickel(II) complex of this ligand was studied by X-ray diffraction.<sup>72</sup> The inspection of molecular models suggested that this ligand would be hexadentate. The X-ray study showed the unique metal-nitrogen distance is  $3.25 \text{ \AA}$ , whereas the other Ni(II)-N distances are  $2.10 \text{ \AA}$ , but the lone pair of electrons on the central tertiary amino nitrogen atom is directed toward the nickel atom.

The ligand cis,cis-1,3,5-tris(pyrindine-2-aldimino)cyclohexane, Figure 7g, was studied as a hexadentate chelating agent.<sup>68,73-75</sup> The structures of the zinc(II) and nickel(II) complexes of this

ligand were determined by single crystal X-ray diffraction.<sup>73,75</sup> Zinc(II) forms a trigonal prismatic complex, but Ni(II) complex has a geometry intermediately between trigonal prismatic and octahedral. The average angle of twist from trigonal prismatic in the zinc(II) complex is only  $4.5^\circ$ ,<sup>73</sup> but in Ni(II) complex it is around  $32^\circ$ .<sup>75</sup> The  $\alpha$ -pyridyl group in this ligand can also be replaced by o-hydroxyphenyl fragment.<sup>68</sup>

Figure 7h shows cis,cis-1,3,5-triaminocyclohexane-N,N',N''-tri-acetic acid, which acts as a hexadentate ligand in Co(III) complex.<sup>76</sup>

Figure 7i shows 15,18-dithia-1,5,8,12-tetraaza-3,4:9,10:13,14:19,20-tetrabenzocycloicosane-1,11-diene ( $N_4S_2$ ), which acts as a hexadentate and gives  $[M(N_4S_2)](ClO_4)_2 \cdot CH_3OH$ , where M = iron(II), cobalt(II), nickel(II), and zinc(II). The  $[Fe(N_4S_2)]^{2+}$  ion structure was determined by a single crystal X-ray diffraction.<sup>77</sup> The structure is distorted slightly from octahedral geometry, because iron-sulfur bonds are longer than iron-nitrogen bonds, and the N-Fe-N bond angle in trans position is about  $175^\circ$ .

The crystal structures of cobalt(II) and cobalt(III) with the cage ligand (Figure 7j) 1,8-bis(fluoroboro)-2,7,9,14,15,20-hexaoxa-3,6,10,13,16,19-hexaaza-4,5,11,12,17,18-hexamethylbicyclo[6.6.6]-eicosa-3,5,10,12,16,18-hexaene, were studied by X-ray diffraction.<sup>78</sup> The polyhedron in the Co(II) complex has  $D_3$  symmetry and is slightly ( $8.6^\circ$ ) distorted from prismatic; in the Co(III) complex it has a configuration between octahedral and trigonal-prismatic.

Figure 7k shows fluoroborotris-(2-carboxaldimino-6-pyridyl)phosphine. A single crystal X-ray study of  $[(FB(ONCH \cdot C_5H_3N)_3P)Ni(II)][BF_4]$

indicates that the cation has  $C_{3v}$  symmetry. The nickel atom is coordinated to six nitrogen atoms, and is distorted only  $1.6^\circ$  from trigonal-prismatic;<sup>79</sup> but the iron(II) complex is distorted by approximately  $21.5^\circ$  from the ideal trigonal prism.<sup>80</sup>

There are many macrocyclic hexadentate ligands available in addition to those mentioned above. For example, a series of cyclic polyethers<sup>81</sup> and polyether sulfides<sup>82</sup> have been studied by Pedersen.

The new planar hexadentate 2,9-diformyl-1,10-phenanthroline bis (semicarbazone), PHENSC (Figure 8), has been prepared and found to yield a series of complexes which are described in this research. This ligand is typical of hexadentate chelating agents, which would be forced to form metal complexes involving six donors in the plane.

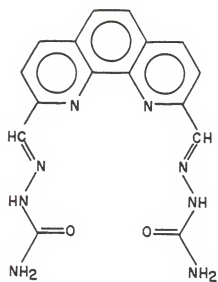


Figure 8. 2,9-Diformyl-1,10-phenanthroline bis(semicarbazone).



## CHAPTER II

### GENERAL DIFFRACTION EXPERIMENTAL

The following is a general description of the experimental method used in the determination of molecular structures.

Precession and Weissenburg photographs were used to determine the space group and unit cell dimensions.<sup>83-85</sup> The accurate cell constants with estimated standard deviations and the intensity data were measured by using a Syntex P $\bar{I}$  diffractometer. The cell volume and its estimated standard deviation were determined from the cell constants. The calculated density is usually in agreement with the crystal density as determined by the flotation method.<sup>86</sup> The density of the flotation liquid was measured to  $\pm 0.002 \text{ g/cm}^3$  with a precision hygrometer.

Graphite-monochromatized molybdenum radiation was used for the measurements of the intensity data. A variable speed  $\theta$ - $2\theta$  scan technique was used to measure intensities. All intensity measurements were taken at room temperature with a Syntex P $\bar{I}$  diffractometer. The scan rate varied linearly from  $1^\circ/\text{minute}$  for counts of 150 or less to  $24^\circ/\text{minute}$  for 1500 counts or more. The intensity,  $I$ , is equal to

$$I = (\text{scan rate})[(\text{total scan counts}) - \frac{(\text{background counts})}{(\text{background to scan ratio})}]$$

The estimated standard deviation,  $\sigma(I)$ , for each reflection is given by

$$(I) = [(total\ scan\ counts) + \frac{(background\ counts)^2}{(background\ to\ scan\ ratio)}]^{1/2}$$

Structures were solved by the heavy-atom method and refined by least-squares techniques. The heavy atom position was determined from a Patterson function,

$$P(UVW) = \frac{1}{V_c} \sum_{h=-\infty}^{\infty} \sum_{k=-\infty}^{\infty} \sum_{l=-\infty}^{\infty} |F(hkl)|^2 \cos 2\pi(hU + kV + lW),$$

and the remaining nonhydrogen atoms were determined by successive Fourier Syntheses,<sup>87</sup>

$$\rho(XYZ) = \frac{1}{V_c} \sum_{h=-\infty}^{\infty} \sum_{k=-\infty}^{\infty} \sum_{l=-\infty}^{\infty} |F(hkl)| \cos[\theta - \alpha(hkl)]$$

Scattering factors were determined from the International Tables.<sup>88</sup> Anisotropic temperature factors for the nonhydrogen atoms of the form

$$\exp[-(\beta_{11}h^2 + \beta_{22}k^2 + \beta_{33}l^2 + \beta_{12}hk + \beta_{13}hl + \beta_{23}kl)]$$

were used in all block-diagonal least-squares calculations. Isotropic thermal parameters only were used in the refinement of the hydrogen atom positions. The differences between observed and calculated structure-factor amplitudes, expressed as an R value, where

$$R = \frac{\sum ||F_{obs}| - |F_{calc}||}{\sum |F_{obs}|},$$

give a measure of the precision of the crystal structure.<sup>83,89</sup>

An R value of about 0.05 shows a well-refined structure. There are a number of factors which limit the agreement between the observed

and calculated  $F$  values. The accuracy of measurement of intensities is not high, and it is often difficult to correct for absorption and extinction. The scattering factor curves are known with only moderate precision. The problems of anisotropic thermal motions and non-spherical electron distributions in bonded atoms are difficult to solve.<sup>89</sup>

All calculations were carried out on an Amdahl-470/V6 using local programs written or modified by G.J. Palenik.

Table 1

Crystal Data for  $\text{Mn}[\text{OC}(\text{NH}_2)_2]_6(\text{ClO}_4)_3$ 

Formula	$\text{C}_6\text{H}_{24}\text{O}_{18}\text{N}_{12}\text{Cl}_3\text{Mn}$
Molecular Weight	713.62
Space Group	$\text{R}\bar{3}\text{c}$
a, Å	18.124(4)
b, Å	18.124(4)
c, Å	14.042(3)
$\alpha$ , deg	90*
$\beta$ , deg	90*
$\gamma$ , deg	120*
Volume, Å <sup>3</sup>	3995(1)
Z	6
$D_m$ , gcm <sup>-3</sup>	1.788
$D_c$ , gcm <sup>-3</sup>	1.780
Crystal Size, mm	0.14 x 0.12 x 0.12
$\mu$ , cm <sup>-1</sup>	8.7
Radiation Used	Mo K $\alpha$ - graphite monochromator
2 $\theta$ Range	0 - 45°
No. of Measured Reflections	642
No. of Reliable Reflections	364
K [in I $\leq$ K $\sigma$ (I)]	2.0
Goodness of Fit	0.98
R	0.055

\* Required by symmetry of space group.

Table 2

Crystal Data for  $[\text{Co}(\text{PHENSC})(\text{H}_2\text{O})_2](\text{NO}_3)_2$ 

Formula	$\text{C}_{16}\text{H}_{18}\text{O}_{10}\text{N}_{10}\text{Co}$
Molecular Weight	569.32
Space Group	$\text{P2}_1/\text{c}$
a, Å	8.012(3)
b, Å	10.257(9)
c, Å	26.260(15)
$\alpha$ , deg	90*
$\beta$ , deg	92.71(4)
$\gamma$ , deg	90*
Volume, Å <sup>3</sup>	2155(2)
z	4
$D_{\text{m}}$ , g cm <sup>-3</sup>	1.714
$D_{\text{c}}$ , g cm <sup>-3</sup>	1.754
Crystal Size, mm	0.25 x 0.09 x 0.09
$\mu$ , cm <sup>-1</sup>	8.7
Radiation Used	Mo K $\alpha$ - graphite monochromator
2 $\theta$ Range	0 - 45°
No. of Measured Reflections	2824
No. of Reliable Reflections	2103
K [in $I \leq K\sigma(I)$ ]	2.0
F (low)	14.0
F (high)	56.0
Goodness of Fit	2.0
R	0.044

\*

Required by symmetry of space group.

Table 3  
Crystal Data for  $[\text{Pb}(\text{PHENSC})(\text{NO}_3)_2]$

Formula	$\text{C}_{16}\text{H}_{14}\text{O}_8\text{N}_{10}\text{Pb}$
Molecular Weight	681.54
Space Group	C2/c
a, Å	14.831(4)
b, Å	16.722(4)
c, Å	8.399(2)
$\alpha$ , deg	90*
$\beta$ , deg	95.27(2)
$\gamma$ , deg	90*
Volume, Å <sup>3</sup>	2074(1)
z	4
$D_m$ , g cm <sup>-3</sup>	2.175
$D_c$ , g cm <sup>-3</sup>	2.198
Crystal Size, mm	0.12 x 0.07 x 0.07
$\mu$ , cm <sup>-1</sup>	82.6
Radiation Used	Mo K $\alpha$ - graphite monochromator
2 $\theta$ Range	0 - 45°
No. of Measured Reflections	1598
No. of Reliable Reflections	1241
K [in $I \leq K\sigma(I)$ ]	2.0
Goodness of Fit	0.23
R	0.039

\* Required by symmetry of space group.

Table 4

Crystal Data for  $[(\text{Th}[\text{PHENSC}])_2\text{O}(\text{NO}_3)_2(\text{H}_2\text{O})_2](\text{NO}_3)_4 \cdot \text{H}_2\text{O}$ 

Formula	$\text{C}_{32}\text{H}_{34}\text{O}_{26}\text{N}_{22}\text{Th}_2$
Molecular Weight	1606.83
Space Group	$\text{P2}_1/\text{c}$
a, Å	14.423(3)
b, Å	25.833(10)
c, Å	13.140(3)
$\alpha$ , deg	90*
$\beta$ , deg	93.52(2)
$\gamma$ , deg	90*
Volume, Å <sup>3</sup>	4887(2)
Z	4
$D_m$ , g cm <sup>-3</sup>	2.190
$D_c$ , g cm <sup>-3</sup>	2.146
Crystal Size, mm	0.20 x 0.16 x 0.06
$\mu$ , cm <sup>-1</sup>	64.0
Radiation Used	Mo K $\alpha$ - Graphite Monochromator
2 $\theta$ Range	0 - 45°
No. of Measured Reflections	5151
No. of Reliable Reflections	3489
K [in $I \leq K\sigma(I)$ ]	2.0
Goodness of Fit	1.9
R	0.086

\* Required by symmetry of space group.

CHAPTER III  
PREPARATION AND CRYSTAL STRUCTURE OF  
HEXAUREAMANGANESE(III)PERCHLORATE

Manganese(III) complexes have not been well characterized compared to many of the other tripositive, first-row transition elements. The factors responsible for the lack of data on manganese(III) complexes include its strength as an oxidizing agent, the tendency for photolytic instability<sup>90</sup> in many cases, and the propensity for the commercially available fluoride and acetate to form mixed-ligand complexes. However, a carefully-documented and reasoned interpretation of the visible spectral data for a number of manganese(III) complexes has been presented.<sup>37</sup> The authors noted that the presence of two prominent bands lying between 5 kK and 25 kK--and sometimes a third which may lie within the envelope of the higher energy absorption, sometimes appearing as a shoulder upon it--are most easily rationalized as arising from the transitions  ${}^5B_{1g} \rightarrow {}^5A_{1g}$  and the  ${}^5B_{1g} \rightarrow {}^5B_{2g}$ , respectively; the shoulder they assigned to the  ${}^5B_{1g} \rightarrow {}^5E_g$  transition. These term levels arise from a splitting of the octahedral terms by a Jahn-Teller distortion. The splitting of the ground octahedral term ( ${}^5E_g$ ) is greater than that of the excited term ( ${}^5T_{2g}$ ).<sup>37</sup>

On the basis of solution, diffuse reflectance, and mull spectra data, the hexaureamanganese(III) complex seems to be typically distorted.<sup>48</sup> However, the structures of the anhydrous hexakisurea



complexes of titanium(III),<sup>91-93</sup> vanadium(III),<sup>94</sup> and aluminum(III)<sup>95</sup> have been reported to be essentially identical ( $R\bar{3}c$ ). This structure requiring a symmetrical molecule, i.e., equivalence of M-O distances, would be compatible with a Jahn-Teller distorted complex. These considerations and the absence of reported structure data for the hexaureamanganese(III) complex have prompted the preparation and study of this interesting ion.

#### A. Experimental Section

##### Preparation of Hexaureamanganese(III)Perchlorate

Powdered manganese (10.0 g, 0.182 mol) was added to 400 ml of refluxing glacial acetic acid. The manganese slowly dissolved in the stirred solution over about 4 h. To the hot, stirred suspension of manganese(II) acetate was added  $KMnO_4$  (6.5 g, 0.041 mol). After 25 min, perchloric acid (250 ml of 60% acid) saturated with urea was added to the warm, dark red solution. A dark purple microcrystalline solid formed immediately and was separated by filtration, washed with 50% (V/V) absolute ethanol-dry ether, and placed in a dessicator over  $CaCl_2$ . The yield was 80% based upon the  $KMnO_4$  used. Anal. Calcd. for  $MnC_6N_{12}H_{24}Cl_3O_{18}$ : C, 10.10; H, 3.39; N, 23.55. Found: C, 9.67; H, 3.66; N, 22.66.

Single crystals were grown from a hot solution of 60% perchloric acid nearly saturated with urea at room temperature. The complex is insoluble in this solution at room temperature, but a small quantity dissolves at 75-80°C. Slow cooling of the solution in a dewar over a period of 24 h gave suitable single crystals. The crystalline complex

decomposes in a few days in room air or in the X-ray beam. This decomposition is presumably caused by water vapor since the complex decomposes quickly in water.

### Magnetic Measurements

The Gouy method was used to measure the magnetic susceptibility of the complex. The magnetic susceptibility is 5.02 B.M. corresponding to a high-spin  $d^4$  ion (spin only value 4.90 B.M.). The  $\text{Hg}[\text{Co}(\text{NCS})_4]$  complex was used as a standard.

### Data Collection and Reduction

Preliminary photographs indicated that the space group was either  $R\bar{3}c$  or  $R3c$ . The complex appeared to be isomorphous with the corresponding  $\text{Ti}(\text{III})$  derivative.<sup>92</sup> The unit cell dimensions reported in Table 1 and the intensity data were measured using a Syntex  $\text{P}\bar{1}$  diffractometer. The pertinent crystal data, together with some details of the intensity measurements, are given in Table 1. The  $\theta$ - $2\theta$  scan technique with a scan rate of  $12^\circ/\text{min}$  was used in measuring the intensity. The rather fast scan was used because crystal decomposition had occurred on a previous crystal. Four standard reflections were measured after every 96 reflections and were used to correct for a 6% decrease in their intensities during the course of the data collection. Absorption corrections were not made because of the small value of  $\mu$  and the size of the crystal.

### Structure Determination and Refinement

The final positional parameters from the isomorphous titanium complex were used as starting values for an isotropic refinement. After three cycles the R value ( $R = \Sigma ||F_{\text{obs}}| - |F_{\text{calc}}|| / \Sigma |F_{\text{obs}}|$ ) was 0.098.

Anisotropic thermal refinement gave an R of 0.068 after three cycles. A difference Fourier synthesis gave reasonable positions for the four hydrogen atoms. The contribution of the hydrogen atoms was included in subsequent least-squares cycles, but the positional and thermal parameters were not varied. After three cycles, the final R was 0.055 and the shifts were much less than the estimated standard deviations so that the refinement was terminated. The weighting scheme was  $\omega = 1.5/\sigma(F)^2$  where  $\sigma(F)^2 = [\sigma(I) + 0.04 \sigma(I)][LP \text{ corrections}]$ . The LP correction was calculated assuming a 50% perfect and 50% mosaic graphite monochromator. The scattering factors were taken from the usual sources.<sup>88</sup> The final positional parameters and thermal parameters for the nonhydrogen atoms are given in Tables 5 and 6; the bond distances and angles are given in Tables 7 and 8; and the hydrogen atom parameters and distances are given in Table 9.

## B. Results and Discussion

Hexaureamanganese(III)perchlorate is isomorphous with the corresponding titanium(III)<sup>92</sup> and aluminum(III)<sup>95</sup> salts. The crystal consists of the  $Mn(urea)_6^{3+}$  cation (site symmetry  $\bar{3}$ ) illustrated in Figures 9 and 10 and the  $ClO_4^-$  anions (site symmetry 2) shown in Figure 11 and joined by weak hydrogen bonds (see Table 10). The large deviations of the N-H...O angles from 180° and the long H...O and N...O distances are characteristic of weak hydrogen bonds.

The most remarkable feature of the structure is the  $\bar{3}$  symmetry of the cation which requires all six Mn-O bonds to be equivalent, an apparent violation of the Jahn-Teller theorem. To our knowledge, there is no other reported structural data on a high-spin Mn(III) complex

with six identical monodentate ligands, although a number of trisbi-dentate complexes are known. The Mn-O distance of 1.986(7) Å found in the hexaurea complexes is comparable to the average Mn-O distances observed in tris(2,4-pentanedionato)manganese(III) [1.981(32) Å<sup>41</sup> in the  $\beta$  form and 1.993(91) Å in the  $\gamma$  form],<sup>42</sup> and in tris(tropolonato)manganese(III) of 2.004(97) and 1.995(49) Å.<sup>43</sup> However, there is some question as to the validity of averaging Mn-O distances in distorted molecules where the range can be from 1.931 to 2.020 Å.<sup>41</sup> Certainly the Mn-O distance observed in this study is not unreasonable relative to other Mn-O bond lengths. The important question is why are the Mn-O bonds equivalent in an apparent violation of the Jahn-Teller theorem?

Before we discuss the Mn-O bond length in more detail, let us focus on the urea molecule to see if there are any unusual features in the ligand. There are a large number of urea-metal ion complexes reported, but we will consider only the isomorphous Ti(III) and Al(III) complexes, the  $\text{Ti(urea)}_6^{3+} \cdot 3\text{I}^-$ <sup>91</sup> and the  $\text{Cr(urea)}_6^{3+} \cdot 3\text{Cl}^- \cdot 3\text{H}_2\text{O}$  structures<sup>96</sup> which all crystallize in a hexagonal space group. In these four structures, the average distances in the coordinated urea molecule are C-O of 1.283(16) Å, C-N of 1.325(27) Å and 1.316(18) Å. The free urea molecule in the solid state<sup>97</sup> has dimensions of C-O 1.270(7) and C-N 1.326(6) Å, which are not significantly different from those in the coordinated molecule. The dimensions in our manganese complex are C-O 1.283(15), C-N 1.320(16), and C-N 1.305(14) Å (see Figure 12), which are indistinguishable from the average values in the four complexes or in the free urea. Therefore, we conclude that the urea molecule has no unusual features which could account for the six equivalent Mn-O bonds.

The most reasonable explanation for the equivalence of the Mn-O bond lengths is in terms of the "dynamic" Jahn-Teller effect. The differences in the mean-square-displacements given in Table 11 for the three isomorphous  $M(\text{urea})_6^{3+}$  complexes are in agreement with the "dynamic" Jahn-Teller effect. The mean-square-displacements for the metal ions are very similar in magnitude and orientation relative to the M-O bond. If there were major errors in the intensity data, we might have expected greater discrepancies in the thermal parameters and the mean-square-displacements. In contrast, only the mean-square-displacements for the oxygen atom in the Mn complex are much larger in the direction of the bond. These differences in the mean-square-displacements are in agreement with the predictions for a dynamic Jahn-Teller distorted molecule.

An extensive analysis of the dynamic Jahn-Teller in Cu(II) complexes has been reported,<sup>11</sup> and we will use the same notation. Since there are no examples of a statically distorted hexaureamanganese(III) cation, we can only compare our results with various tris-ligand-manganese(III) complexes. The average Mn-O bond distances in the five tris-ligand molecules are essentially identical (vide supra), in spite of a large spread in the individual values. However, the Jahn-Teller radii,  $R_{JT}$ , calculated from the observed Mn-O distances vary markedly. The values of  $R_{JT}$  are 0.203 Å for the  $\gamma$ -tris-acac, 0.072 Å for the  $\beta$ -tris-acac, 0.171 Å in the tris-oxalato, and 0.217 and 0.110 Å for the two crystallographically independent tris-tropolonato complexes.<sup>98</sup> In comparison, the values of  $R_{JT}$  for twelve different Cu(II) complexes range from 0.252 to 0.355 Å.<sup>11</sup>

The value of  $R_{JT}$  for the hexaureamanganese(III) cation can be estimated from the difference in the mean-square-displacement between the Mn(III) and Ti(III) and Al(III) complexes. A value of  $0.306 \text{ \AA}$  was calculated from  $\Delta U(\text{Mn-O}) - \Delta U(\text{Ti-O})$ . In the Al(III) complex,  $U(\text{O}) - U(\text{Al})$  was negative which was somewhat surprising. However, using the absolute value of  $U(\text{O}) - U(\text{Al})$ ,  $R_{JT}$  for Mn(III) is  $0.355 \text{ \AA}$ . These two values are in reasonable agreement with each other and with the Cu(II) values but not with the values calculated from the observed bond distances in the tris-complexes. Whether the large variation in  $R_{JT}$  for Mn(III) complexes versus Cu(II) complexes is a consequence of a  $d^4$  system compared to a  $d^9$  case or reflects the more reactive nature of tris-Mn(III) complexes compared to Cu(II) can only be decided as additional data become available.

Additional support for a dynamic Jahn-Teller distortion is also found in the electronic spectral properties of the hexaurea complex. The room-temperature visible absorption spectra of this complex (both the mull and the diffuse reflectance spectra) contain two very broad absorption envelopes centered at 8.70 kK and 19.10 kK, respectively. But in the mull spectrum taken near liquid nitrogen temperature, the 19.10 kK absorption was resolved into two broad, overlapping bands, one maximum lying at 16.70 kK and the other at 20.00 kK.<sup>48</sup> The lowest energy absorption was assigned as  ${}^5B_{1g} \rightarrow {}^5A_{1g}$  (the components of the split octahedral  ${}^5E_g$  ground term), the 16.70 kK absorption as  ${}^5B_{1g} \rightarrow {}^5E_g$ . These assignments, in accord with those made by Davis et al.,<sup>37</sup> assume a tetragonally elongated manganese(III) complex

during the time of the electronic transition (see Figure 13). The ordering of term energies implicit in these assignments leads to a Dq value of 1.67 kK, a Ds value of 1.71 kK, and a Dt value of 0.372 kK.<sup>10</sup> These parameters are of similar value to those obtained for manganese(III) complexes shown to be statically distorted.<sup>37</sup> Furthermore, no other assignment of absorptions or ordering of terms proposed to account for the spectral properties of manganese(III) complexes leads to such close agreement of the Dq values reported for the isomorphous hexaurea complexes of Ti(III),<sup>99</sup> V(III),<sup>100</sup> and Cr(III)<sup>101</sup> (1.67-1.70 kK). Taking the stabilization of the tetragonal structure over that of the reference, undistorted octahedral structure to be  $\underline{D_t} - 2\underline{D_s}$ , the apparent Jahn-Teller stabilization ( $E_{JT}$ ) is -3.05 kK, similar to those values reported for both manganese(III)<sup>37</sup> and for copper(II)<sup>11</sup> complexes.

An alternative means of estimating the stabilization energy of the distorted complex has been suggested provided  $E_{JT} \gg h\nu > kT$  (where  $\nu$  is the frequency of the Mn-O vibrational mode of  $e_g$  symmetry),<sup>11</sup> namely,  $4E_{JT} \approx E(^5B_{1g} \rightarrow ^5A_{1g})$  or  $E_{JT} \approx 2.20$  kK. This estimated stabilization energy is similar to that calculated by the application of simple perturbation treatment; but the extension of the treatment leads to unacceptable values of the crystal field splitting parameter.

We conclude that  $[Mn(urea)_6](ClO_4)_3$  is the first example of a dynamic Jahn-Teller effect in a high-spin Mn(III) complex. The  $Mn(urea)_6^{3+}$  cation is required by the space group symmetry to have six equivalent Mn-O bonds. However, the mean-square-displacement of

the oxygen atom is much larger in the direction of the Mn-O bond compared to the isomorphous Ti(III) and Al(III) hexaurea complexes, and the visible absorption spectrum can be interpreted in terms of a tetragonally distorted cation. The above three observations are typical of dynamically distorted Cu(II) complexes and by extrapolation, high-spin Mn(III) complexes.



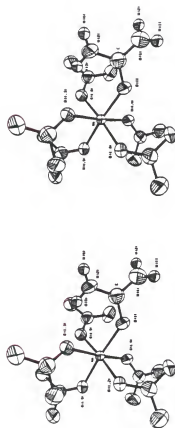
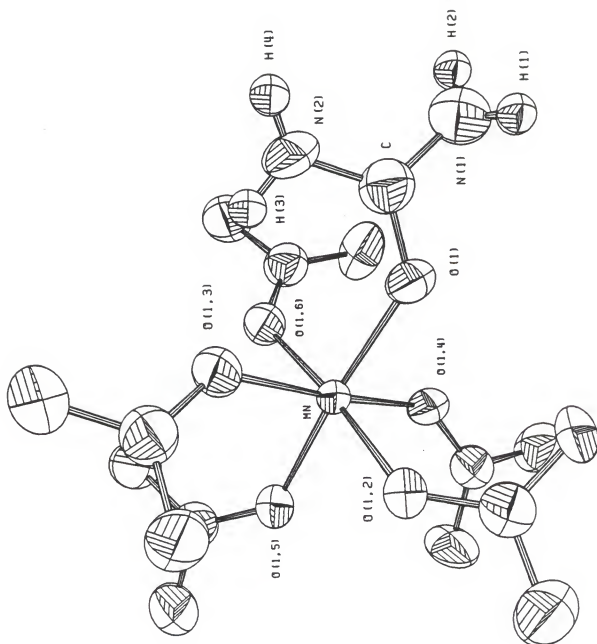


Figure 9. Stereoscopic view of the  $[\text{Mn}(\text{urea})_6](\text{ClO}_4)_3 \cdot$ .

Figure 10. An ORTEP view of  $[\text{Mn}(\text{urea})_6](\text{ClO}_4)_3$  showing the atomic numbering and the thermal ellipsoids (50% probability level). Hydrogen atoms are shown for only one urea. The other hydrogen atoms are omitted for clarity.



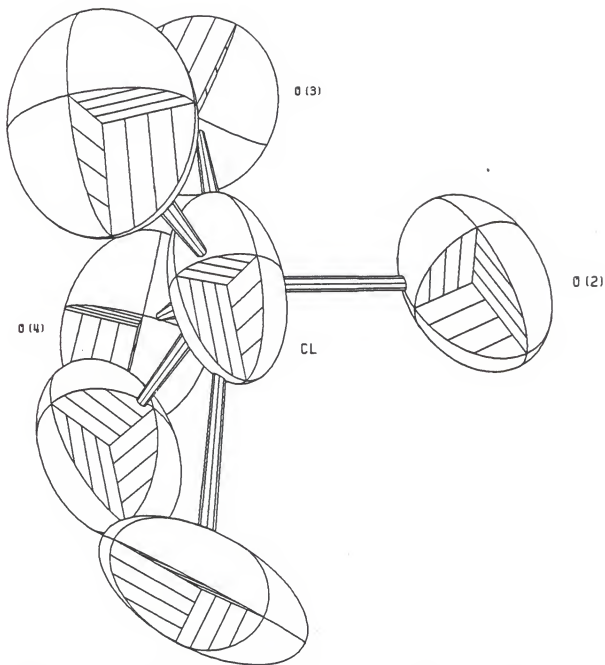
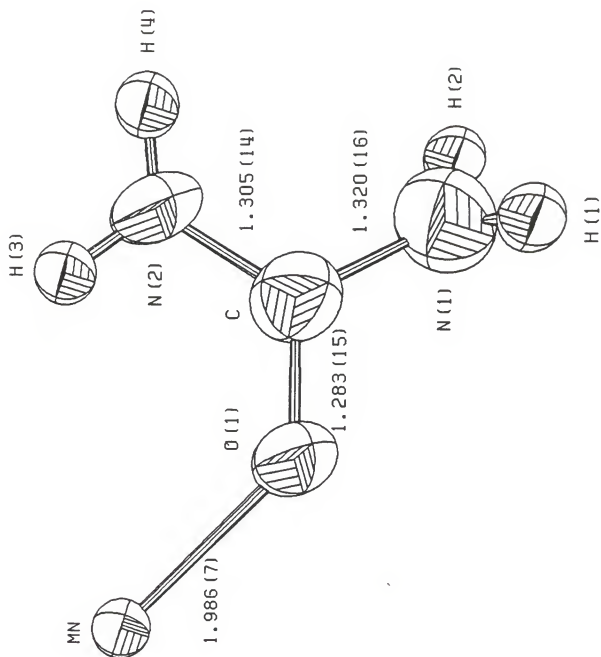


Figure 11. An ORTEP view of perchlorate ion in  $[\text{Mn}(\text{urea})_6](\text{ClO}_4)_3$  showing the atomic numbering and the thermal ellipsoids (50% probability level). Oxygen O(3) and O(4) are disordered and are only half-atoms.

Figure 12. An ORTEP view of the coordinated urea molecule in  $[\text{Mn}(\text{urea})_6](\text{ClO}_4)_3$  showing the atomic number and thermal ellipsoids (50% probability level), and bond distances (Å) with estimated standard deviations in parenthesis.



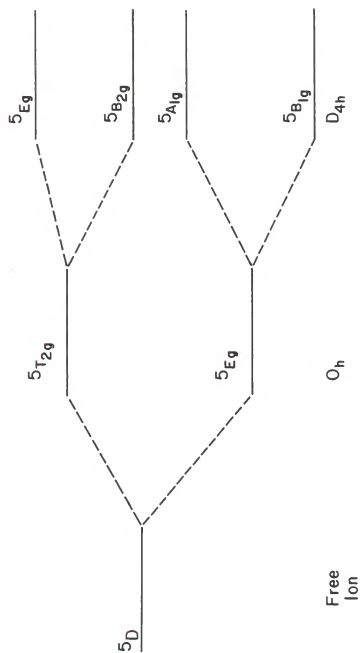


Figure 13. Term level diagram for a  $d^4$  ion in three fields.

Table 5

Final Positional Parameters ( $\times 10^4$ ) for  $\text{Mn}[\text{OC}(\text{NH}_2)_2]_6(\text{C}_6\text{H}_5)_3$ 

	x	y	z
Mn	0*	0*	2500*
Cl	3685(2)	0*	2500*
O(1)	1040(4)	569(4)	1698(5)
O(2)	3568(6)	585(5)	3004(7)
O(3)	4163(11)	612(10)	1567(14)
O(4)	4466(14)	216(25)	2276(29)
N(1)	2334(5)	923(6)	1159(9)
N(2)	1325(6)	-473(6)	1287(8)
C	1549(7)	329(7)	1374(8)

\* Position required by the space group symmetry.



Table 6

Final Thermal Parameters ( $\times 10^4$ ) for  $\text{Mn}[\text{OC}(\text{NH}_2)_2]_6(\text{ClO}_4)_3$

The Form of the Thermal Parameter is  
 $\exp[-2\pi^2(U_{11}h^2a^{*2} + U_{22}k^2b^{*2} + U_{33}l^2c^{*2} + 2U_{12}hka^{*b*} + 2U_{13}hla^{*c*} + 2U_{23}klb^{*c*})]$

	$U_{11}$	$U_{22}$	$U_{33}$	$U_{12}$	$U_{13}$	$U_{23}$
Mn	19(1)	19 <sup>†</sup>	42(2)	19 <sup>†</sup>	0*	0*
Cl	37(2)	52(2)	127(4)	52	-35	-71(5)
O(1)	33(3)	33(3)	84(5)	39(6)	7(6)	-14(7)
O(2)	75(5)	57(4)	116(8)	82(8)	-22(11)	-24(9)
O(3)	64(8)	65(8)	104(14)	12(14)	79(19)	58(18)
O(4)	47(10)	94(34)	147(45)	40(26)	15(25)	-55(47)
N(1)	42(4)	57(5)	105(8)	54(8)	26(10)	22(10)
N(2)	47(5)	40(4)	125(9)	41(8)	44(11)	-52(10)
C	40(6)	41(6)	61(7)	40(10)	-5(11)	-13(11)

<sup>†</sup> Value equal to  $U_{11}$  by symmetry.

\* Required to be zero by symmetry.

Table 7

Bond Distances (in Å) for  $\text{Mn}[\text{OC}(\text{NH}_2)_2]_6(\text{ClO}_4)_3$  with  
Estimated Standard Deviations

---

<u>In the Cation</u>	
Mn-O(1)	1.986(7)
O(1)-C	1.283(15)
C-N(1)	1.320(16)
C-N(2)	1.305(14)
<u>In the Perchlorate Ion</u>	
Cl-O(2)	1.38(1)
Cl-O(3)	1.66(2)
Cl-O(4)	1.30(3)

---

Table 8

Bond Angles (in deg) in  $\text{Mn}[\text{OC}(\text{NH}_2)_2]_6(\text{ClO}_4)_3$ 


---

<u>In the Cation</u>	
O(1)-Mn-O(1,2)	91.0(3)
O(1)-Mn-O(1,4)	85.5(3)
O(1)-Mn-O(1,5)	174.9(3)
O(1)-Mn-O(1,6)	92.8(3)
Mn-O(1)-C	133.0(7)
O(1)-C-N(1)	118.0(11)
O(1)-C-N(2)	122.3(11)
N(1)-C-N(2)	119.7(11)
H(1)-N(1)-C	111
H(2)-N(1)-C	126
H(1)-N(1)-H(2)	117
H(3)-N(2)-C	112
H(4)-N(2)-C	126
H(3)-N(2)-H(4)	120
<u>In the Perchlorate Ion</u>	
O(2)-Cl-O(2')	114.7(6)
O(2)-Cl-O(3')	94.7(8)
O(2)-Cl-O(4)	117.1(17)
O(2')-Cl-O(3')	96.9(8)
O(2')-Cl-O(4)	123.6(17)
O(3')-Cl-O(4)	99.6(18)

---

Table 9  
 Hydrogen Atom Position ( $\times 10^3$ ) and Isotropic Thermal Parameter  
 In  $\text{Mn}[\text{OC}(\text{NH}_2)_2\text{I}_6(\text{ClO}_4)_3]$

Atom	Bonded to	Distance ( $\text{\AA}$ )	x	y	z	B(iso)
H(1)	N(1)	0.89	233	125	69	6.0
H(2)	N(1)	0.70	270	89	121	6.0
H(3)	N(2)	0.87	81	-81	149	5.0
H(4)	N(2)	0.77	155	-65	98	5.0

Table 10

Hydrogen Bonds in  $\text{Mn}[\text{OC}(\text{NH}_2)_2]_6(\text{C}_{10}\text{H}_4)_3$ 

Bond D-H....A	Position of A	Dist, Å		Angle, deg D-H-A
		D-H	H....A	
N(1)-H(1)....O(2)	2/3 - x, 1/3 - y, 1/3 - z	0.89	2.406(8)	135.9(7)
N(1)-H(2)....O(3)	1/3 + y, 2/3 + x - 1, 1/6 - z	0.70	2.789(21)	139.9(10)
N(2)-H(3)....O(1)	y - x, -x, z	0.87	2.158(7)	149.1(7)
N(2)-H(4)....O(2)	1/3 - y, 2/3 + x - y, 2/3 + z	0.77	2.682(10)	147.4(8)

Table 11

$M[OC(NH_2)_2]_6 (ClO_4)_3$  Mean Square Displacements ( $M = Mn, Ti, Al$ )\*

	MSQ1	Angle	MSQ2	Angle	MSQ3	Angle
Mn	0.155	133.6	0.155	116.7	0.204	55.4
01	0.209	137.1	0.179	117.0	0.294	59.5
Ti	0.146	133.4	0.146	115.8	0.153	54.4
01	0.156	144.2	0.194	125.5	0.240	94.2
Al	0.148	134.1	0.148	116.0	0.224	55.4
01	0.158	155.4	0.188	104.8	0.246	70.9

\* MSQ<sub>n</sub> is the nth mean square displacement ( $\text{\AA}^2$ ) for the appropriate atom. Angle (degree) is the angle that the MSQ<sub>n</sub> makes with the M-O bond.

## CHAPTER IV

### ELECTRON PARAMAGNETIC RESONANCE AND DIFFERENTIAL SCANNING CALORIMETRY OF THE HEXAUREAMANGANESE(III)PERCHLORATE

Thermal analysis can be defined as techniques in which a few physical parameters of the system are determined as a function of temperature. Thermal methods of analysis are based on the fact that thermal energy is absorbed or evolved during a physical or chemical change of a sample.<sup>102,103</sup> Differential Scanning Calorimetry (DSC) is the only technique which measures these changes directly in energy units. DSC was first used by Watson et al. to explain the instrumental technique developed by the Perkin-Elmer Corporation in 1963.<sup>104</sup> The theory of the Perkin-Elmer Calorimeter has been presented by O'Neill,<sup>105</sup> Gray,<sup>106</sup> and Flynn.<sup>107</sup> Figure 14 shows a typical DSC curve.<sup>103</sup> An increase in enthalpy (or endothermic transformation) is represented by a peak in upward direction; an exothermic transformation is represented by a peak in the opposite direction.<sup>103</sup>

The basic differences between differential thermal analysis (DTA) and DSC lie in the design of the heating system and the mode of operation of the instrument.<sup>108</sup>

The DSC technique can determine, directly, the total heat transferred to/from the sample and the rate of a reaction, as a function of time or of temperature. DSC can be used for the measurement of

specific heat, temperature and heat of fusion, phase transitions, dehydrations, decompositions; identification and analysis of solid state reactions and transformations; stability, decomposition thermodynamics and kinetics of metal complexes; temperature and heat of crystallization. Heats of transition and specific heats can be determined with a precision of about  $\pm 2\%$ .<sup>108</sup>

The area of the DSC curve peak is directly proportional to the enthalpy change,  $\text{area} = K\Delta Hm$ , where  $\Delta H$  is the heat of transition (or reaction),  $K$  is the calibration coefficient, and  $m$  is the mass of reactive sample.<sup>103</sup>

Electron Paramagnetic Resonance (EPR), Electron Spin Resonance (ESR), or Electron Magnetic Resonance is a powerful tool that can give a wealth of information about the electronic, magnetic, and the structure or environment of a paramagnetic species. EPR is a branch of absorption spectroscopy. When a paramagnetic specimen is placed in a permanent magnetic field and subjected to radiation of microwave frequency, microwave power is absorbed by the specimen at a particular frequency. As a general rule, to minimize interference between neighboring paramagnetic units, dilute solutions, solid or liquid, are studied. It is also better to work at low temperature, where line-broadening effects are reduced.<sup>109-114</sup>

#### A. Experimental Section

##### Preparation of Hexaureaaluminum Perchlorate

Hydrated aluminum chloride,  $\text{AlCl}_3 \cdot 6\text{H}_2\text{O}$ , (8.0 g, 0.033 mol) was dissolved in the minimum amount of water (total solution volume, 20 ml).



To this solution, perchloric acid (140 ml of 60% acid) saturated with urea was added. A white microcrystalline solid formed immediately and was separated by filtration, washed with 50% (V/V) absolute ethanol-dry ether and placed in a dessicator over  $\text{CaCl}_2$ . The yield was 92% based upon the  $\text{AlCl}_3 \cdot 6\text{H}_2\text{O}$  used. Anal. Calcd. for  $\text{AlC}_6\text{N}_{12}\text{H}_{24}\text{Cl}_3\text{O}_{18}$ : C, 10.51; H, 3.53; N, 24.51. Found: C, 10.60; H, 3.40; N, 24.60.

Single crystals of  $[\text{Al}(\text{urea})_6](\text{ClO}_4)_3$  doped with manganese(III) were grown from a hot solution of 60% perchloric acid nearly saturated with urea at room temperature. The urea complexes are nearly insoluble in this solution at room temperature; however, a significant amount dissolves at 75-80°C. Slow cooling of the solution in a dewar over a period of 24 hours gave single crystals. Some difficulties were experienced in growing large single crystals ( $\approx 2 \times 2 \times 1$  mm). However, suitable crystals were obtained by selective and repetitive seeding. A weighed amount of the sample was placed in the DSC-2C (Perkin-Elmer) and equilibrated at -70°C for several hours -- in one case, overnight.

EPR spectra were obtained both at room temperature and at liquid nitrogen temperature on microcrystalline of  $[\text{Mn}(\text{urea})_6](\text{ClO}_4)_3$  and manganese(III)-doped  $[\text{Al}(\text{urea})_6](\text{ClO}_4)_3$ , on glasses of  $[\text{Mn}(\text{urea})_6](\text{ClO}_4)_3$  in  $\text{C}_2\text{H}_5\text{OH}$  (absolute) and in perchloric acid (60%) saturated with urea. All EPR spectra were recorded by means of a Varian E-3 spectrometer at a microwave power of 8.0 mW, a microwave frequency of  $9.10 \pm 0.01$  GHz, and a modulation amplitude of 1 to 5 G.

## B. Results and Discussion

Microcrystalline  $[\text{Mn}(\text{urea})_6](\text{ClO}_4)_3$  was studied by differential scanning calorimetry in an attempt to identify a temperature at which the complex would cease to pseudorotate and, instead, assume a static Jahn-Teller-distorted geometry. The DSC curve taken from  $-60^\circ\text{C}$  to  $20^\circ\text{C}$  is simply a straight line, i.e., no transition occurs within this temperature range. However, the curve from  $-10^\circ\text{C}$  to  $50^\circ\text{C}$  (Figure 15) shows an endothermic transition occurring between  $16.86^\circ\text{C}$  to  $43.77^\circ\text{C}$ . The area of the peak corresponds to  $1.31 \text{ kJ/mole}$ . It is likely that the observed endothermic transition corresponds to the second-order phase transition observed for  $[\text{Cr}(\text{urea})_6](\text{ClO}_4)_3$  near room temperature.<sup>115</sup>

An octahedral perturbation of the free ion  $^5\text{D}$  term gives a  $^5\text{E}$  ground term. This term should be further split by a Jahn-Teller effect manifested as an axial elongation to give a  $^5\text{B}_{1g}$  ground term.<sup>116</sup> From the  $^5\text{B}_{1g}$ , via zero-field splitting, there are obtained the  $\text{M}_S = 0$  ground term with the excited  $\text{M}_S = \pm 1$  and  $\pm 2$  term lying above it by an energy  $\text{D}$  and  $3\text{D}$ , respectively. There are then four  $\Delta\text{M}_S = \pm 1$  EPR transitions allowed between these levels if  $\text{D}$  is not large. If  $\text{D}$  is very small or zero, the four transitions will be degenerate; or if  $\text{D}$  is rather large, there may be only one transition. If  $\text{D}$  is large, no transitions may be seen by an X-band spectrometer. Because the only isotope of manganese is  $^{55}\text{Mn}$  having a nuclear spin of  $5/2$ , each of the spectral lines seen should be split into six  $(2\text{I}+1)$  components.<sup>109-114</sup>

The EPR spectra of the pure microcrystalline solid  $[\text{Mn}(\text{urea})_6](\text{ClO}_4)_3$  at room temperature and at  $50^\circ\text{C}$  contain a strong and very

broad resonance with  $g = 2.00$ , a value which is expected for a pseudo-rotated  $d^4$  ion complex. The resonance has the expected hyperfine splitting for  $I = 5/2$  with  $A \approx 91G$ . That  $A$  increases with increasing field ( $H$ ) is characteristic of a second-order perturbation effect.<sup>110</sup> A much weaker resonance lying downfield from the principal one has superimposed hyperfine splitting which is one-half that of the  $g \approx 2$  resonance. These are considered to be forbidden transition arising from spin-spin interaction. The forbidden resonances are more pronounced at the higher temperature (Figure 16). At liquid nitrogen temperature, the resonances at low field disappear. Previous work on  $Mn^{3+}$  in  $Al_2O_3$  indicated that the hyperfine structure for  $Mn^{3+}$  could only be resolved below about 2.5K.<sup>117</sup>

To minimize interference between neighboring paramagnetic units, dilute solution and solids were also studied. The EPR spectra of  $Mn^{3+}$ -doped  $[Al(urea)_6](ClO_4)_3$  at room temperature and liquid nitrogen temperature are given in Figures 17 and 18, respectively. The room temperature spectrum contains only one sharp peak at  $g = 1.98$ , but at liquid nitrogen temperature this peak splits into at least two resonances which we assign as  $g_{||} = 1.99$  and  $g_{\perp} = 1.95$ . No hyperfine structure is observed for  $Mn^{3+}$ -doped  $[Al(urea)_6](ClO_4)_3$  either at room temperature or liquid nitrogen temperature. These spectra were obtained not only with a 1000-gauss sweep, but with a 5000-gauss sweep as well to ensure that no resonance had been missed. The several weak resonances lying downfield from the  $g \approx 2$  resonance were shown to be impurities by dilution of the  $Mn^{3+}$ -doped samples. Indeed, these resonances attributed to sample impurities are observed for the Mn-free  $[Al(urea)_6](ClO_4)_3$ .

In an attempt to support the assignment of the resonances observed at  $g_{\parallel} = 1.99$  and at  $g_{\perp} = 1.95$  to  $\text{Mn}^{3+}$  rather than to attribute it to small amounts of  $\text{Mn}^{2+}$  impurity from some decomposition of the  $\text{Mn}^{3+}$ , the EPR spectrum of  $[\text{Al}(\text{urea})_6](\text{ClO}_4)_3$  doped with  $\text{Mn}(\text{ClO}_4)_2 \cdot 6\text{H}_2\text{O}$  was run at liquid nitrogen temperature. In the region of interest, the two spectra (one containing only  $\text{Mn}^{2+}$  and the other thought to contain only  $\text{Mn}^{3+}$ ) were indistinguishable. There is no doubt that the sample doped with the  $\text{Mn}^{3+}$  compound contains predominantly  $\text{Mn}^{3+}$ . The sample has a pronounced pink color even when the  $\text{Mn}^{3+}$  to  $\text{Al}^{3+}$  ratio is 15:1000. A sample of pure  $\text{Mn}(\text{ClO}_4)_2$  is scarcely colored because of the spin-forbiddenness of the optical transitions. Also, the  $\text{Mn}^{3+}$ -containing samples give the familiar evidence of disproportionation to  $\text{Mn}^{2+}$  and  $\text{MnO}_2$  when placed in water. Should the EPR spectra be those of  $\text{Mn}^{2+}$ , the  $\text{Mn}^{2+}$  impurity must be present in trace amount.

The EPR spectrum of  $[\text{Mn}(\text{urea})_6](\text{ClO}_4)_3$  in absolute ethanol glass at liquid nitrogen temperature is identical with that obtained in urea-saturated  $\text{HClO}_4$  (60%) (in which it is improbable that reduction of  $\text{Mn}^{3+}$  will take place). These spectra contain six prominent lines with forbidden transition lying midway between them (Figure 19) ( $g = 2.00$  and  $A \approx 92$ ), essentially identical to that reported for  $\text{Mn}^{2+}$ . Again, either the resonance is attributable to  $\text{Mn}^{2+}$  impurity with absolutely no  $\text{Mn}^{3+}$  resonance or it is of  $\text{Mn}^{3+}$  which happens to be the same as that for the  $\text{Mn}^{2+}$  because of the isotropic nature of the  $\text{Mn}^{3+}$  caused by pseudorotation, a most disconcerting situation, indeed. It is surprising that pseudorotation should be operative at liquid nitrogen temperatures in the light of other published data for Jahn-Teller prone systems investigated at these temperatures.

Should the EPR spectra obtained be entirely from the  $\text{Mn}^{2+}$  impurity, one could suggest two possible explanations for the absence of  $\text{Mn}^{3+}$  resonance(s). Either there is distortion leading to such a large zero-field splitting that no resonance is seen, or the spin-lattice relaxation  $T_1$  is unsuitable for the obtaining of EPR spectra. These questions must remain to be answered by a more exhaustive investigation.

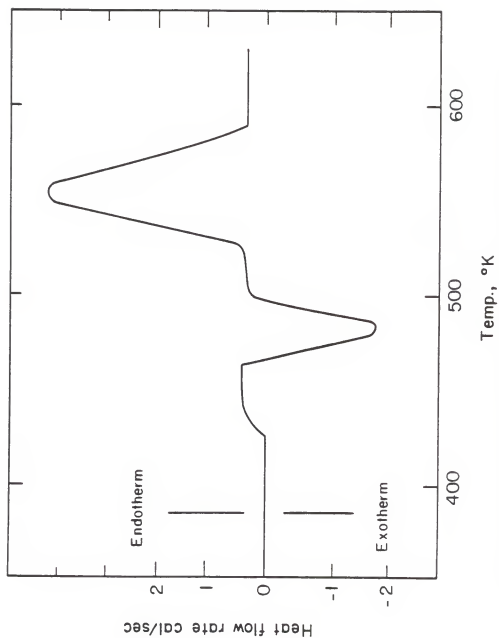


Figure 14. A typical Differential Scanning Calorimetry curve.

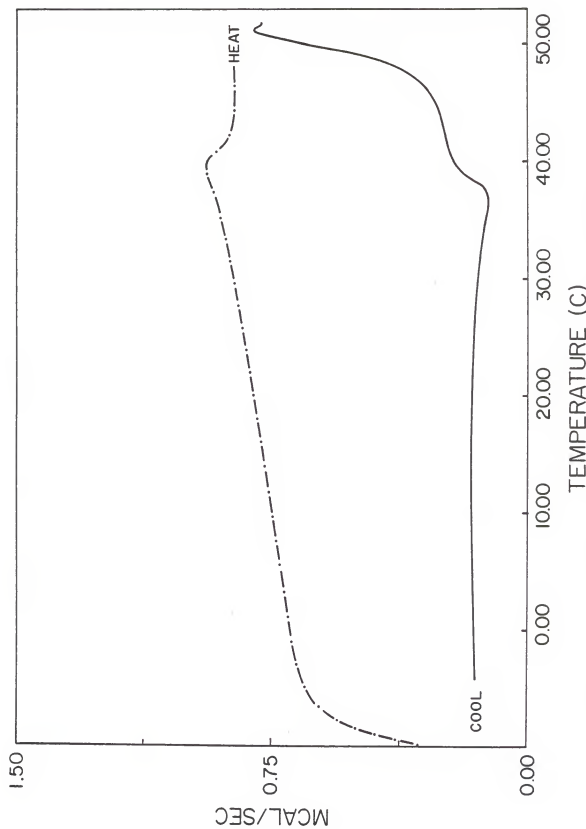
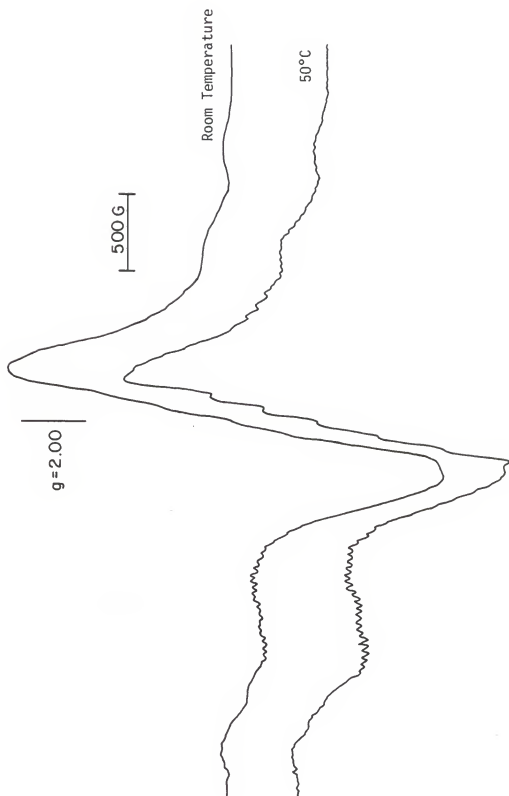


Figure 15. Differential scanning calorimetry of  $[\text{Mn}(\text{urea})_6](\text{ClO}_4)_3$ .

Figure 16. EPR spectra of microcrystalline  $[\text{Mn}(\text{urea})_6](\text{ClO}_4)_3 \cdot$





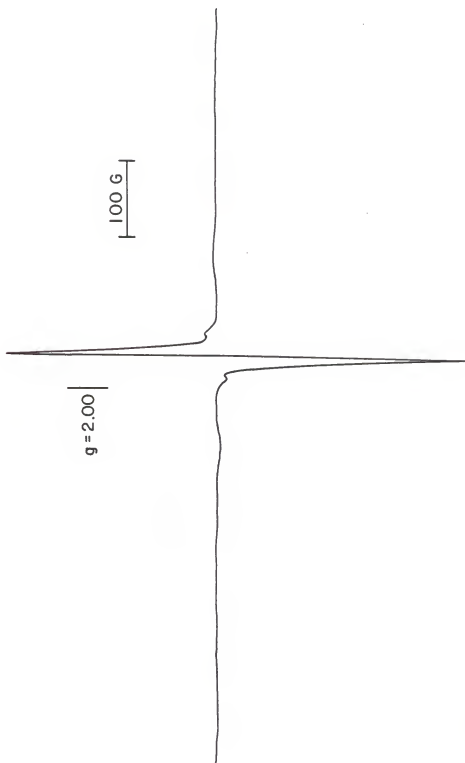
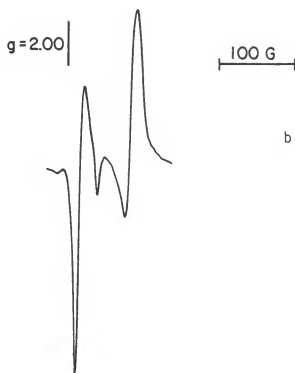
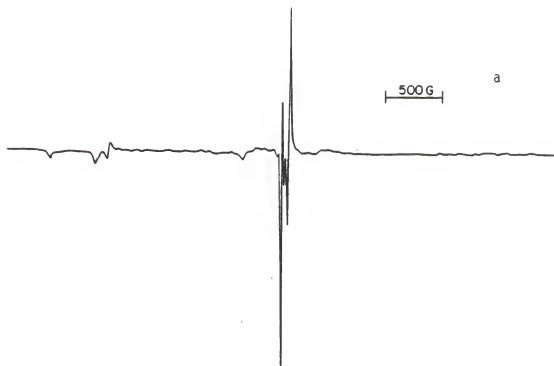


Figure 17. EPR spectrum of microcrystalline manganese(III)-doped  $[\text{Al}(\text{urea})_6(\text{ClO}_4)_3]$  at room temperature.

Figure 18. EPR spectra of manganese(III)-doped  $[\text{Al}(\text{urea})_6](\text{ClO}_4)_3$  at liquid nitrogen temperature (a)  $\pm 2500$  and (b)  $\pm 500$  scan range.



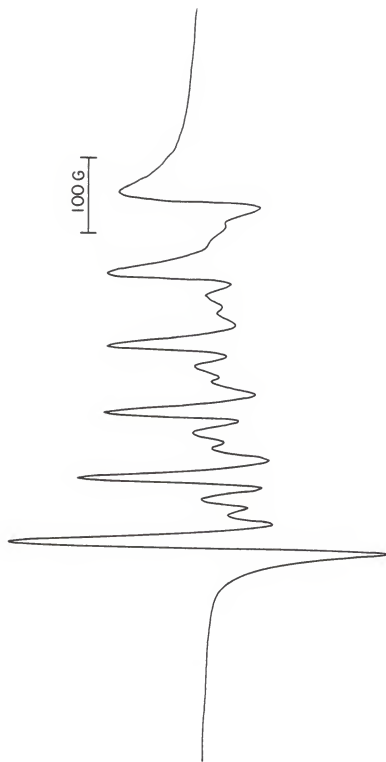


Figure 19. EPR spectrum of  $[\text{Mn}(\text{urea})_6](\text{ClO}_4)_3$  in perchloric acid (60%) saturated with urea at liquid nitrogen temperature.

## CHAPTER V

### THE CRYSTAL STRUCTURE OF DIAQUA[2,9-DIFORMYL-1,10-PHENANTHROLINE BIS(SEMICARBAZONE)] COBALT(II) NITRATE, $[\text{Co}(\text{PHENSC})(\text{H}_2\text{O})_2](\text{NO}_3)_2$

The most extensively studied hexadentate chelating agent is probably ethylenediaminetetraacetic acid (EDTA or  $\text{H}_4\text{Y}$ ). Hoard and co-workers have determined the geometry of seven coordinate aqua complexes of the type  $[\text{M}(\text{EDTA})(\text{H}_2\text{O})]^{n-}$  with  $\text{M} = \text{Fe}(\text{III}), \text{Mg}(\text{II}), \text{Mn}(\text{II})$ .<sup>50-52</sup> They have noted that two kinds of geometries can be obtained, viz., pentagonal-bipyramid and capped trigonal prism. Trans 1,2-diaminocyclohexane- $\text{N}, \text{N}'$ -tetraacetic acid (DCTA) also functions as a hexadentate ligand in  $\text{Ca}[\text{Fe}(\text{H}_2\text{O})(\text{DCTA})]_2 \cdot 2\text{H}_2\text{O}$ . The  $[\text{Fe}(\text{H}_2\text{O})(\text{DCTA})]^-$  is a seven-coordinate aqua complex.<sup>56</sup>

The ligand 2,6-diacetylpyridine bis(semicarbazone), DAPSC, was postulated to be ideally suited to form pentagonal-bipyramidal complexes with a variety of different metal ions.<sup>118-122</sup> Indeed, the complexes  $[\text{M}(\text{DAPSC})(\text{H}_2\text{O})(\text{Cl})]\text{Cl} \cdot 2\text{H}_2\text{O}$ , where  $\text{M} = \text{Mn}(\text{II}), \text{Fe}(\text{II}), \text{Co}(\text{II}),$  and  $\text{Zn}(\text{II})$ , were found to be isomorphous, each cation assuming a pentagonal-bipyramidal shape.<sup>118</sup> In addition,  $[\text{Cu}(\text{DAPSC})(\text{H}_2\text{O})_2](\text{NO}_3)_2 \cdot \text{H}_2\text{O}$ ,<sup>119</sup>  $[\text{Ni}(\text{DAPSC})(\text{H}_2\text{O})_2](\text{NO}_3)_2 \cdot \text{H}_2\text{O}$ ,<sup>119</sup>  $[\text{Cr}(\text{DAPSC})(\text{H}_2\text{O})_2](\text{NO}_3)_2(\text{OH}) \cdot \text{H}_2\text{O}$ ,<sup>120</sup>  $[\text{Fe}(\text{DAPSC})\text{Cl}_2]\text{Cl} \cdot 2\text{H}_2\text{O}$ ,<sup>120</sup>  $[\text{Sc}(\text{DAPSC})(\text{H}_2\text{O})_2](\text{NO}_3)_2(\text{OH})$ ,<sup>121</sup> and  $[\text{Mn}(\text{DAPSC})(\text{H}_2\text{O})_2](\text{NO}_3)_2$ <sup>122</sup> are best described as pentagonal-bipyramidal complexes. A few other planar, pentadentate ligands such as 2,6-diacetylpyridine bis(2'-pyridylhydrazone ( $\text{H}_2\text{DAPP}$ );

2,6-diacetylpyridine bis(benzoic acid hydrazone) (DAPBH); and 2,6-diacetylpyridine bis(salicylic acid hydrazone) (DAPSAH) also have been prepared and found to yield the pentagonal-bipyramidal complexes  $[M(H_2DAPP)(H_2O)_2]Cl_2$ <sup>123</sup> [ $M = Co(II), Zn(II)$ ];  $[Co(DAPBH)(H_2O)(NO_3)](NO_3)$ ,<sup>124</sup>  $[Ni(DAPBH)(H_2O)_2](NO_3)_2 \cdot 2H_2O$ ,<sup>124</sup> and  $[Co(DAPSAH)(H_2O)_2](NO_3)_2 \cdot H_2O$ .<sup>125</sup>

A pentagonal-bipyramidal complex of  $Co(II)$ ,  $[Co(BIPYSC)(H_2O)_2](NO_3)_2$ ,<sup>126</sup> was synthesized using the BIPYSC, a hexadentate ligand 6,6'-diformyl-2,2'-bipyridine bis(semicarbazone) related to DAPSC and characterized by a single-crystal X-ray investigation. Another hexadentate ligand, 2,9-diformyl-1,10-phenanthroline bis(semicarbazone), PHENSC, was used to prepare  $[Co(PHENSC)(H_2O)_2](NO_3)_2$ , which was studied by X-ray diffraction.

#### A. Experimental Section

##### Preparation of $[Co(PHENSC)(H_2O)_2](NO_3)_2$

The ligand 2,9-diformyl-1,10-phenanthroline bis(semicarbazone) was prepared from 1,10-phenanthroline-2,9-dicarboxaldehyde and semicarbazide hydrochloride. Equimolar amounts of cobalt nitrate hexahydrate and 2,9-diformyl-1,10-phenanthroline bis(semicarbazone) were heated in 95% ethanol for one-half hour. Addition of a small amount of water and continued heating gave a clear solution within one hour. After filtering, orange crystals were obtained by slow evaporation of the solvent.

##### Data Collection and Reduction

Preliminary photographs indicated that the space group was  $P2_1/c$ . The unit cell dimensions are reported in Table 2, and the intensity

data were measured using a Syntex PT diffractometer. The pertinent crystal data, together with some details of the intensity measurements, are given in Table 2. The  $\theta$ - $2\theta$  scan technique with a variable scan rate of 1 to  $24^\circ/\text{min}$  was used in measuring the intensity. Four standard reflections were measured every 96 reflections to monitor the beam and crystal stability. Scale factors varying from 0.988 to 1.024 were used to place all the data on approximately the same scale.

#### Structure Determination and Refinement

The position of the cobalt atom was determined from the Patterson function and the remaining non-hydrogen atoms from successive Fourier syntheses. The R value ( $R = \Sigma ||F_{\text{obs}}| - |F_{\text{calc}}|| / \Sigma |F_{\text{obs}}|$ ) was 0.17 at the start of the least-squares refinement. After three cycles, the R value was 0.093. Anisotropic thermal refinement gave an R of 0.060 after three cycles. A difference Fourier synthesis gave reasonable positions for all the eighteen hydrogen atoms. Three additional least squares cycles, in which the H atoms were included in the structure factors calculation but were not refined, reduced R to 0.047. Three more cycles, in which all the atoms were refined, reduced R to the final value of 0.044.

The scattering factors were taken from the usual sources.<sup>88</sup> The final positional parameters and thermal parameters for the non-hydrogen atoms are given in Tables 12 and 13, respectively. The bond distances and angles are given in Tables 14 and 15, respectively. The hydrogen atom parameters and distances are given in Tables 16 and 17, respectively.



## B. Results and Discussion

The crystal consists of  $[\text{Co}(\text{PHENSC})(\text{H}_2\text{O})_2]^{2+}$  cation, illustrated in Figures 20 and 21. The cobalt atom is in the center of a pentagonal bipyramidal arrangement consisting of five of the six donor atoms of the planar ligand in the equatorial plane and two axial water molecules. The  $\text{NO}_3^-$  anions are joined by hydrogen bonds (see Table 18). The range of D-H---A angles and the variation of the H---A and D---A distances indicate the presence of both strong and weak hydrogen bonds. The  $[\text{Co}(\text{PHENSC})(\text{H}_2\text{O})_2](\text{NO}_3)_2$  and  $[\text{Co}(\text{BIPYSC})(\text{H}_2\text{O})_2](\text{NO}_3)_2$  are the only two seven-coordinate cobalt complexes with hexadentate ligands which have been characterized by X-ray diffraction studies. The two hexadentate ligands act as pentadentate ligands because the size of  $\text{Co}(\text{II})$  ion is too small to form bonds to all six donors in the equatorial plane. In the four cobalt complexes with planar pentadentate ligands (as mentioned above), the Co-N bond distances range from 2.171 to 2.268 Å; the Co-O bond distances range from 2.150 to 2.253 Å. In  $[\text{Co}(\text{BIPYSC})(\text{H}_2\text{O})_2](\text{NO}_3)_2$ , the average Co-N bond distance is 2.222 Å, and the Co-O bond distance in the plane is 2.191 Å.<sup>126</sup> We found in  $[\text{Co}(\text{PHENSC})(\text{H}_2\text{O})_2](\text{NO}_3)_2$  the Co-O bond distance in the plane is 2.138 Å, and the average Co-N bond length is 2.220 Å, which are similar to the values in the other seven-coordinate cobalt complexes. The axial Co-O (to  $\text{H}_2\text{O}$ ) bond distances are (2.146(4), 2.153(4) Å) in  $[\text{Co}(\text{H}_2\text{DAPP})(\text{H}_2\text{O})_2]^{2+}$ , (2.060(9), 2.146(8) Å) in the purpurato-Co(II) complex,<sup>127</sup> (2.110(6), 2.125(6) Å) in  $[\text{Co}(\text{DAPSAH})(\text{H}_2\text{O})_2]^{2+}$  and (2.131(6), 2.159(6) Å) in  $[\text{Co}(\text{BIPYSC})(\text{H}_2\text{O})_2]^{2+}$ .<sup>126</sup> The

O-Co-O angles (axial) are 176.1°, 168.8°, 174.2°, and 176.2°, respectively, and only the purpurato-Co(II) complex shows a significant deviation from linearity. The axial Co-O (to H<sub>2</sub>O) bond distances of (2.113(4), 2.119(4) Å) and O-Co-O angle (axial) of 176.2° in [Co(PHENSC)(H<sub>2</sub>O)<sub>2</sub>]<sup>2+</sup> again are indistinguishable from other seven-coordinate cobalt complexes.

The least-squares planes data are given in Table 19. The deviations of the five donor atoms from the pentagonal plane are from -0.038 to 0.034 Å in [Co(BIPYSC)(H<sub>2</sub>O)<sub>2</sub>](NO<sub>3</sub>)<sub>2</sub>,<sup>126</sup> from -0.038 to 0.047 Å in [Co(PHENSC)(H<sub>2</sub>O)<sub>2</sub>](NO<sub>3</sub>)<sub>2</sub>, from -0.068 to 0.069 Å in [Co(DAPSAH)(H<sub>2</sub>O)<sub>2</sub>](NO<sub>3</sub>)<sub>2</sub>·H<sub>2</sub>O,<sup>125</sup> from -0.100 to 0.111 Å in [Co(DAPBH)(H<sub>2</sub>O)(NO<sub>3</sub>)](NO<sub>3</sub>),<sup>124</sup> from -0.116 to 0.115 Å in [Co(DAPSC)(H<sub>2</sub>O)Cl]Cl·2H<sub>2</sub>O,<sup>118</sup> from -0.140 to 0.160 Å in [CoL(NO<sub>3</sub>)(H<sub>2</sub>O)<sub>2</sub>·2H<sub>2</sub>O (L = purpurate),<sup>127</sup> and from -0.364 to 0.363 Å in [Co(H<sub>2</sub>DAPP)(H<sub>2</sub>O)<sub>2</sub>]Cl<sub>2</sub>.<sup>123</sup> Therefore, the maximum and minimum deviations from planarity are found in [Co(H<sub>2</sub>DAPP)(H<sub>2</sub>O)<sub>2</sub>]Cl<sub>2</sub> and [Co(BIPYSC)(H<sub>2</sub>O)<sub>2</sub>](NO<sub>3</sub>)<sub>2</sub>, respectively; but the deviation for Co(PHENSC)(H<sub>2</sub>O)<sub>2</sub>](NO<sub>3</sub>)<sub>2</sub> is very close to that found for [Co(BIPYSC)(H<sub>2</sub>O)<sub>2</sub>](NO<sub>3</sub>)<sub>2</sub>. Dihedral angles for [Co(PHENSC)(H<sub>2</sub>O)<sub>2</sub>]<sup>2+</sup> are given in Table 20. The two side arms are twisted slightly (side (1), 3.7° and side (2), 3.4°) relative to the 1,10-phenanthroline ring.

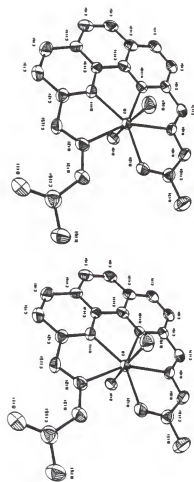


Figure 20. Stereoscopic view of  $[\text{Co}(\text{PHENS})(\text{H}_2\text{O})_2](\text{NO}_3)_2 \cdot$

Figure 21. An ORTEP view of  $[\text{Co}(\text{PHENSC})(\text{H}_2\text{O})_2](\text{NO}_3)_2$  showing the atomic numbering and the thermal ellipsoids (50% probability level).

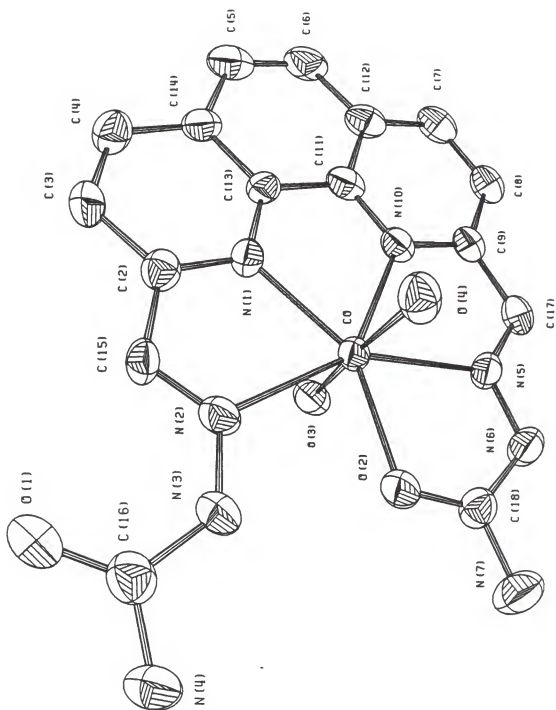


Table 12

Final Positional Parameters ( $\times 10^4$  except for Co  
which is  $\times 10^5$ ) for  $[\text{Co}(\text{PHENSC})(\text{H}_2\text{O})_2](\text{NO}_3)_2$

ATOM	X	Y	Z
CO	-28691(11)	13009(8)	37633(3)
O(1)	2090(6)	-1098(5)	4696(2)
O(2)	-3701(5)	-630(4)	3924(2)
O(3)	-3904(6)	1928(4)	4447(2)
O(4)	-1995(5)	643(4)	3059(2)
O(5)	-5366(7)	-259(6)	613(2)
O(6)	-7766(8)	-225(6)	222(2)
O(7)	-6697(7)	1536(5)	492(2)
O(8)	196(6)	3144(5)	2616(2)
O(9)	-802(6)	4131(5)	1953(2)
O(10)	-2183(6)	2578(5)	2274(2)
N(1)	-898(6)	2704(5)	3838(2)
N(2)	-502(7)	387(5)	4187(2)
N(3)	-516(7)	-876(5)	4336(2)
N(4)	274(8)	-2760(5)	4710(2)
N(5)	-5441(5)	1021(5)	3421(2)
N(6)	-6089(6)	-173(5)	3473(2)
N(7)	-5587(7)	-2211(5)	3785(3)
N(8)	-6596(7)	323(6)	442(2)
N(9)	-926(6)	3275(5)	2292(2)
N(10)	-3782(6)	3059(5)	3389(2)
C(2)	548(8)	2455(6)	4076(2)
C(3)	1791(8)	3413(6)	4140(2)
C(4)	1474(8)	4643(7)	3959(3)
C(5)	-566(9)	6149(7)	3478(2)
C(6)	-2061(9)	6316(7)	3239(3)
C(7)	-4810(9)	5360(7)	2946(2)
C(8)	-5852(8)	4287(7)	2936(2)
C(9)	-5297(8)	3140(6)	3162(2)
C(11)	-2774(8)	4081(6)	3402(2)
C(12)	-3248(8)	5288(6)	3187(2)
C(13)	-1198(7)	3900(6)	3657(2)
C(14)	-50(8)	4912(6)	3700(2)
C(15)	757(7)	1122(6)	4264(2)
C(16)	703(8)	-1558(6)	4593(2)
C(17)	-6233(7)	1938(6)	3185(2)
C(18)	-5030(7)	-1004(6)	3740(2)

Table 13

Final Thermal Parameters ( $\times 10^{-4}$  except for Co which is  $\times 10^{-5}$ ) for  
 $[\text{Co}(\text{PHENSC})(\text{H}_2\text{O})_2](\text{NO}_3)_2$ . The Form of the Thermal Parameter is

$$\exp[-2\pi^2(U_{11}h^2a^2 + U_{22}k^2b^2 + U_{33}l^2c^2 + 2U_{12}hka + 2U_{13}hla + 2U_{23}klb)]$$

ATOM	U11	U22	U33	U12	U13	U23
CO						
O(1)	312(4)	223(4)	329(5)	3(3)	-81(3)	15(4)
O(2)	49(3)	49(3)	60(4)	6(2)	-13(2)	17(2)
O(3)	60(3)	29(2)	55(4)	0(2)	-24(2)	9(2)
O(4)	52(3)	39(2)	36(4)	2(2)	-4(2)	2(2)
O(5)	46(2)	34(2)	42(4)	3(2)	-7(2)	-20(2)
O(6)	67(3)	81(4)	76(5)	21(3)	-1(3)	60(3)
O(7)	90(4)	58(4)	74(5)	-27(3)	-12(3)	-18(3)
O(8)	88(4)	32(3)	95(5)	1(2)	-10(3)	-18(3)
O(9)	40(2)	78(4)	46(4)	9(2)	-14(2)	0(3)
O(10)	50(3)	50(3)	72(5)	-7(2)	-10(2)	23(3)
N(1)	26(2)	66(3)	61(4)	-16(2)	-3(2)	8(3)
N(2)	47(3)	27(2)	34(4)	0(2)	-3(2)	-3(2)
N(3)	45(3)	26(3)	39(4)	1(2)	-11(2)	4(2)
N(4)	70(4)	34(3)	48(5)	4(2)	-12(2)	9(2)
N(5)	33(3)	29(3)	64(5)	2(3)	-21(3)	9(3)
N(6)	36(3)	29(3)	40(4)	-2(2)	-8(2)	-1(2)
N(7)	41(3)	31(3)	55(5)	-4(2)	-10(2)	0(3)
N(8)	46(3)	34(3)	87(6)	-8(2)	-7(3)	6(3)
N(9)	34(3)	45(3)	45(5)	-2(2)	-1(2)	-5(3)
N(10)	42(3)	41(4)	41(4)	0(2)	2(2)	-4(2)
C(2)	37(3)	27(3)	28(4)	3(2)	-3(2)	0(2)
C(3)	33(3)	37(3)	34(5)	-1(3)	1(2)	-3(3)
C(4)	35(3)	45(4)	39(5)	-5(3)	-10(3)	0(3)
C(5)	40(4)	41(4)	46(5)	-11(3)	-3(3)	-5(3)
C(6)	68(5)	37(4)	38(5)	-8(3)	10(3)	3(3)
C(7)	70(5)	28(3)	44(5)	-4(3)	0(3)	14(3)
C(8)	53(4)	40(4)	40(5)	14(3)	-3(3)	13(3)
C(9)	41(4)	47(4)	38(5)	9(3)	-11(3)	9(3)
C(11)	35(3)	37(3)	30(5)	5(3)	-5(3)	3(3)
C(12)	52(4)	27(3)	28(5)	2(3)	2(3)	2(2)
C(13)	54(4)	27(3)	37(5)	6(3)	5(3)	6(3)
C(14)	34(3)	26(3)	30(4)	-5(3)	0(2)	0(2)
C(15)	42(3)	31(3)	33(5)	-7(3)	5(3)	2(2)
C(16)	21(3)	37(3)	43(5)	2(2)	-7(2)	-2(3)
C(17)	49(4)	42(4)	36(5)	1(3)	-8(3)	-1(3)
C(18)	27(3)	42(4)	34(5)	9(3)	-6(2)	0(3)
C(19)	29(3)	33(3)	46(5)	0(2)	-3(3)	-1(3)

Table 14

Bond Distances (in Å) in  $[\text{Co}(\text{PHENSC})(\text{H}_2\text{O})_2](\text{NO}_3)_2$   
 With Estimated Standard Deviations

---

In the Cation:			
Co-O(3)	2.113(4)	Co-O(4)	2.119(4)
Co-N(1)	2.139(5)	Co-N(10)	2.164(5)
Co-N(2)	2.348(5)	Co-N(5)	2.227(5)
Co-O(2)	2.138(4)		
C(2)-C(15)	1.460(9)	C(9)-C(17)	1.446(9)
C(15)-N(2)	1.268(8)	C(17)-N(5)	1.278(8)
N(2)-N(3)	1.353(7)	N(5)-N(6)	1.340(7)
N(3)-C(16)	1.356(9)	N(6)-C(18)	1.371(8)
C(16)-N(4)	1.320(9)	C(18)-N(7)	1.322(8)
C(16)-O(1)	1.225(8)	C(18)-O(2)	1.212(8)
N(1)-C(2)	1.314(8)	N(10)-C(9)	1.329(8)
N(1)-C(13)	1.333(7)	N(10)-C(11)	1.323(8)
C(2)-C(3)	1.404(9)	C(9)-C(8)	1.381(9)
C(13)-C(14)	1.388(8)	C(11)-C(12)	1.406(9)
C(3)-C(4)	1.368(9)	C(8)-C(7)	1.381(10)
C(4)-C(14)	1.397(9)	C(7)-C(12)	1.377(10)
C(5)-C(6)	1.337(10)	C(11)-C(13)	1.412(9)
C(5)-C(14)	1.449(9)	C(6)-C(12)	1.423(10)
In the Nitrate Ions:			
N(8)-O(5)	1.219(8)	N(9)-O(8)	1.216(7)
N(8)-O(6)	1.216(8)	N(9)-O(9)	1.259(7)
N(8)-O(7)	1.254(8)	N(9)-O(10)	1.234(7)

---



Table 15

Bond Angles (in deg) in  $[\text{Co}(\text{PHENSC})(\text{H}_2\text{O})_2](\text{NO}_3)_2$   
 With Estimated Standard Deviations

<u>In the Cation</u>	
O(2)-Co-O(3)	88.6(2)
O(2)-Co-O(4)	89.8(2)
O(2)-Co-N(2)	77.8(2)
O(2)-Co-N(5)	70.7(2)
O(3)-Co-O(4)	176.2(2)
O(3)-Co-N(1)	92.0(2)
O(3)-Co-N(2)	93.4(2)
O(3)-Co-N(5)	89.4(2)
O(3)-Co-N(10)	89.7(2)
O(4)-Co-N(1)	91.2(2)
O(4)-Co-N(2)	89.6(2)
O(4)-Co-N(5)	86.8(2)
O(4)-Co-N(10)	89.3(2)
N(1)-Co-N(2)	69.4(2)
N(1)-Co-N(10)	73.4(2)
N(5)-Co-N(10)	68.7(2)
Co-O(2)-C(18)	119.4(4)
Co-N(1)-C(2)	122.9(4)
Co-N(1)-C(13)	117.8(4)
Co-N(2)-N(3)	120.1(4)
Co-N(2)-C(15)	117.2(4)
Co-N(5)-N(6)	115.6(4)

Table 15 Continued

Co-N(5)-C(17)	122.0(4)
Co-N(10)-C(9)	122.6(4)
Co-N(10)-C(11)	117.1(4)
C(2)-N(1)-C(13)	119.2(5)
N(3)-N(2)-C(15)	122.8(5)
N(2)-N(3)-C(16)	128.5(5)
N(6)-N(5)-C(17)	122.4(5)
N(5)-N(6)-C(18)	112.8(5)
C(9)-N(10)-C(11)	120.4(5)
N(1)-C(2)-C(3)	121.7(6)
N(1)-C(2)-C(15)	115.3(5)
C(3)-C(2)-C(15)	123.0(6)
C(2)-C(3)-C(4)	119.0(6)
C(3)-C(4)-C(14)	119.6(6)
C(6)-C(5)-C(14)	122.3(6)
C(5)-C(6)-C(12)	122.0(6)
C(8)-C(7)-C(12)	120.1(6)
C(7)-C(8)-C(9)	119.2(6)
N(10)-C(9)-C(8)	121.0(6)
N(10)-C(9)-C(17)	113.0(5)
C(8)-C(9)-C(17)	126.0(6)
N(10)-C(11)-C(12)	122.3(6)
N(10)-C(11)-C(13)	116.1(5)
C(12)-C(11)-C(13)	121.7(6)
C(6)-C(12)-C(7)	126.4(6)

Table 15 Continued

C(6)-C(12)-C(11)	116.5(6)
C(7)-C(12)-C(11)	117.0(6)
N(1)-C(13)-C(11)	115.6(5)
N(1)-C(13)-C(14)	123.4(5)
C(11)-C(13)-C(14)	121.0(5)
C(4)-C(14)-C(5)	126.5(6)
C(4)-C(14)-C(13)	117.0(6)
C(5)-C(14)-C(13)	116.5(6)
N(2)-C(15)-C(2)	115.2(5)
O(1)-C(16)-N(3)	122.3(6)
O(1)-C(16)-N(4)	123.5(6)
N(3)-C(16)-N(4)	114.2(6)
N(5)-C(17)-C(9)	113.6(5)
O(2)-C(18)-N(6)	121.2(6)
O(2)-C(18)-N(7)	123.7(6)
N(6)-C(18)-N(7)	115.1(6)

In the Nitrate Ions

O(5)-N(8)-O(6)	122.8(6)
O(5)-N(8)-O(7)	120.1(6)
O(6)-N(8)-O(7)	117.1(6)
O(8)-N(9)-O(9)	119.5(5)
O(8)-N(9)-O(10)	122.6(5)
O(9)-N(9)-O(10)	117.9(5)

---

Table 16

Final Hydrogen Atom Parameters for  $[\text{Co}(\text{PHENSC})(\text{H}_2\text{O})_2](\text{NO}_3)_2 \cdot$

ATOM	The positional parameters are $\times 10^3$			B
	X	Y	Z	
H(1)	-354(9)	152(7)	473(3)	5.6(1.8)
H(2)	-406(8)	250(7)	451(2)	4.6(1.6)
H(3)	-189(7)	125(6)	286(2)	3.6(1.4)
H(4)	-241(13)	23(8)	297(3)	7.0(2.0)
H(5)	274(7)	314(6)	435(2)	3.3(1.4)
H(6)	230(8)	526(7)	402(3)	5.3(1.7)
H(7)	-32(9)	642(8)	364(3)	7.0(2.0)
H(8)	-232(7)	717(6)	312(2)	3.2(1.4)
H(9)	-514(8)	619(6)	280(2)	4.3(1.5)
H(10)	-679(8)	432(5)	275(2)	2.0(1.2)
H(11)	-728(8)	181(6)	302(2)	4.3(1.6)
H(12)	174(9)	87(6)	442(2)	3.9(1.4)
H(13)	-176(8)	-119(7)	438(3)	5.2(1.7)
H(14)	-736(9)	-45(8)	333(3)	6.3(2.0)
H(15)	-645(8)	-241(7)	363(3)	5.3(1.8)
H(16)	-516(13)	-274(8)	398(3)	7.3(2.1)
H(17)	-67(7)	-305(6)	466(2)	2.8(1.4)
H(18)	107(9)	-327(7)	485(3)	5.3(1.8)

and B is the isotropic thermal parameter.

Table 17

Bond Distances (in Å) for Hydrogens of  $[\text{Co}(\text{PHENSC})(\text{H}_2\text{O})_2](\text{NO}_3)_2$   
With Estimated Standard Deviations

---

H(1)-O(3)	0.90(7)
H(2)-O(3)	0.62(7)
H(3)-O(4)	0.83(6)
H(4)-O(4)	0.58(8)
H(5)-C(3)	0.95(6)
H(6)-C(4)	0.92(7)
H(7)-C(5)	0.53(8)
H(8)-C(6)	0.95(6)
H(9)-C(7)	0.97(6)
H(10)-C(8)	0.88(5)
H(11)-C(17)	0.94(6)
H(12)-C(15)	0.90(6)
H(13)-N(3)	1.06(7)
H(14)-N(6)	1.11(7)
H(15)-N(7)	0.82(7)
H(16)-N(7)	0.82(8)
H(17)-N(4)	0.82(6)
H(18)-N(4)	0.89(7)

---

Table 18  
Hydrogen Bonds in  $[\text{Co}(\text{PHENSC})(\text{H}_2\text{O})_2](\text{NO}_3)_2$

Bond D-H....A	Position of A	Dist, Å		Angle, deg D-H-A
		D-H	H....A	
O(3)-H(1).....O(1)	2 - x, - y, 1 - z	0.90(7)	1.91(7)	158(7)
O(3)-H(2).....O(5)	1 - x, 1/2 + y, 1/2 - z	0.62(7)	2.37(7)	158(8)
O(4)-H(3).....O(10)	x, y, z	0.83(6)	2.05(6)	166(6)
O(4)-H(3).....N(9)	x, y, z	0.83(6)	2.68(6)	168(5)
N(3)-H(13).....O(7)	1 - x, -1/2 + y, 1/2 - z	1.06(7)	2.67(7)	137(5)
N(6)-H(14).....O(9)	1 - x, -1/2 + y, 1/2 - z	1.11(7)	1.67(7)	174(6)
N(7)-H(15).....O(10)	1 - x, -1/2 + y, 1/2 - z	0.82(7)	2.56(7)	142(6)
N(7)-H(16).....O(7)	1 - x, -1/2 + y, 1/2 - z	0.82(8)	2.12(8)	156(7)
N(4)-H(17).....O(7)	1 - x, -1/2 + y, 1/2 - z	0.82(6)	2.17(6)	170(6)
N(4)-H(18).....O(6)	1 + x, -1/2 - y, 1/2 + z	0.89(7)	2.03(7)	162(6)
			2.887(8)	

Table 19  
Least-Squares Planes for  $[\text{Co}(\text{PHENSC})(\text{H}_2\text{O})_2](\text{NO}_3)_2^{\text{a}}$

Atom	PHEN	Side (1)	Side (2)	Donors
Co	86	-153	-22	25
O(1)	-85	-589	-27*	-160
O(2)	198	8*	10	47*
N(1)	-9*	-358	4	19*
N(2)	20	-347	-3*	-38*
N(3)	17	-345	-36*	-92
N(4)	93	-311	33*	-79
N(5)	75	-19*	-155	-38*
N(6)	80	25*	-207	-92
N(7)	65	-13*	-247	-180
N(10)	15*	-175	-94	11*
C(2)	-13*	-442	60	30
C(3)	-11*	-512	139	90
C(4)	19*	-469	184	164
C(5)	9*	-368	117	181
C(6)	2*	-291	46	157
C(7)	-25*	-162	-127	47
C(8)	2*	-74	-171	14
C(9)	18*	-87	-157	-8
C(11)	-6*	-254	-46	47
C(12)	-10*	-234	-43	84

Table 19 Continued

Atom	PHEN	Side (1)	Side (2)	Donors
C(13)	5*	-330	33	77
C(14)	4*	-398	107	135
C(15)	-19	-457	31*	-27
C(16)	14	-414	1*	-102
C(17)	51	0*	-194	-39
C(18)	111	-2*	-147	-77
$\ell$	-0.4190	-0.4771	-0.3684	-0.3971
m	0.2731	0.2631	0.2994	0.3111
n	0.8659	0.8386	0.8802	0.8634
p	6.628	6.278	7.177	6.830

<sup>a</sup> The title of the plane is followed by the deviations ( $\times 10^3$  Å) of the atoms listed in the left-hand column. The atoms used to define the plane are denoted by asterisks. The deviation equals  $\ell X + mY + nZ - p$ , where X, Y, and Z are the orthogonal coordinates (in Å) relative to a, b, and  $c \sin \beta$ ;  $\ell$ , m and n are the direction cosines; and p is the distance of the plane from the origin (in Å).



Table 20

Dihedral Angles for Various Planes in  $[\text{Co}(\text{PHENSC})(\text{H}_2\text{O})_2](\text{NO}_3)_2$ 

Plane (1)	Plane (2)	Angle (deg)
Phen	Side (1)	3.7
Phen	Side (2)	3.4
Side (1)	Side (2)	7.0

## CHAPTER VI

### THE CRYSTAL STRUCTURE OF DINITRATO[2,9-DIFORMYL-1,10-PHENANTHROLINE BIS(SEMICARBAZONE)]LEAD(II), $[\text{Pb}(\text{PHENSC})(\text{NO}_3)_2]$

The Pb(II) ion is a good example for consideration of low and high coordination number complexes. In addition, the lone pair of electrons on lead(II) ion in some cases has an important effect on the stereochemistry of Pb(II).<sup>128-130</sup> In spite of the large size of the lead(II) ion, complexes with low coordination numbers are known. However, high coordination numbers such as seven to ten are usually found, with eight coordination being the most common. Only two nine-<sup>131,132</sup> and one ten-<sup>133</sup> coordinate lead(II) complexes have been reported. A few hexadentate macrocyclic lead(II) compounds have been studied by X-ray diffraction method.<sup>130,131,134,135</sup> Another hexadentate ligand, 2,9-diformyl-1,10-phenanthroline bis(semicarbazone), PHENSC, was used to prepare  $[\text{Pb}(\text{PHENSC})(\text{NO}_3)_2]$ , which was studied by X-ray diffraction.

#### A. Experimental Section

##### Preparation of $[\text{Pb}(\text{PHENSC})(\text{NO}_3)_2]$

Equimolar amounts of lead nitrate and 2,9-diformyl-1,10-phenanthroline bis(semicarbazone) were heated for six hours in methanol-water (2:1). After filtering the slurry and collecting one crop of crystals, clear yellow crystals suitable for X-ray diffraction studies were obtained.

### Data Collection and Reduction

Preliminary photographs indicated that the space group was C2/c, and the molecule has a twofold axis. The unit cell dimensions are reported in Table 3, and the intensity data were measured using a Syntex PT diffractometer. The pertinent crystal data, together with some details of the intensity measurements, are given in Table 3. The  $\theta$ - $2\theta$  scan technique with a variable scan rate of 1 to 24°/min was used in measuring the intensity. Four standard reflections were measured every 96 reflections to monitor the beam and crystal stability. Scale factors varying from 0.978 to 1.005 were used to place all the data on approximately the same scale.

### Structure Determination and Refinement

The position of the lead atom was determined from the Patterson function and the remaining non-hydrogen atoms from successive Fourier syntheses. The R value ( $R = \Sigma ||F_{\text{obs}}| - |F_{\text{calc}}|| / \Sigma |F_{\text{obs}}|$ ) was 0.15 at the start of the least-squares refinement. After three cycles, the R value was 0.076. Anisotropic thermal refinement gave an R of 0.039 after three cycles.

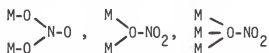
The scattering factors were taken from the usual sources.<sup>88</sup> The final positional parameters and thermal parameters for the non-hydrogen atoms are given in Tables 21 and 22, respectively. The bond distances and angles are given in Tables 23 and 24, respectively.

### B. Results and Discussion

The crystal consists of  $[\text{Pb}(\text{PHENSC})(\text{NO}_3)_2]$ , illustrated in Figures 22 and 23. The lead atom has an unusual coordination number of ten involving six donor atoms of the planar ligand in the equatorial plane and four oxygen atoms from two axial bidentate nitrate groups.

### The Nitrate Groups

A great many nitrate complexes have been studied. Several modes of coordination have been proposed for the nitrate group, and so far four of these types of nitrate-groups have been identified-- unidentate, unsymmetrically bidentate, symmetrically bidentate, and bridging. The unidentate form is a less common alternative, in  $[\text{Au}(\text{NO}_3)_4]^-$  ion, Au(III) is coordinated in an essentially square-planar manner by four unidentate nitrate groups.<sup>136</sup> In unsymmetrical bidentate nitrate groups, there is a small but real difference (e.g., 0.2 - 0.7 Å) between the distances from the metal atom to the two coordinated oxygen atoms of each nitrate group. For example, in  $[\text{Co}(\text{NO}_3)_4]^{2-}$ ,<sup>137</sup> the Co-O distances are 2.03, 2.36 Å and 2.11, 2.54 Å. The symmetrical bidentate nitrate group is preferred where the metal atom is equidistant from the two-coordinated oxygen atoms. For bridging nitrate-groups, the coordination to more than one metal atom is possible.<sup>138</sup>



The Pb-O (bidentate nitrate groups) distances range from 2.564 to 2.809 Å for nine and eight coordinations of binuclear  $\text{TPyMTpPb}_2(\text{NO}_3)_4(\text{H}_2\text{O})_2$  complex (TPyMT = 2,4,6-tris(2-pyrimidyl)-1,3,5-triazine)<sup>132</sup> containing symmetrical bidentate nitrate groups. In eight coordination  $[\text{Pb}(\text{L})(\text{NO}_3)_2]$  complex (L = 1,4,8,11-tetra-azacyclotetradecane), the Pb-O (nitrate) bond distances are 2.96, 3.31 Å and 2.88, 3.08 Å (unsymmetrical bidentate nitrate groups).<sup>129</sup> We found in  $[\text{Pb}(\text{PHENSC})(\text{NO}_3)_2]$ , the Pb-O bond distances are 2.735(10) and 2.823(10) Å, which

are similar to the values in the two lead complexes. The N-O bond lengths are 1.232(14), 1.234(15), 1.235(14) Å and ONO bond angles are 119.2(11)°, 120.7(11)°, 120.0(11)°, which indicates a very symmetrical nitrate group in this complex. Dimensions of symmetrical bidentate nitrato-groups are given in Table 25.<sup>132,138</sup> In most instances, the terminal N-O bond is shorter, and the N-O bonds involving the coordinated oxygens are longer than the N-O bond in an uncoordinated nitrate group (nitrate ion). Also, the ONO bond angle involving the coordinated oxygen atoms is less than 120°. <sup>138</sup> However, in [Pb(PHENSC)(NO<sub>3</sub>)<sub>2</sub>] and (TPymT)Pb<sub>2</sub>(NO<sub>3</sub>)<sub>4</sub>(H<sub>2</sub>O)<sub>2</sub> complexes, the bidentate nitrato-groups are very similar to a nitrate ion with all the N-O distances being equal.

#### The Hexadentate Ligand

In the [Pb(PHENSC)(NO<sub>3</sub>)<sub>2</sub>] complex, four nitrogen atoms (Pb-N bond distances 2.731(9) and 2.727(9) Å) and two oxygen atoms (Pb-O bond length 2.739(9) Å) of the hexadentate ligand (PHENSC) are coordinated. In comparison, the average Pb-N bond distance is 2.704 in [(TPymT)Pb<sub>2</sub>(NO<sub>3</sub>)<sub>4</sub>(H<sub>2</sub>O)<sub>2</sub>];<sup>132</sup> 2.884 (Pb-N cryptate), 2.642 (Pb-NCS) in [Pb(cryptate)(NCS)(SCN)];<sup>133</sup> 2.49 in [Pb(L)(NO<sub>3</sub>)<sub>2</sub>];<sup>129</sup> 2.75 in [Pb(L)(H<sub>2</sub>O)](ClO<sub>4</sub>)<sub>2</sub>·H<sub>2</sub>O;<sup>130</sup> 2.751 in [Pb(L)(SCN)<sub>2</sub>];<sup>135</sup> and 2.618 Å in [Pb(L)(SCN)(NCS)];<sup>131</sup> where the L's are macrocyclic ligands. The Pb-O bond distances in lead(II) complexes range from 2.564 to 3.130 Å.<sup>131-133,135</sup> Therefore, the Pb-N and Pb-O bond distances in the [Pb(PHENSC)(NO<sub>3</sub>)<sub>2</sub>] complex are within the range of values found in the other lead(II) complexes.

The least-squares planes data are given in Table 26. The deviations of the atoms in plane I are from -0.061 to 0.046 Å and in plane II are from -0.042 to 0.081 Å. The dihedral angle between plane I and plane II is 21.6°, and six donor atoms in the equatorial are planar.

### The Coordination Polyhedron

Robertson's polyhedron analysis was used to evaluate the structural results for this complex.<sup>139</sup> The dihedral angles of the polyhedron were calculated after the metal-donor distances were reduced to a unit sphere. Then these angles were compared to the dihedral angles formed by the idealized polyhedron (see Figures 24 and 25)<sup>140</sup> when inscribed in a unit sphere. The coordinates of the idealized polyhedron were calculated by an energy minimization technique based on  $R_{ij}^{-n}$  repulsion potential (where  $R_{ij}$  is the separation of atoms  $i$  and  $j$ ). The dihedral angles were calculated for the case of  $n = 6$ . A bicapped square antiprism (1-4-4-1) polyhedron and a 2-6-2 (0° twist) polyhedron were considered for this complex. In the case of the 2-6-2 polyhedron, the two pairs of capping vertices were rotated from the eclipsed position in opposite directions. The root mean square (RMS) of the differences in the dihedral angles between the observed and idealized polyhedron are given in Table 27. The dihedral angles for the 2-6-2 polyhedron with twists of 20° and 40° are essentially similar to the bicapped square antiprism. The RMS values for 2-6-2 (0° twist) and 1-4-4-1 polyhedron are very similar (15.69 and 14.68, respectively). Therefore, the polyhedron in the lead complex has features common to both 2-6-2 and 1-4-4-1 geometries. We also

considered the 2-6-2 polyhedron without the energy minimization procedure for  $20^\circ$ ,  $40^\circ$  and  $60^\circ$  (see Table 28). The dihedral angles for the  $80^\circ$  twist are very similar to those for the  $40^\circ$  twist. Therefore, the coordination polyhedron is probably best described in terms of the 2-6-2 polyhedron with a  $60^\circ$  twist.

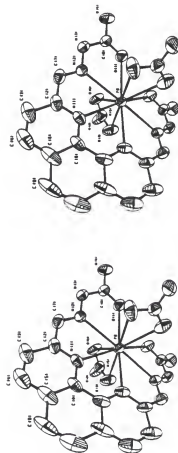
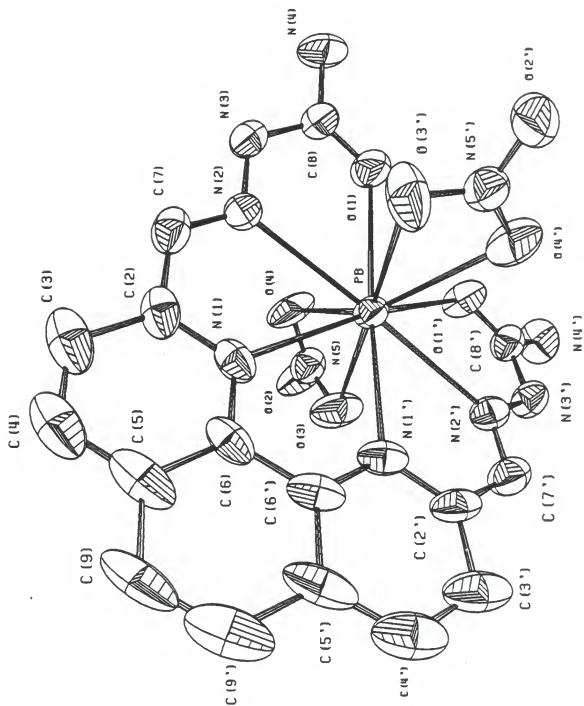


Figure 22. Stereoscopic view of  $[\text{Pb}(\text{PHENC})(\text{NO}_3)_2]$ .



Figure 23. An ORTEP view of [Pb(PHNSC)(NO<sub>3</sub>)<sub>2</sub>] showing the atomic numbering and the thermal ellipsoids (50% probability level).



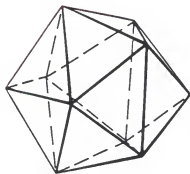
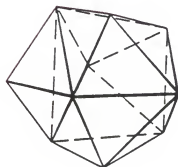
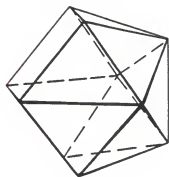
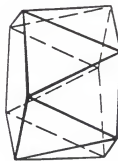
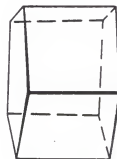
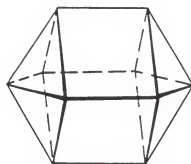
1. *Biccapped Square Antiprism*2. *Tetracapped Trigonal Prism*3. *Tetradecahedron*4. *Pentagonal Antiprism*5. *Pentagonal Prism*6. *Biccapped Square Prism*

Figure 24. Six possible polyhedra for a coordination number of ten.

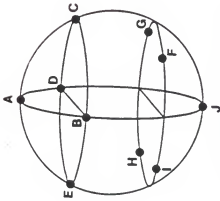
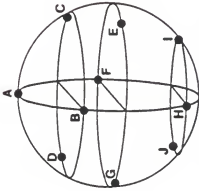
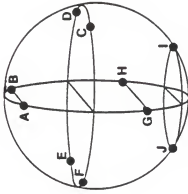
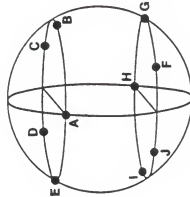
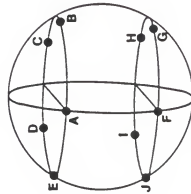
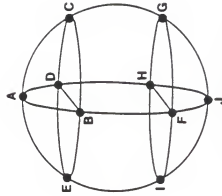
1. *Biccapped Square Antiprism*2. *Tetracapped Trigonal Prism*3. *Tetradecahedron*4. *Pentagonal Antiprism*5. *Pentagonal Prism*6. *Biccapped Square Prism*

Figure 25. Six possible polyhedra represented as points on a sphere for a coordination number of ten.

Table 21

Final Positional Parameters ( $\times 10^4$  except for Pb  
which is  $\times 10^5$ ) for  $[\text{Pb}(\text{PHENSC})(\text{NO}_3)_2]$

ATOM	X	Y	Z
PB	0 *	22513(3)	-25000 *
O(1)	394(6)	914(5)	-685(11)
O(2)	2045(7)	1563(6)	-5669(12)
O(3)	941(7)	2327(6)	-5269(12)
O(4)	1637(6)	1705(6)	-3301(12)
N(1)	688(6)	3668(5)	-1316(10)
N(2)	1181(6)	2291(6)	186(11)
N(3)	1356(6)	1616(6)	1066(11)
N(4)	986(8)	322(7)	1618(14)
N(5)	1553(7)	1874(6)	-4737(12)
C(2)	1381(8)	3669(7)	-153(14)
C(3)	1852(10)	4375(9)	371(17)
C(4)	1530(10)	5090(9)	-253(17)
C(5)	773(9)	5116(8)	-1365(16)
C(6)	393(7)	4380(7)	-1913(13)
C(7)	1613(8)	2917(7)	655(15)
C(8)	861(8)	937(7)	604(14)
C(9)	374(9)	5851(9)	-1981(17)

\* Required by symmetry of space group.

Table 22

Final Thermal Parameters ( $\times 10^4$  except for Pb which is  $\times 10^5$ ) for  $[\text{Pb}(\text{PHENSC})(\text{NO}_3)_2]$

The Form of the Thermal Parameter is  
 $\exp[-2\pi^2(U_{11}^2 a^2 + U_{22}^2 b^2 + U_{33}^2 c^2 + 2U_{12}^2 ab + 2U_{13}^2 ac + 2U_{23}^2 bc)]$

ATOM	U11	U22	U33	U12	U13	U23
Pb	4458(46)	3137(42)	3201(38)	0*	-430(25)	0*
O(1)	79(5)	49(6)	49(5)	-13(4)	-14(4)	3(4)
O(2)	72(6)	118(7)	47(6)	43(5)	0(5)	3(5)
O(3)	69(7)	84(7)	83(6)	34(6)	11(5)	34(5)
O(4)	92(6)	106(7)	25(6)	6(5)	-10(5)	9(5)
N(1)	55(5)	35(5)	42(5)	-13(4)	15(4)	-8(4)
N(2)	47(5)	46(5)	32(5)	-3(5)	4(4)	-3(4)
N(3)	52(5)	50(6)	40(5)	-2(5)	-7(4)	4(4)
N(4)	86(7)	58(8)	58(7)	8(6)	-2(6)	30(6)
N(5)	49(6)	62(6)	43(6)	0(5)	2(5)	-1(5)
C(2)	51(7)	57(7)	40(6)	-15(6)	14(5)	-22(5)
C(3)	75(9)	70(9)	63(9)	-32(7)	35(7)	-23(7)
C(4)	85(9)	55(9)	72(9)	-28(7)	42(7)	-22(7)
C(5)	91(8)	33(8)	72(8)	-10(7)	55(7)	-13(6)
C(6)	60(8)	34(7)	44(6)	-13(5)	28(4)	-9(5)
C(7)	49(7)	56(7)	41(6)	-1(5)	3(5)	-12(5)
C(8)	47(7)	56(7)	40(6)	0(5)	-2(5)	-4(5)
C(9)	125(10)	33(9)	73(9)	-2(7)	62(6)	0(7)

\* Required by symmetry of space group.

Table 23  
Bond Distances (in Å) in  $[\text{Pb}(\text{PHENSC})(\text{NO}_3)_2]$   
With Estimated Standard Deviations

---

Pb-O(1)	2.739(9)
Pb-O(3)	2.823(10)
Pb-O(4)	2.735(10)
Pb-N(1)	2.731(9)
Pb-N(2)	2.727(9)
N(1)-C(2)	1.352(14)
N(1)-C(6)	1.348(14)
N(2)-N(3)	1.361(13)
N(2)-C(7)	1.271(15)
N(3)-C(8)	1.388(15)
N(4)-C(8)	1.337(16)
N(5)-O(2)	1.232(14)
N(5)-O(3)	1.234(15)
N(5)-O(4)	1.235(14)
C(2)-C(3)	1.421(19)
C(2)-C(7)	1.456(17)
C(3)-C(4)	1.373(21)
C(4)-C(5)	1.393(20)
C(5)-C(6)	1.413(18)
C(5)-C(9)	1.440(20)
C(8)-O(1)	1.231(14)

---

Table 24

Bond Angles (in deg) in [Pb(PHENSC)(NO<sub>3</sub>)<sub>2</sub>]  
With Estimated Standard Deviations

---

O(3)-Pb-O(1)	113.5(3)
O(3)-Pb-N(1)	93.7(3)
O(3)-Pb-N(2)	110.6(3)
O(4)-Pb-O(1)	73.5(3)
O(4)-Pb-N(1)	94.0(3)
O(4)-Pb-N(2)	72.2(3)
O(3)-Pb-O(4)	45.2(3)
N(1)-Pb-N(2)	59.2(3)
N(2)-Pb-O(1)	58.1(3)
Pb-O(1)-C(8)	122.5(7)
Pb-O(3)-N(5)	94.4(7)
Pb-O(4)-N(5)	98.7(7)
Pb-N(1)-C(2)	119.9(7)
Pb-N(1)-C(6)	122.2(7)
Pb-N(2)-N(3)	120.4(6)
Pb-N(2)-C(7)	122.9(8)
C(2)-N(1)-C(6)	117.8(9)
N(3)-N(2)-C(7)	116.7(9)
N(2)-N(3)-C(8)	117.1(9)
O(2)-N(5)-O(3)	119.2(11)
O(2)-N(5)-O(4)	120.7(11)
O(3)-N(5)-O(4)	120.0(11)

---



Table 24 Continued

N(1)-C(2)-C(3)	123.0(11)
N(1)-C(2)-C(7)	117.8(10)
C(3)-C(2)-C(7)	119.1(11)
C(2)-C(3)-C(4)	117.4(13)
C(3)-C(4)-C(5)	121.0(13)
C(4)-C(5)-C(6)	117.6(12)
C(4)-C(5)-C(9)	123.2(13)
C(6)-C(5)-C(9)	119.2(12)
N(1)-C(6)-C(5)	122.8(10)
N(2)-C(7)-C(2)	118.5(11)
O(1)-C(8)-N(3)	120.8(10)
O(1)-C(8)-N(4)	124.7(11)
N(3)-C(8)-N(4)	114.3(10)

---

Table 25  
Dimensions of Symmetrically Bidentate Nitrate-Groups in Å and Degrees

Compound	M-O <sub>I</sub>	M-O <sub>I'</sub>	N-O <sub>I</sub>	Average Values		α	β	β'
				N-O <sub>I'</sub>	N-O <sub>II</sub>			
Ti(NO <sub>3</sub> ) <sub>4</sub>	2.06	2.08	1.30	1.29	1.19	111	125	125
(Ph <sub>4</sub> As)[Fe(NO <sub>3</sub> ) <sub>4</sub> ]	2.13	2.14	1.27	1.27	1.22	114	123	123
Co(NO <sub>3</sub> ) <sub>3</sub>	1.89	1.90	1.28	1.29	1.19	110	124	126
Cu(NO <sub>3</sub> )(Ph <sub>3</sub> P) <sub>2</sub>	2.22	2.22	1.25	1.25	1.16	118	121	121
Sn(NO <sub>3</sub> ) <sub>4</sub>	2.15	2.18	1.29	1.29	1.18	112	124	124
La(NO <sub>3</sub> ) <sub>3</sub> bipy <sub>2</sub>	2.59	2.61	1.24	1.24	1.20	117	121	121
Mg <sub>3</sub> [Ce(NO <sub>3</sub> ) <sub>6</sub> ] <sub>2</sub> ·24H <sub>2</sub> O	2.61	2.65	1.26	1.26	1.22	117	122	122
(NH <sub>4</sub> ) <sub>2</sub> [Ce(NO <sub>3</sub> ) <sub>6</sub> ]	2.49	2.51	1.28	1.27	1.21	115	124	122
Th(NO <sub>3</sub> ) <sub>4</sub> (H <sub>2</sub> O) <sub>3</sub> ·2H <sub>2</sub> O	2.54	2.60	1.27	1.26	1.20	115	123	122
Rb[LuO <sub>2</sub> (NO <sub>3</sub> ) <sub>3</sub> ]	2.48	2.48	1.26	1.26	1.21	118	121	121

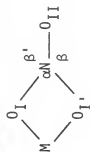


Table 25 Continued

Compound	M-O <sub>I</sub>	M-O <sub>I</sub> '	N-O <sub>I</sub>	Average Values		
				N-O <sub>I</sub> '	N-O <sub>II</sub>	
UO <sub>2</sub> (NO <sub>3</sub> ) <sub>2</sub> (H <sub>2</sub> O) <sub>2</sub> ·4H <sub>2</sub> O	2.53	2.53	1.27	1.27	1.22	122
[Pb(PHENS)(NO <sub>3</sub> ) <sub>2</sub> ]	2.82	2.74	1.23	1.24	1.23	119
(TPymT)Pb <sub>2</sub> (NO <sub>3</sub> ) <sub>4</sub> (H <sub>2</sub> O) <sub>2</sub>	2.72	2.63	1.24	1.24	1.24	122
					118	120

Table 26

Least-Squares Planes for  $[\text{Pb}(\text{PHENSC})(\text{NO}_3)_2]^a$ 

Atom	Plane I	Plane II
Pb	211	-250
N(1)	8*	-595
C(2)	-61*	-272
C(3)	10*	-255
C(4)	39*	-696
C(5)	7*	-1135
C(6)	46*	-1014
C(9)	-48*	-1684
C(7)	-301	-11*
N(2)	-377	-42*
N(3)	-726	81*
C(8)	-867	-8*
O(1)	-483	18*
N(4)	-1361	-37*
$\ell$	0.6824	0.8363
m	-0.0489	-0.2754
n	-0.7293	-0.4741
p	1.261	0.3657

<sup>a</sup> The title of the plane is followed by the deviations ( $\times 10^3$  Å) of the atoms listed in the left-hand column. The atoms used to define the plane are denoted by asterisks. The deviation equals  $\ell X + mY + nZ - p$ , where X, Y, and Z are the orthogonal coordinates (in Å) relative to a, b, and c sin  $\beta$ ;  $\ell$ , m and n are the direction cosines; and p is the distance of the plane from the origin (in Å).

Table 27

A Comparison of the Interplanar Angles for the  
Coordination Polyhedron in  $[\text{Pb}(\text{PHENSC})(\text{NO}_3)_2]$  Complex

Edge	Observed* Angle	Theoretical Polyhedron	
		1-4-4-1	2-6-2
O(4')-N(2')	52.83	56.34	53.45
O(3)-N(2')	46.34	56.34	53.45
N(1')-N(2')	70.73	56.34	53.45
O(1')-N(2')	57.50	56.34	53.45
N(2)-O(1)	57.50	56.34	53.45
N(2)-O(3')	46.34	56.34	53.45
N(2)-O(4)	52.83	56.34	53.45
N(2)-N(1)	70.73	56.34	53.45
O(3')-O(4')	77.61	56.16	90.00
O(1)-O(4')	35.58	56.16	**
O(4)-O(3)	77.61	56.16	90.00
N(1)-O(3)	31.16	56.16	**
O(3')-N(1')	31.16	56.16	**
N(1)-N(1')	80.18	56.16	90.00
O(1)-O(1')	54.20	56.16	90.00
O(4)-O(1')	35.58	56.16	**
O(1')-O(4')	43.58	30.86	50.50
O(3)-N(1')	41.27	30.86	50.50
O(4')-N(1')	22.72	30.86	50.50
O(3)-O(1')	35.51	30.86	50.50

Table 27 Continued

Edge	Observed* Angle	Theoretical 1-4-4-1	Polyhedron 2-6-2
O(4)-O(1)	43.58	30.86	50.50
O(1)-O(3')	35.51	30.86	50.50
N(1)-O(4)	22.72	30.86	50.50
N(1)-O(3')	41.27	30.86	50.50
RMS =			14.68      15.69

\*Angle calculated after all Pb-donor distances were normalized to 1.0 Å.

\*\*No value was calculated, since this is not an external edge of the polyhedron.

Table 28

A Comparison of the Interplanar Angles for the Coordination Polyhedron in  $[\text{Pb}(\text{PHENSC})(\text{NO}_3)_2]$  Complex

Edge	Observed* Angle	Theoretical Polyhedron		
		2-6-2 20°	2-6-2 40°	2-6-2 60°
N(1)-N(1')	80.18	83.96	77.50	70.85
O(3)-O(4)	77.61	85.33	82.66	81.79
O(3')-O(4')	77.61	85.33	82.66	81.79
N(1)-N(2)	70.73	53.73	55.50	58.34
N(1')-N(2')	70.73	53.73	55.50	58.34
O(1')-N(2')	57.50	53.73	55.50	58.34
O(1)-N(2)	57.50	53.73	55.50	58.34
O(1)-O(1')	54.20	83.96	77.50	70.85
O(4')-N(2')	52.83	53.15	53.16	53.06
O(4)-N(2)	52.83	53.15	53.16	53.06
O(3)-N(2')	46.34	53.15	53.16	53.06
N(2)-O(3')	46.34	53.15	53.16	53.06
O(1')-O(4')	43.58	51.96	52.70	53.06
O(1)-O(4)	43.58	51.96	52.70	53.06
N(1)-O(3')	41.27	51.96	52.70	53.06
O(3)-N(1')	41.27	51.96	52.70	53.06
O(1)-O(4')	35.58	8.89	17.45	25.82
O(4)-O(1')	35.58	8.89	17.45	25.82
O(3)-O(1')	35.51	42.39	34.11	25.82
O(1)-O(3')	35.51	42.39	34.11	25.82

Table 28 Continued

Edge	Observed* Angle	Theoretical Polyhedron		
		2-6-2 20°	2-6-2 40°	2-6-2 60°
O(3')-N(1')	31.16	8.89	17.45	25.82
O(3)-N(1)	31.16	8.89	17.45	25.82
O(4)-N(1)	22.72	42.39	34.11	25.82
O(4')-N(1')	22.72	42.39	34.11	25.82
RMS =		15.28	11.21	8.62

\* Angle calculated after all Pb-donor distances were normalized to 1.0 Å.



## CHAPTER VII

THE CRYSTAL STRUCTURE OF  $\mu$ -OXO-BIS{NITRATO[2,9-DIFORMYL-1,10-PHENANTHROLINE BIS(SEMICARBAZONE)]AQUA THORIUM(IV)}NITRATE MONOHYDRATE,  $\{[\text{Th}(\text{PHENSC})(\text{H}_2\text{O})(\text{NO}_3)]_2\text{O}\}(\text{NO}_3)_4 \cdot \text{H}_2\text{O}$

The coordination numbers eight to twelve have been reported for Th(IV) complexes, even up to sixteen in the case of  $\pi$ -complexes.<sup>141,142</sup> However, an unusual four coordination in  $\text{BH}_4\text{Th}[\text{N}(\text{Si}(\text{CH}_3)_3)_2]_3$ , which is isostructural with  $\text{CH}_3\text{Th}[\text{N}(\text{Si}(\text{CH}_3)_3)_2]_3$ , has been confirmed by an X-ray diffraction study.<sup>143</sup> Dinuclear thorium(IV) complexes are common, and the two metal atoms can be linked by various bridging groups,<sup>142,144-147</sup> but no example of bridging oxo groups has been found for Th(IV) complexes.

There are several varieties of oxo bridging compounds with the other metals. Singly-bridged complexes may have either bent or linear bridges, and the M-O-M angle can vary from  $\sim 122^\circ$  to  $180^\circ$ . These angles are  $121.7^\circ$  in  $(\text{Ph}_2\text{TeNCS})_2\text{O}$ ;<sup>148</sup>  $126-129^\circ$  in  $[(\text{CH}_3)_3\text{SbX}]_2\text{O}$  ( $\text{X} = \text{ClO}_4^-$ ,  $\text{Cl}^-$  and  $\text{N}_3^-$ );<sup>149</sup>  $157.2^\circ$  in  $\{[\text{Ru}(\text{bPy})_2(\text{NO}_2)]_2\text{O}\}(\text{ClO}_4)_2 \cdot 2\text{H}_2\text{O}$ ;<sup>150</sup>  $178 \pm 4^\circ$  in  $[(\text{C}_2\text{H}_5\text{OCS}_2)_2\text{MoO}]_2\text{O}$ ;<sup>151</sup> linear in  $\text{K}_2[\text{MoO}_2(\text{C}_2\text{O}_4)(\text{H}_2\text{O})]_2\text{O}$ ;<sup>152</sup> and  $\{[(\text{H}_2\text{O})\text{LFe}]_2\text{O}\}(\text{ClO}_4)_4$ ;<sup>153</sup> (L = pentadentate macrocyclic ligand).

In  $\mu$ -oxo-bis[4-chloro-2,6-pyridinedicarboxylatodiaquairon(III) tetrahydrate, Fe-O-Fe angle is about  $178^\circ$ .<sup>154</sup> The molecular structures of the  $\mu$ -dioxo complexes  $\text{Na}_2\text{Mo}_2\text{O}_4(\text{cysteine})_2 \cdot 5\text{H}_2\text{O}$ <sup>155</sup> and  $\{[\text{MoO}(\text{C}_2\text{O}_4)(\text{H}_2\text{O})]_2\text{O}\}^{2-}$ ,<sup>156</sup> have been studied by X-ray diffraction. A pyramidal

$\mu_3\text{-O}$  unit ( $\mu_3\text{-O}$ ) is found in  $[\text{NEt}_4]_2[\text{Re}_3\text{O}(\text{H})_3(\text{CO})_9]$  with an average Re-Re bond length of 2.968 Å.<sup>157</sup> Oxo-centered complexes  $\mu_3\text{-O}$  in  $[\text{Mn}_3(\text{Py})_3\text{O}(\text{O}_2\text{CMe})_6]^{158}$  with Mn---Mn distance 3.363 Å and  $\mu_4\text{-O}$  in  $\text{Cu}_4\text{OCl}_6(\text{Ph}_3\text{PO})_4^{159}$  and  $(\text{Et}_2\text{NH}_2)_4[\text{Cu}_4\text{OCl}_{10}]^{160}$  which oxygen atom is at the central of a tetrahedron were studied by X-ray. Finally,  $\mu_5\text{-O}$  in  $[\text{Fe}_5\text{O}(\text{O}_2\text{CMe}_2)_{12}]^+$  which spectroscopic properties of this complex shows the central oxygen atom would be five coordinate in trigonal bipyramidal geometry.<sup>161</sup>

No complex of a hexadentate ligand with Th(IV) has been reported. However, 2,9-diformyl-1,10-phenanthroline bis(semicarbazone), PHENSC, was used to produce  $[\{\text{Th}(\text{PHENSC})(\text{H}_2\text{O})(\text{NO}_3)\}_2\text{O}](\text{NO}_3)_4 \cdot \text{H}_2\text{O}$ , which was studied by X-ray diffraction. This complex is the first example of a hexadentate ligand coordinated to Th(IV) and the first oxo bridged Th(IV) complex reported.

#### A. Experimental Section

##### Preparation of $[\{\text{Th}(\text{PHENSC})(\text{H}_2\text{O})(\text{NO}_3)\}_2\text{O}](\text{NO}_3)_4 \cdot \text{H}_2\text{O}$

A slurry of equimolar amounts of thorium nitrate tetrahydrate and 1,10-phenanthroline-2,9-dicarboxaldehyde disemicarbazone was heated in 95% ethanol. Additional water was added, and the mixture was heated for about four hours. The resulting clear golden solution was filtered and provided suitable crystals after slow evaporation of the solvent. Anal. Calcd. for  $\text{C}_{32}\text{H}_{34}\text{N}_{22}\text{O}_{26}\text{Th}_2$ : C, 23.92; H, 2.13; N, 19.18. Found: C, 24.36; H, 2.23; N, 19.27.

##### Data Collection and Reduction

Preliminary photographs indicate that the space group was  $P2_1/c$ . The unit cell dimensions are reported in Table 4, and the intensity

data were measured using a Syntex PT diffractometer. The pertinent crystal data, together with some details of the intensity measurements, are given in Table 4. The  $\theta$ - $2\theta$  scan technique with a variable scan rate of 1 to  $24^\circ/\text{min}$  was used in measuring the intensity. Four standard reflections were measured every 96 reflections to monitor the beam and crystal stability. Scale factors varying from 0.983 to 1.057 were used to place all the data on approximately the same scale.

Structure Determination and Refinement

The position of the two unique thorium atoms were determined from the Patterson function and the remaining non-hydrogen atoms from successive Fourier Syntheses. The R value ( $R = \sum |F_{\text{obs}}| - |F_{\text{calc}}| / \sum |F_{\text{obs}}|$ ) was 0.13 after three least-squares cycles with 81 atoms isotropic. A difference Fourier synthesis at this point indicated a water of crystallization which was included in the subsequent calculations. Anisotropic thermal refinement of the two thorium atoms with all other atoms isotropic gave an R of 0.086 after three cycles.

The scattering factors were taken from the usual sources.<sup>88</sup> The final positional parameters for the non-hydrogen atoms and thermal parameters for thorium atoms are given in Table 29. The bond distances and angles are given in Tables 30 and 31, respectively.

### B. Results and Discussion

The two thorium atoms in the binuclear, oxo-bridged complex both have coordination numbers of ten involving six donor atoms of the planar ligand, two oxygen atoms from one bidentate nitrate group, one oxygen from water, and one oxygen from the unusual oxo bridge (see

Figures 26 and 27). The Th(1)-O(23)-Th(2) bridging angle is  $174.4(11)^\circ$ , and the Th(1)-Th(2) separation is  $4.245(2) \text{ \AA}$ . The Th-O (bridging) distances,  $2.10(2)$  and  $2.15(2) \text{ \AA}$  (average =  $2.125 \text{ \AA}$ ), are not significantly different but are much shorter than those of the Th-O(nitrate), with average distance  $2.65 \text{ \AA}$ , and Th-O(water), with average distance  $2.53 \text{ \AA}$ . The oxygen atom in Th(1)-O(23)-Th(2) linkage is much more tightly bound than that of the nitrate or water groups. The bridge bonding can be considered in terms of a three-center molecular orbital treatment. A combination of the d orbitals of the two metal atoms and the P orbital of the oxygen atom produces one bonding, one non-bonding, and one anti-bonding MO, with four electrons occupying the lower two. The linearity probably results from  $d_\pi$ - $P_\pi$  bonding through overlap of the P orbital on oxygen and the d orbitals on two thorium atoms. In tetranitratobis(triphenylphosphine oxide)thorium(IV),  $[\text{Th}(\text{NO}_3)_4(\text{OPPh}_3)_2]$ , the average Th-O (bridging) distance ( $2.35 \text{ \AA}$ ) is shorter than the average Th-O(nitrate) distance ( $2.55 \text{ \AA}$ ). These differences are smaller than those found in the Th-PHENSC complex, and also shows accordingly we conclude that the Th(1)-O(23)-Th(2) linkage is much more tightly bound than that in  $[\text{Th}(\text{NO}_3)_4(\text{OPPh}_3)_2]$ .<sup>162</sup>

#### The Water and Nitrate Groups

The average Th-O (water) and the average Th-O (nitrate) bond distances are  $2.53$  and  $2.65 \text{ \AA}$ , respectively, in  $[\text{Th}_2(\text{OH})_2(\text{NO}_3)_6(\text{H}_2\text{O})_6]$ ;<sup>147</sup>  $2.461$  and  $2.568 \text{ \AA}$ , respectively, in  $[\text{Th}(\text{NO}_3)_4(\text{H}_2\text{O})_3] \cdot 2\text{H}_2\text{O}$ .<sup>163</sup> In  $[\text{Th}(\text{NO}_3)_3(\text{PMe}_3\text{O})_4]_2[\text{Th}(\text{NO}_3)_6]$  complex,<sup>164</sup> the Th-O (nitrate) bond

distances range from 2.46 Å to 2.94 Å (average = 2.61 Å), which are similar to our results. The two bidentate nitrate groups are similar to the uncoordinated nitrate ion (see Table 25 and discussion in Chapter VI); all nitrate groups in this complex are planar.

#### The Hexadentate Ligand

The two PHENSC hexadentate ligands in the  $\{[\text{Th}(\text{PHENSC})(\text{H}_2\text{O})(\text{NO}_3)]_2\text{O}(\text{NO}_3)_4 \cdot \text{H}_2\text{O}\}$  complex are involving four nitrogen atoms and two oxygen atoms. No hexadentate ligand containing nitrogen atoms have been reported for Th(IV), and no Th-N bond lengths are available for ten coordination of Th(IV) to compare with our results. The average Th-O (PHENSC) bond distance is 2.46 Å, and the average Th-N bond length is 2.74 Å, which is larger than Th-N bond distances in the eight coordinations of tetrakisothiocyanato tetrakis (tetramethylurea) thorium(IV) (average = 2.52 Å)<sup>165</sup> and bis(N,N'-O-phenylenebis(salicylaldiminato) thorium(IV) (average = 2.66 Å),<sup>166</sup> which is not surprising.

The least-squares planes data are given in Tables 32 and 33 for Th(1) and Th(2), respectively. The deviations of the six donor atoms are from -0.371 to 0.366 Å for Th(1) and from -0.324 to 0.476 Å for Th(2), which are significantly larger than the deviations of the five donor atoms in  $[\text{Co}(\text{PHENSC})(\text{H}_2\text{O})_2](\text{NO}_3)_2$ . Dihedral angles for the  $\{[\text{Th}(\text{PHENSC})(\text{H}_2\text{O})(\text{NO}_3)]_2\text{O}(\text{NO}_3)_4 \cdot \text{H}_2\text{O}\}$  are given in Table 34. The two side arms are twisted (side (1), 6.7° and side (2), 7.3°) for Th(1) and (side (1), 7.1° and side (2), 17.6°) for Th(2) relative to the 1,10-phenanthroline rings. The 1,10-phenanthroline rings and planes containing six donors in Th(1) and Th(2) (with angles 1.2° and 2.8°,

respectively) are almost parallel. However, the angle between side (1) - side (1) is  $11.3^\circ$ , which is slightly smaller than angle between side(2) - side (2) ( $13.4^\circ$ ) (see Table 34). Therefore, the two side (1) arms are twisted in the opposite direction, but the two side (2) arms are twisted in the same direction.

### The Coordination Polyhedron

We have evaluated the relative stabilities of eclipsed 1-6-3 and staggered 1-6-3 polyhedron geometries. After energy minimization procedure, we found the eclipsed form is of lower energy, because the six donors in the plane deviate markedly from planarity with respect to the staggered form (three donors go up and three donors go down). The RMS around Th(1) and Th(2) in this complex are given in Tables 35 and 36, respectively. The RMS indicates that the staggered form is more favorable for both thoriums but is significantly better for Th(2), which is not surprising. We have also considered the 1-3-6 (eclipsed and staggered) polyhedron without the energy minimization procedure to see which form is more favorable for Th(1) and Th(2) (see Tables 37 and 38). The RMS values indicate the eclipsed form is more favorable for Th(1), and the staggered form is more favorable for Th(2) in this complex.

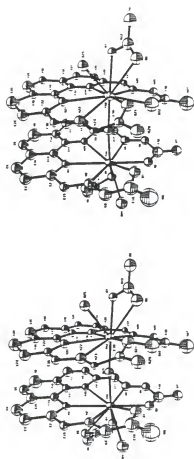


Figure 26. Stereoscopic view of  $\{[\text{Th}(\text{PHNSC})(\text{H}_2\text{O})(\text{NO}_3)_2\text{O}]_2(\text{NO}_3)_4 \cdot 4\text{H}_2\text{O}\}$ .

Figure 27. An ORTEP view of  $\{[\text{Th}(\text{PHENSC})(\text{H}_2\text{O})(\text{NO}_3)]_2\text{O}\}(\text{NO}_3)_4 \cdot \text{H}_2\text{O}$  showing the atomic numbering and the thermal ellipsoids (50% probability level).





Table 29

Final Parameters for  $[(\text{Th}[\text{PHENSC}])_2\text{O}(\text{NO}_3)_2(\text{H}_2\text{O})_2](\text{NO}_3)_4 \cdot 2\text{H}_2\text{O}$ .  
 The positional parameters are  $\times 10^5$  for the Th atoms and  $\times 10^3$   
 for the light atoms. The B is the isotropic  
 thermal parameter for the light atoms.

ATOM	X	Y	Z	B
TH(1)	18080(11)	43557(4)	60368(5)	*
TH(2)	19013(11)	39556(4)	91537(9)	*
O(1)	72(2)	505(1)	671(2)	3.2(5)
O(2)	17(2)	417(1)	578(2)	2.7(5)
O(3)	181(2)	391(1)	425(2)	3.0(5)
O(4)	290(2)	453(1)	453(2)	2.8(5)
C(5)	301(2)	402(1)	323(2)	4.9(6)
O(6)	91(2)	383(1)	1074(2)	3.4(5)
O(7)	194(2)	323(1)	1061(1)	2.1(4)
C(8)	126(2)	329(1)	1200(2)	3.7(6)
O(9)	407(2)	349(1)	140(2)	5.4(7)
C(10)	494(3)	415(1)	136(2)	5.6(7)
O(11)	551(3)	345(2)	211(4)	10.4(10)
O(12)	879(3)	328(1)	96(4)	8.3(9)
C(13)	983(2)	271(1)	68(3)	6.0(7)
O(14)	850(3)	245(1)	118(3)	6.2(7)
O(15)	908(2)	296(1)	344(3)	5.7(7)
O(16)	767(2)	326(1)	350(3)	7.5(9)
O(17)	794(3)	243(1)	354(3)	7.0(7)
C(18)	199(2)	550(1)	306(2)	4.9(7)
O(19)	170(3)	476(1)	236(3)	7.8(9)
O(20)	222(3)	537(1)	149(2)	6.6(5)
C(21)	112(2)	475(1)	958(2)	3.1(5)
O(22)	22(2)	390(1)	869(3)	5.4(6)
C(23)	191(1)	415(1)	760(1)	2.5(5)
O(24)	118(2)	502(1)	469(2)	3.9(5)
O(25)	279(2)	423(1)	1079(1)	2.4(5)
C(26)	292(2)	627(1)	888(2)	5.6(6)
N(1)	362(2)	463(1)	632(2)	1.8(4)
N(2)	238(2)	539(1)	659(2)	2.1(6)
N(3)	168(3)	572(1)	669(2)	3.6(7)
N(4)	18(3)	588(1)	697(4)	6.0(10)
N(5)	127(2)	339(1)	594(2)	3.1(7)
N(6)	34(2)	330(1)	582(2)	2.6(5)
N(7)	-110(2)	365(1)	574(3)	3.4(7)
N(10)	317(2)	363(1)	617(2)	1.8(5)
N(11)	256(2)	413(1)	393(2)	2.8(5)
N(12)	129(2)	346(1)	1111(2)	3.2(7)
N(13)	482(2)	366(1)	162(3)	5.4(8)
N(14)	898(3)	280(1)	87(3)	5.4(9)
N(15)	825(2)	290(1)	343(3)	4.9(8)
N(16)	196(2)	521(1)	232(2)	3.5(7)
N(21)	378(2)	403(1)	896(2)	2.2(4)
N(22)	277(2)	489(1)	902(2)	2.6(7)
N(23)	215(2)	532(1)	912(2)	1.0(5)
N(24)	71(2)	561(1)	955(2)	3.0(6)
N(25)	104(2)	305(1)	856(2)	2.1(6)
N(26)	12(2)	304(1)	843(2)	2.4(6)
N(27)	-124(3)	354(1)	834(3)	6.0(9)
N(30)	256(2)	309(1)	876(2)	2.2(6)
C(2)	398(3)	511(1)	646(2)	2.9(7)
C(3)	494(3)	528(1)	650(3)	3.5(7)
C(4)	559(3)	488(1)	642(3)	3.7(8)
C(5)	595(3)	393(2)	632(3)	3.4(7)
C(6)	572(3)	344(2)	625(3)	6.6(14)
C(7)	440(4)	279(2)	617(4)	4.5(13)
C(8)	348(3)	272(1)	617(2)	2.8(7)
C(9)	278(3)	313(1)	612(2)	2.7(7)
C(11)	405(2)	372(1)	618(3)	2.5(7)
C(12)	468(3)	333(1)	619(2)	3.0(7)
C(13)	432(2)	427(1)	634(2)	2.3(8)

Table 29 Continued

ATOM	X	Y	Z	B
C(14)	531(2)	436(1)	638(3)	3.7(9)
C(15)	327(2)	551(1)	659(2)	2.1(7)
C(16)	81(3)	556(1)	679(3)	4.3(10)
C(17)	188(3)	301(1)	603(3)	3.1(9)
C(18)	-25(3)	372(1)	571(3)	3.9(8)
C(22)	423(2)	449(1)	897(2)	1.8(6)
C(23)	515(3)	455(1)	887(3)	3.1(7)
C(24)	585(3)	413(1)	902(3)	4.4(8)
C(25)	582(3)	316(1)	888(3)	4.6(9)
C(26)	542(2)	268(1)	879(2)	2.3(7)
C(27)	394(3)	219(1)	859(3)	2.5(7)
C(28)	303(3)	216(1)	846(2)	2.3(6)
C(29)	248(3)	263(1)	860(2)	2.4(5)
C(31)	384(3)	311(1)	879(2)	2.1(7)
C(32)	441(3)	266(1)	871(3)	2.5(7)
C(33)	433(3)	360(1)	889(2)	2.0(6)
C(34)	529(3)	364(1)	892(2)	2.2(6)
C(35)	369(2)	494(1)	900(2)	1.7(6)
C(36)	132(3)	522(1)	941(3)	1.8(5)
C(37)	149(2)	260(1)	851(2)	1.4(5)
C(38)	-33(3)	352(1)	853(2)	2.7(7)

\* THE ANISOTROPIC VALUES (UIJ) FOR TH(1) AND TH(2) ARE GIVEN BELOW.

ATOM	U11	U22	U33	U12	U13	U23
TH(1)	432(12)	147(6)	290(6)	-21(6)	32(7)	18(5)
TH(2)	412(12)	133(6)	293(6)	-8(6)	44(7)	-1(5)

Table 30

Bond Distances (in Å) for  $[(\text{Th}[\text{PHENSC}])_2\text{O}(\text{NO}_3)_2(\text{H}_2\text{O})_2](\text{NO}_3)_4 \cdot \text{H}_2\text{O}$   
 With Estimated Standard Deviations

<u>In the Cation</u>			
Th(1)-O(1)	2.50(2)	Th(2)-O(21)	2.42(2)
Th(1)-O(2)	2.45(3)	Th(2)-O(22)	2.46(3)
Th(1)-O(3)	2.66(2)	Th(2)-O(6)	2.62(3)
Th(1)-O(4)	2.63(2)	Th(2)-O(7)	2.69(2)
Th(1)-O(23)	2.15(2)	Th(2)-O(23)	2.10(2)
Th(1)-O(24)	2.52(2)	Th(2)-O(25)	2.54(2)
Th(1)-N(1)	2.69(3)	Th(2)-N(21)	2.75(3)
Th(1)-N(2)	2.77(2)	Th(2)-N(22)	2.73(2)
Th(1)-N(5)	2.71(2)	Th(2)-N(25)	2.74(2)
Th(1)-N(10)	2.78(3)	Th(2)-N(30)	2.79(3)
Th(1)-Th(2)	4.245(2)		
O(1)-C(16)	1.33(4)	O(21)-C(36)	1.30(3)
O(2)-C(18)	1.31(4)	O(22)-C(38)	1.28(4)
O(3)-N(11)	1.32(4)	O(6)-N(12)	1.20(4)
O(4)-N(11)	1.36(3)	O(7)-N(12)	1.33(4)
O(5)-N(11)	1.20(4)	O(8)-N(12)	1.24(3)
N(1)-C(2)	1.34(4)	N(21)-C(22)	1.35(4)
N(1)-C(13)	1.38(4)	N(21)-C(33)	1.37(4)
N(2)-N(3)	1.34(4)	N(22)-N(23)	1.44(3)
N(2)-C(15)	1.32(4)	N(22)-C(35)	1.33(4)
N(3)-C(16)	1.34(6)	N(23)-C(36)	1.30(4)

Table 30 Continued

N(4)-C(16)	1.27(6)	N(24)-C(36)	1.34(4)
N(5)-N(6)	1.37(4)	N(25)-N(26)	1.32(4)
N(5)-C(17)	1.32(4)	N(25)-C(37)	1.34(4)
N(6)-C(18)	1.38(4)	N(26)-C(38)	1.40(4)
N(7)-C(18)	1.24(5)	N(27)-C(38)	1.33(6)
N(10)-C(9)	1.41(4)	N(30)-C(29)	1.39(4)
N(10)-C(11)	1.29(5)	N(30)-C(31)	1.27(5)
C(2)-C(3)	1.44(6)	C(22)-C(23)	1.35(5)
C(2)-C(15)	1.48(5)	C(22)-C(35)	1.40(4)
C(3)-C(4)	1.40(6)	C(23)-C(24)	1.50(5)
C(4)-C(14)	1.40(5)	C(24)-C(34)	1.50(5)
C(5)-C(6)	1.32(7)	C(25)-C(26)	1.38(5)
C(5)-C(14)	1.46(5)	C(25)-C(34)	1.46(5)
C(6)-C(12)	1.53(6)	C(26)-C(32)	1.46(5)
C(7)-C(8)	1.34(7)	C(27)-C(28)	1.32(5)
C(7)-C(12)	1.45(6)	C(27)-C(32)	1.39(4)
C(8)-C(9)	1.45(5)	C(28)-C(29)	1.46(4)
C(9)-C(17)	1.34(6)	C(29)-C(37)	1.43(5)
C(11)-C(12)	1.36(5)	C(31)-C(32)	1.43(4)
C(11)-C(13)	1.48(4)	C(31)-C(33)	1.45(4)
C(13)-C(14)	1.44(5)	C(33)-C(34)	1.38(5)

Table 30 Continued

<u>In the Anions</u>			
N(13)-O(9)	1.21(4)	N(15)-O(15)	1.20(5)
N(13)-O(10)	1.30(4)	N(15)-O(16)	1.26(4)
N(13)-O(11)	1.27(6)	N(15)-O(17)	1.30(4)
N(14)-O(12)	1.28(4)	N(16)-O(18)	1.24(4)
N(14)-O(13)	1.30(5)	N(16)-O(19)	1.22(4)
N(14)-O(14)	1.23(5)	N(16)-O(20)	1.25(4)

---

Table 31

Bond Angles (in deg) in  $[(\text{Th}[\text{PHENSC}])_2\text{O}(\text{NO}_3)_2(\text{H}_2\text{O})_2](\text{NO}_3)_4 \cdot \text{H}_2\text{O}$ 

<u>In the Cation</u>			
O(1)-Th(1)-O(2)	65.5(8)	O(21)-Th(2)-O(22)	68.7(9)
O(1)-Th(1)-N(2)	58.1(8)	O(21)-Th(2)-N(22)	59.5(8)
O(2)-Th(1)-N(5)	59.4(8)	O(22)-Th(2)-N(25)	57.5(9)
O(3)-Th(1)-O(4)	50.4(7)	O(6)-Th(2)-O(7)	48.4(7)
O(3)-Th(1)-O(24)	72.8(8)	O(6)-Th(2)-O(25)	68.3(8)
O(4)-Th(1)-O(24)	66.3(8)	O(7)-Th(2)-O(25)	66.6(7)
O(23)-Th(1)-O(1)	82.4(8)	O(23)-Th(2)-O(21)	93.2(8)
O(23)-Th(1)-O(2)	94.0(8)	O(23)-Th(2)-O(22)	80.8(9)
O(23)-Th(1)-N(1)	85.6(8)	O(23)-Th(2)-N(21)	79.9(8)
O(23)-Th(1)-N(2)	91.1(8)	O(23)-Th(2)-N(22)	72.3(8)
O(23)-Th(1)-N(5)	76.6(8)	O(23)-Th(2)-N(25)	87.8(8)
O(23)-Th(1)-N(10)	73.8(7)	O(23)-Th(2)-N(30)	88.6(8)
N(1)-Th(1)-N(2)	58.8(8)	N(21)-Th(2)-N(22)	57.9(8)
N(1)-Th(1)-N(10)	58.5(8)	N(21)-Th(2)-N(30)	59.0(8)
N(5)-Th(1)-N(10)	61.3(8)	N(25)-Th(2)-N(30)	60.1(8)
Th(1)-O(1)-C(16)	128.9(23)	Th(2)-O(21)-C(36)	130.3(21)
Th(1)-O(2)-C(18)	131.6(23)	Th(2)-O(22)-C(38)	132.6(24)
Th(1)-O(3)-N(11)	96.8(17)	Th(2)-O(6)-N(12)	99.5(20)
Th(1)-O(4)-N(11)	97.3(17)	Th(2)-O(7)-N(12)	92.9(16)
Th(1)-N(1)-C(2)	126.2(22)	Th(2)-N(21)-C(22)	122.6(20)
Th(1)-N(1)-C(13)	123.1(20)	Th(2)-N(21)-C(33)	121.4(21)
Th(1)-N(2)-N(3)	114.0(20)	Th(2)-N(22)-N(23)	112.6(16)

Table 31 Continued

Th(1)-N(2)-C(15)	120.1(20)	Th(2)-N(22)-C(35)	123.3(20)
Th(1)-N(5)-N(6)	116.5(20)	Th(2)-N(25)-N(26)	118.3(18)
Th(1)-N(5)-C(17)	122.0(22)	Th(2)-N(25)-C(37)	123.3(20)
Th(1)-N(10)-C(9)	112.1(20)	Th(2)-N(30)-C(29)	116.2(20)
Th(1)-N(10)-C(11)	124.9(22)	Th(2)-N(30)-C(31)	120.7(21)
O(1)-C(16)-N(3)	113.2(34)	O(21)-C(36)-N(23)	117.5(29)
O(1)-C(16)-N(4)	126.9(39)	O(21)-C(36)-N(24)	121.0(30)
O(2)-C(18)-N(6)	114.1(32)	O(22)-C(38)-N(26)	113.8(30)
O(2)-C(18)-N(7)	125.1(36)	O(22)-C(38)-N(27)	127.8(35)
O(3)-N(11)-O(4)	114.9(25)	O(6)-N(12)-O(7)	118.9(28)
O(3)-N(11)-O(5)	128.8(29)	O(6)-N(12)-O(8)	127.9(30)
O(4)-N(11)-O(5)	116.2(28)	O(7)-N(12)-O(8)	112.0(26)
N(1)-C(2)-C(3)	130.1(34)	N(21)-C(22)-C(23)	125.2(30)
N(1)-C(2)-C(15)	113.2(30)	N(21)-C(22)-C(35)	117.3(28)
N(1)-C(13)-C(11)	118.1(28)	N(21)-C(33)-C(31)	116.2(28)
N(1)-C(13)-C(14)	126.5(29)	N(21)-C(33)-C(34)	121.5(30)
N(2)-N(3)-C(16)	122.0(32)	N(22)-N(23)-C(36)	117.9(24)
N(2)-C(15)-C(2)	120.5(28)	N(22)-C(35)-C(22)	118.6(28)
N(3)-N(2)-C(15)	125.3(28)	N(23)-N(22)-C(35)	123.6(24)
N(3)-C(16)-N(4)	119.9(39)	N(23)-C(36)-N(24)	121.5(30)
N(5)-N(6)-C(18)	118.4(28)	N(25)-N(26)-C(38)	116.7(26)
N(5)-C(17)-C(9)	117.7(32)	N(25)-C(37)-C(29)	115.7(27)
N(6)-C(18)-N(7)	119.4(35)	N(26)-C(38)-N(27)	118.0(32)
N(10)-C(9)-C(8)	113.7(30)	N(30)-C(29)-C(28)	117.4(28)
N(10)-C(9)-C(17)	126.8(33)	N(30)-C(29)-C(37)	123.2(28)



Table 31 Continued

N(10)-C(11)-C(12)	122.4(33)	N(30)-C(31)-C(32)	121.7(29)
N(10)-C(11)-C(13)	114.4(30)	N(30)-C(31)-C(33)	121.7(29)
C(2)-N(1)-C(13)	110.7(28)	C(22)-N(21)-C(33)	115.9(27)
C(2)-C(33)-C(4)	114.8(34)	C(22)-C(23)-C(24)	123.9(33)
C(3)-C(2)-C(15)	116.8(31)	C(23)-C(22)-C(35)	117.3(30)
C(3)-C(4)-C(14)	120.2(35)	C(23)-C(24)-C(34)	104.7(32)
C(4)-C(14)-C(5)	122.8(34)	C(24)-C(34)-C(25)	115.5(32)
C(4)-C(14)-C(13)	117.1(32)	C(24)-C(34)-C(33)	126.2(32)
C(5)-C(6)-C(12)	115.6(40)	C(25)-C(26)-C(32)	116.2(30)
C(5)-C(14)-C(13)	120.0(32)	C(25)-C(34)-C(33)	118.3(31)
C(6)-C(5)-C(14)	125.4(38)	C(26)-C(25)-C(34)	123.4(34)
C(6)-C(12)-C(7)	117.4(35)	C(26)-C(32)-C(27)	120.4(30)
C(6)-C(12)-C(11)	121.1(34)	C(26)-C(32)-C(31)	123.1(29)
C(7)-C(8)-C(9)	125.3(35)	C(27)-C(28)-C(29)	117.6(30)
C(7)-C(12)-C(11)	121.4(35)	C(27)-C(32)-C(31)	116.4(30)
C(8)-C(7)-C(12)	114.1(38)	C(28)-C(27)-C(32)	123.3(32)
C(8)-C(9)-C(17)	119.5(33)	C(28)-C(29)-C(37)	119.2(28)
C(9)-N(10)-C(11)	122.7(29)	C(29)-N(30)-C(31)	122.9(28)
C(11)-C(13)-C(14)	114.9(29)	C(31)-C(33)-C(34)	122.3(30)
C(12)-C(11)-C(13)	122.5(32)	C(32)-C(31)-C(33)	116.5(28)
C(17)-N(5)-N(6)	121.5(28)	C(37)-N(25)-N(26)	118.0(26)
Th(1)-O(23)-Th(2)	174.4(11)		

Table 31 Continued

<u>In the Anions</u>			
O(9)-N(13)-O(10)	115.3(34)	O(15)-N(15)-O(16)	124.2(35)
O(10)-N(13)-O(11)	116.0(37)	O(16)-N(15)-O(17)	116.2(34)
O(11)-N(13)-O(9)	128.6(39)	O(17)-N(15)-O(15)	118.6(34)
O(12)-N(14)-O(13)	114.2(34)	O(18)-N(16)-O(19)	123.3(34)
O(13)-N(14)-O(14)	119.4(34)	O(19)-N(16)-O(20)	117.4(34)
O(14)-N(14)-O(12)	124.2(36)	O(20)-N(16)-O(18)	119.2(32)

---

Table 32

Least-Squares Planes for Th(1)-PHENSC in  
 $[(\text{Th}[\text{PHENSC}])_2\text{O}(\text{NO}_3)_2(\text{H}_2\text{O})_2](\text{NO}_3)_4 \cdot \text{H}_2\text{O}^a$

Atom	PHEN	Side (1)	Side (2)	Donors
Th(1)	-294	176	-528	-281
O(1)	526	1256	13*	366*
O(2)	-521	18*	-1005	-371*
N(1)	-36*	353	8	-168*
N(2)	238	925	-26*	-85*
N(3)	354	1184	-71*	-48
N(4)	755	1750	47*	352
N(5)	-237	10*	-441	108*
N(6)	-341	-44*	-693	70
N(7)	-441	63*	-1080	-83
N(10)	-46*	114	41	150*
C(2)	48*	534	94	-247
C(3)	47*	501	236	-337
C(4)	-30*	267	320	-314
C(5)	-9*	9	517	-13
C(6)	-17*	-111	530	142
C(7)	45*	-116	443	455
C(8)	92*	-14	340	558
C(9)	-21*	37	61	345
C(11)	-84*	28	145	53

Table 32 Continued

Atom	PHEN	Side (1)	Side (2)	Donors
C(12)	-35*	-76	347	198
C(13)	26*	262	232	-19
C(14)	19*	202	382	-94
C(15)	181	831	55*	-214
C(16)	539	1397	-19*	217
C(17)	-70	27*	-127	369
C(18)	-528	-74*	-1029	-223
$\ell$	-0.0282	-0.0834	0.0909	-0.0539
m	-0.0639	0.0384	-0.1098	-0.1834
n	0.9976	0.9958	0.9898	0.9816
p	7.406	7.967	7.310	5.855

<sup>a</sup> The title of the plane is followed by the deviations ( $\times 10^3$  Å) of the atoms listed in the left-hand column. The atoms used to define the plane are denoted by asterisks. The deviation equals  $\ell X + mY + nZ - p$ , where X, Y, and Z are the orthogonal coordinates (in Å) relative to a, b, and c sin  $\beta$ ;  $\ell$ , m and n are the direction cosines; and p is the distance of the plane from the origin (in Å).

Table 33

Least-Squares Planes for Th(2)-PHENSC in  
 $[(\text{Th}[\text{PHENSC}])_2\text{O}(\text{NO}_3)_2(\text{H}_2\text{O})_2](\text{NO}_3)_4 \cdot \text{H}_2\text{O}^{\text{a}}$

Atom	PHEN	Side (1)	Side (2)	Donors
Th(2)	490	226	-441	287
O(21)	950	641	37*	476*
O(22)	-1	-10*	-1554	-278*
N(21)	99*	-442	-88	-11*
N(22)	81	-481	-125*	-324*
N(23)	166	-391	-96*	-396
N(24)	766	351	66*	33
N(25)	-50	-11*	-1653	-43*
N(26)	-166	6*	-2105	-208
N(27)	-296	-23*	-2534	-551
N(30)	75*	-167	-805	181*
C(22)	-11*	-702	162	-221
C(23)	-208*	-1040	337	-380
C(24)	21*	-831	640	4
C(25)	36*	-627	246	285
C(26)	35*	-477	-105	396
C(27)	-36*	-244	-919	375
C(28)	-138*	-208	-1371	232
C(29)	-8*	-92	-1254	199
C(31)	54*	-318	-489	203

Table 33 Continued

Atom	PHEN	Side (1)	Side (2)	Donors
C(32)	-7*	-372	-525	300
C(33)	63*	-473	-99	104
C(34)	24*	-654	233	110
C(35)	-23	-723	135*	-388
C(36)	610	183	-16*	20
C(37)	-65	-2*	-1688	94
C(38)	-105	39*	-2017	-306
l	-0.0446	-0.1427	0.2138	-0.0042
m	-0.0754	-0.1490	0.0874	-0.1816
n	0.9962	0.9785	0.9730	0.9834
p	10.609	9.712	13.444	9.655

<sup>a</sup> The title of the plane is followed by the deviations ( $\times 10^3$  Å) of the atoms listed in the left-hand column. The atoms used to define the plane are denoted by asterisks. The deviation equals  $lX+mY+nZ-p$ , where X, Y, and Z are the orthogonal coordinates (in Å) relative to a, b, and c sin  $\beta$ ; l, m and n are the direction cosines; and p is the distance of the plane from the origin (in Å).

Table 34

Dihedral Angles for Various Planes In  $[(\text{Th}[\text{PHENSC}])_2\text{O}(\text{NO}_3)_2(\text{H}_2\text{O})_2](\text{NO}_3)_4 \cdot \text{H}_2\text{O}$ 

In Th(1)-PHENSC		In Th(2)-PHENSC	
Plane (1)	Plane (2)	Plane (1)	Plane (2)
Angle (deg)		Angle (deg)	
Phen	Side (1)	Phen	Side (1)
			7.1
Phen	Side (2)	Phen	Side (2)
			17.6
Side (1)	Side (2)	Side (1)	Side (2)
			24.7

Plane In Th(1)-PHENSC	Plane In Th(2)-PHENSC	Angle (deg)
Phen	Phen	1.2
6 Donors	6 Donors	2.8
Side (1)	Side (1)	11.3
Side (2)	Side (2)	13.4

Table 35

A Comparison of the Interplanar Angles for the Coordination Polyhedron in  $\{[\text{Th}(\text{PHENSC})(\text{H}_2\text{O})(\text{NO}_3)]_2\text{O}\}(\text{NO}_3)_4 \cdot \text{H}_2\text{O}$  Around Th(1)

Edge	Observed* Angle	Theoretical Polyhedron	
		1-6-3 Staggered	1-6-3 Eclipsed
O(1)-O(23)	56.27	40.09	70.90
O(2)-O(23)	27.04	40.09	10.27
N(1)-O(23)	37.68	40.09	70.90
N(2)-O(23)	33.21	40.09	10.27
N(5)-O(23)	50.39	40.09	70.90
N(10)-O(23)	48.67	40.09	10.27
O(1)-O(2)	66.17	75.50	62.36
O(2)-N(5)	68.45	58.85	62.36
N(5)-N(10)	55.04	75.50	62.36
N(10)-N(1)	59.28	58.85	62.36
N(1)-N(2)	71.68	75.50	62.36
N(2)-O(1)	66.66	58.85	62.36
O(3)-O(4)	60.19	61.30	46.35
O(3)-O(24)	41.53	61.30	46.35
O(4)-O(24)	51.66	61.30	46.35
O(3)-N(5)	52.59	57.98	38.58
O(3)-O(2)	33.29	57.98	47.58
O(3)-N(10)	31.74	**	47.58
O(4)-N(1)	57.79	57.98	38.58
O(4)-N(10)	27.62	57.98	47.58
O(4)-N(2)	18.57	**	47.58



Table 35 Continued

Edge	Observed* Angle	Theoretical Polyhedron	
		1-6-3 Staggered	1-6-3 Eclipsed
O(24)-O(1)	47.00	57.98	38.58
O(24)-N(2)	45.46	57.98	47.58
O(24)-O(2)	45.13	**	47.58
		RMS = 13.53	17.23

\*Angle calculated after all Th-donor distances were normalized to 1.0 Å.

\*\*No value was calculated, since this is not an external edge of the polyhedron.

Table 36

A Comparison of the Interplanar Angles for the Coordination Polyhedron in  $\{[\text{Th}(\text{PHENSC})(\text{H}_2\text{O})(\text{NO}_3)]_2\text{O}\}(\text{NO}_3)_4 \cdot \text{H}_2\text{O}$  Around Th(2)

Edge	Observed* Angle	Theoretical Polyhedron	
		1-6-3 Staggered	1-6-3 Eclipsed
O(21)-O(23)	25.37	40.09	10.27
O(22)-O(23)	55.76	40.09	70.90
N(21)-O(23)	41.01	40.09	10.27
N(22)-O(23)	56.00	40.09	70.90
N(25)-O(23)	38.31	40.09	10.27
N(30)-O(23)	36.97	40.09	70.90
O(21)-O(22)	60.42	58.85	62.36
O(22)-N(25)	70.01	75.50	62.36
N(25)-N(30)	63.43	58.85	62.36
N(30)-N(21)	78.30	75.50	62.36
N(21)-N(22)	57.47	58.85	62.36
N(22)-O(21)	67.44	75.50	62.36
O(6)-O(7)	62.88	61.30	46.35
O(6)-O(25)	41.52	61.30	46.35
O(7)-O(25)	54.26	61.30	46.35
O(6)-O(22)	50.44	57.98	38.58
O(6)-O(21)	50.07	57.98	47.58
O(6)-N(25)	13.98	**	47.58
O(7)-N(30)	58.58	57.98	38.58
O(7)-N(25)	45.54	57.98	47.58

Table 36 Continued

Edge	Observed* Angle	Theoretical Polyhedron	
		1-6-3 Staggered	1-6-3 Eclipsed
O(7)-N(21)	**	**	47.58
O(25)-N(21)	56.19	57.98	47.58
O(25)-O(21)	32.55	**	47.58
O(25)-N(22)	44.48	57.98	38.58
RMS = 9.38			16.93

\*Angle calculated after all Th-donor distances were normalized to 1.0 Å.

\*\*No value was calculated, since this is not an external edge of the polyhedron.

Table 37

A Comparison of the Interplanar Angles for the Coordination Polyhedron in  $\{[\text{Th}(\text{PHENSC})(\text{H}_2\text{O})(\text{NO}_3)]_2\text{O}\}(\text{NO}_3)_4 \cdot \text{H}_2\text{O}$  Around Th(1)

Edge	Observed* Angle	Theoretical Polyhedron	
		1-6-3 Staggered	1-6-3 Eclipsed
O(1)-O(23)	56.27	44.42	44.42
O(2)-O(23)	27.04	44.42	44.42
N(1)-O(23)	37.68	44.42	44.42
N(2)-O(23)	33.21	44.42	44.42
N(5)-O(23)	50.39	44.42	44.42
N(10)-O(23)	48.67	44.42	44.42
O(1)-O(2)	66.17	76.32	67.46
O(2)-N(5)	68.45	63.80	67.46
N(5)-N(10)	55.04	76.32	67.46
N(10)-N(1)	59.28	63.80	67.46
N(1)-N(2)	71.68	76.32	67.46
N(2)-O(1)	66.66	63.80	67.46
O(3)-O(4)	60.19	54.57	49.11
O(3)-O(24)	41.53	54.57	49.11
O(4)-O(24)	51.66	54.57	49.11
O(3)-N(5)	52.59	53.06	53.13
O(3)-O(2)	33.29	53.06	28.56
O(3)-N(10)	31.74	**	28.56
O(4)-N(1)	57.79	53.06	53.13
O(4)-N(10)	27.62	53.06	28.56

Table 37 Continued

Edge	Observed* Angle	Theoretical Polyhedron	
		1-6-3 Staggered	1-6-3 Eclipsed
O(4)-N(2)	18.57	**	28.56
O(24)-O(1)	47.00	53.06	53.13
O(24)-N(2)	45.46	53.06	28.56
O(24)-O(2)	45.13	**	28.56
		RMS = 11.53	8.97

\* Angle calculated after all Th-donor distances were normalized to 1.0 Å.

\*\*No value was calculated, since this is not an external edge of the polyhedron.

Table 38

A Comparison of the Interplanar Angles for the Coordination Polyhedron in  $\{[\text{Th}(\text{PHENSC})(\text{H}_2\text{O})(\text{NO}_3)]_2\text{O}\}(\text{NO}_3)_4 \cdot \text{H}_2\text{O}$  Around Th(2)

Edge	Observed* Angle	Theoretical Polyhedron	
		1-6-3 Staggered	1-6-3 Eclipsed
O(21)-O(23)	25.37	44.42	44.42
O(22)-O(23)	55.76	44.42	44.42
N(21)-O(23)	41.01	44.42	44.42
N(22)-O(23)	56.00	44.42	44.42
N(25)-O(23)	38.31	44.42	44.42
N(30)-O(23)	36.97	44.42	44.42
O(21)-O(22)	60.42	63.80	67.46
O(22)-N(25)	70.01	76.32	67.46
N(25)-N(30)	63.43	63.80	67.46
N(30)-N(21)	78.30	76.32	67.46
N(21)-N(22)	57.47	63.80	67.46
N(22)-O(21)	67.44	76.32	67.46
O(6)-O(7)	62.88	54.57	49.11
O(6)-O(25)	41.52	54.57	49.11
O(7)-O(25)	54.26	54.57	49.11
O(6)-O(22)	50.44	53.06	53.13
O(6)-O(21)	50.07	53.06	28.56
O(6)-N(25)	13.98	**	28.56
O(7)-N(30)	58.58	53.06	53.13
O(7)-N(25)	45.54	53.06	28.56

Table 38 Continued

Edge	Observed* Angle	Theoretical Polyhedron	
		1-6-3 Staggered	1-6-3 Eclipsed
O(7)-N(21)	**	**	28.56
O(25)-N(21)	56.19	53.06	28.56
O(25)-O(21)	32.55	**	28.56
O(25)-N(22)	44.48	53.06	53.13
		RMS = 8.15	11.96

\* Angle calculated after all Th-donor distances were normalized to 1.0 Å.

\*\*No value was calculated, since this is not an external edge of the polyhedron.

## APPENDIX

The  $[\text{Mn}(\text{urea})_6](\text{ClO}_4)_3$  was corrected for diamagnetism by using Pascal's constants.<sup>48,109</sup>

### Pascal's Corrections for Diamagnetism

C	$-6.00 \times 10^{-6}$ c.g.s. Units
H	-2.93
N	-5.57
O	-4.61
$\text{ClO}_4^-$	-32.0
$\text{Mn}^{3+}$	-10.0



## REFERENCES

1. H.A. Jahn and E. Teller, Proc. Roy. Soc. A161, 220 (1937).
2. H.A. Jahn, Proc. Roy. Soc. A164, 117 (1938).
3. F. Basolo, R. Johnson, "Coordination Chemistry," W.A. Benjamin, Inc., Menlo Park, California, 1964.
4. J.E. Huheey, "Inorganic Chemistry," 2nd Ed., Harper and Row, New York, 1978.
5. F.A. Cotton, "Chemical Applications of Group Theory," 2nd Ed., John Wiley and Sons, New York, 1971.
6. F.A. Cotton and G. Wilkinson, "Advanced Inorganic Chemistry," 4th Ed., John Wiley and Sons, New York, 1980.
7. B.N. Figgis, "Introduction to Ligand Fields," John Wiley and Sons, New York, 1966.
8. A.D. Liehr, Progress in Inorganic Chemistry 3, 281 (1962).
9. I.B. Bersuker, Coord. Chem. Rev. 14, 357 (1975).
10. C.J. Ballhausen, "Introduction to Ligand Field Theory," McGraw-Hill, New York, 1962.
11. J.H. Ammeter, H.B. Bürgi, E. Gamp, V. Meyer-Sandrin and W.P. Jensen, Inorg. Chem. 18, 733 (1979).
12. D. Reinen and C. Friebe, Struct. Bonding 37, 1 (1979).
13. B. Hathaway, M. Duggan, A. Murphy, J. Mullane, C. Power, A. Walsh and B. Walsh, Coord. Chem. Rev. 36, 267 (1981).
14. J.A. Bertrand and D.A. Carpenter, Inorg. Chem. 5, 514 (1966).
15. J.A. Bertrand, D.A. Carpenter and A.R. Kalyanaraman, Inorg. Chim. Acta. 5, 113 (1971).
16. M.G.B. Drew, R.W. Matthews and R.A. Walton, J. Chem. Soc. (A), 1405 (1970).

17. D.L. Cullen and E.C. Lingafelter, Inorg. Chem. **10**, 1264 (1971).
18. M.D. Joesten, S. Takagi and P.G. Lenhert, Inorg. Chem. **16**, 2680 (1977).
19. B.V. Harrowfield and J.R. Pilbrow, J. Phys. (C): Solid State Phys. **6**, 755 (1973).
20. S. Takagi, M.D. Joesten and P.G. Lenhert, Acta. Cryst. **B32**, 326 (1976).
21. B.V. Harrowfield, A.J. Dempster, T.E. Freeman and J.R. Pilbrow, J. Phys. (C): Solid State Phys. **6**, 2058 (1973).
22. S. Takagi, M.D. Joesten and P.G. Lenhert, Acta. Cryst. **B31**, 1968 (1975).
23. S. Takagi, M.D. Joesten and P.G. Lenhert, J. Am. Chem. Soc. **96**, 6606 (1974).
24. S. Takagi, M.D. Joesten and P.G. Lenhert, Acta. Cryst. **B31**, 596 (1975).
25. S. Takagi, M.D. Joesten and P.G. Lenhert, Acta. Cryst. **B32**, 2524 (1976).
26. S. Takagi, M.D. Joesten and P.G. Lenhert, Acta. Cryst. **B32**, 1278 (1976).
27. D.L. Cullen and E.C. Lingafelter, Inorg. Chem. **9**, 1858 (1970).
28. I. Bertini, P. Dapporto, D. Gatteschi and A. Scozzafava, J. Chem. Soc. Dalton. Trans., 1409 (1979).
29. I. Bertini, D. Gatteschi and A. Scozzafava, Inorg. Chem. **16**, 1973 (1977).
30. M.D. Joesten, M. Sakhawat Hussain and P.G. Lenhert, Inorg. Chem. **9**, 151 (1970).
31. R.C. Koch, M.D. Joesten and J.H. Venable, J. Chem. Phys. **59**, 6312 (1973).
32. O.P. Anderson, J. Chem. Soc. Dalton. Trans., 2597 (1972).
33. O.P. Anderson, J. Chem. Soc. Dalton. Trans., 1237 (1973).
34. F.A. Cotton and G. Wilkinson, "Advanced Inorganic Chemistry," 3rd Ed., John Wiley and Sons, New York, 1972.

35. M.C. Day and J. Selbin, "Theoretical Inorganic Chemistry," 2nd Ed., Nostrand Reinhold Co., New York, 1969.
36. G. Davies, Coord. Chem. Rev. 4, 199 (1969).
37. T.S. Davis, J.P. Fackler and M.J. Weeks, Inorg. Chem. 7, 1994 (1968).
38. J.P. Fackler and I.D. Chawla, Inorg. Chem. 3, 1130 (1964).
39. B. Morosin and J.R. Brathovde, Acta. Cryst. 17, 705 (1964).
40. P.K. Hon and C.E. Pfluger, J. Coord. Chem. 3, 67 (1973).
41. J.P. Fackler, Jr. and A. Avdeef, Inorg. Chem. 13, 1864 (1974).
42. B.R. Stults, R.S. Marianelli and V.W. Day, Inorg. Chem. 18, 1853 (1979).
43. A. Avdeef, J.A. Costamagna and J.P. Fackler, Jr., Inorg. Chem. 13, 1854 (1974).
44. T. Lis, J. Matuszewski and B. Jeżowska-Trzebiatowska, Acta. Cryst. B33, 1943 (1977).
45. P.C. Healy and A.H. White, J. Chem. Soc. Dalton. Trans., 1883 (1972).
46. R.J. Butcher and E. Sinn, J. Chem. Soc. Dalton. Trans., 2517 (1975).
47. R.J. Butcher and E. Sinn, J. Am. Chem. Soc. 98, 5159 (1976).
48. J.C. Summers, Ph.D. Dissertation, University of Florida, 1968.
49. D.St.C. Black and A.J. Hartshorn, Coord. Chem. Rev. 9, 219 (1972-1973).
50. S. Richards, B. Pedersen, J.V. Silverton and J.L. Hoard, Inorg. Chem. 3, 27 (1964).
51. M.D. Lind, M.J. Hamor, T.A. Hamor and J.L. Hoard, Inorg. Chem. 3, 34 (1964).
52. J.J. Stezowski, R. Countryman and J.L. Hoard, Inorg. Chem. 12, 1749 (1973).
53. F.P. Van Remoortere, J.J. Flynn and F.P. Boer, Inorg. Chem. 10, 2313 (1971).

54. J.L. Hoard, B. Lee and M.D. Lind, J. Am. Chem. Soc. 87, 1612 (1965).
55. J.L. Hoard, B. Lee and M.D. Lind, J. Am. Chem. Soc. 87, 1611 (1965).
56. G.H. Cohen and J.L. Hoard, J. Am. Chem. Soc. 88, 3228 (1966).
57. A. Muto, F. Marumo and Y. Saito, Acta. Cryst. B26, 226 (1970).
58. R.B. Kind and M.S. Saran, Inorg. Chem. 10, 1861 (1971).
59. F.P. Dwyer and F. Lions, J. Am. Chem. Soc. 69, 2917 (1947).
60. F.P. Dwyer and F. Lions, J. Am. Chem. Soc. 72, 1545 (1950).
61. F.P. Dwyer, F. Lions and D.P. Mellor, J. Am. Chem. Soc. 72, 5037 (1950).
62. F.P. Dwyer, N.S. Gill, E.C. Gyarfas and F. Lions, J. Am. Chem. Soc. 74, 4188 (1952).
63. J. Collins, F.P. Dwyer and F. Lions, J. Am. Chem. Soc. 74, 3134 (1952).
64. F.P. Dwyer, N.S. Gill, E.C. Gyarfas and F. Lions, J. Am. Chem. Soc. 75, 1526 (1953).
65. F.P. Dwyer, N.S. Gill, E.C. Gyarfas and F. Lions, J. Am. Chem. Soc. 75, 2443 (1953).
66. F.P. Dwyer, N.S. Gill, E.C. Gyarfas and F. Lions, J. Am. Chem. Soc. 76, 383 (1954).
67. F.P. Dwyer, N.S. Gill, E.C. Gyarfas and F. Lions, J. Am. Chem. Soc. 79, 1269 (1957).
68. F. Lions and K.V. Martin, J. Am. Chem. Soc. 79, 1572 (1957).
69. F. Lions and K.V. Martin, J. Am. Chem. Soc. 80, 3858 (1958).
70. B. Das Sarma and J.C. Bailar, J. Am. Chem. Soc. 77, 5476 (1955).
71. L.F. Lindoy, S.E. Livingstone, T.N. Lockyer and N.C. Stephenson, Aust. J. Chem. 19, 1165 (1966).
72. L.J. Wilson and N.J. Rose, J. Am. Chem. Soc. 90, 6041 (1968).
73. W.O. Gillum, J.C. Huffman, W.E. Streib and R.A.D. Wentworth, Chem. Commun., 843 (1969).

74. W.O. Gillum, R.A.D. Wentworth and R.F. Childers, Inorg. Chem. **9**, 1825 (1970).
75. E.B. Fleischer, A.E. Gebala and D.R. Swift, Chem. Commun. 1280 (1971).
76. L.J. Zompa and J.M. Shindler, Chem. Commun., 65 (1971).
77. P.A. Tasker and E.B. Fleischer, J. Am. Chem. Soc. **92**, 7072 (1970).
78. G.A. Zakrzewski, C.A. Ghilardi and E.C. Lingafelter, J. Am. Chem. Soc. **93**, 4411 (1971).
79. M.R. Churchill and A.H. Reis, Chem. Commun. 879 (1970).
80. M.R. Churchill and A.H. Reis, Chem. Commun. 1307 (1971).
81. C.J. Pedersen, J. Am. Chem. Soc. **89**, 7017 (1967).
82. C.J. Pedersen, J. Org. Chem. **36**, 254 (1971).
83. C.W. Bunn, "Chemical Crystallography," Oxford Univ. Press, London, 1961.
84. M.J. Buerger, "The Precession Method," John Wiley and Sons, New York, 1964.
85. M.J. Buerger, "X-ray Crystallography," John Wiley and Sons, New York, 1942.
86. M.F.C. Ladd and R.A. Palmer, "Structure Determination by X-ray Crystallography," Plenum Press, New York, 1977.
87. N.F.M. Henry and K. Lonsdale, Eds., "International Tables For X-ray Crystallography," Vol. 1, The Kynoch Press, Birmingham, 1952.
88. J.A. Ibers and W.C. Hamilton, Eds., "International Tables For X-ray Crystallography," Vol. 4, The Kynoch Press, Birmingham, 1974.
89. M.J. Buerger, "Crystal Structure Analysis," John Wiley and Sons, New York, 1960.
90. A. Harriman, Coord. Chem. Rev. **28**, 147 (1979).
91. P.H. Davis and J.S. Wood, Inorg. Chem. **9**, 1111 (1970).
92. B.N. Figgis, L.G.B. Wadley and J. Graham, Acta Crystallogr., Sect. B **28**, 187 (1972).
93. B.N. Figgis and L.G.B. Wadley, Aust. J. Chem. **25**, 2233 (1972).

94. B.N. Figgis and L.G.B. Wadley, J. C. S. Dalton, 2182 (1972).
95. J.H.M. Mooy, W. Krieger, D. Heijdenrijk and C.H. Stam, Chem. Phys. Lett. 29(2), 179 (1974).
96. M.L. Niven and L.R. Nassimbeni, Cryst. Struct. Comm. 9, 1133 (1980).
97. A. Caron and J. Donohue, Acta Crystallogr., Sect. B 25, 404 (1969).
98. The values of  $R_{JT}^2 = \sum_{i=1}^6 \Delta d_i^2$  were calculated from the values of the Mn-O distances given in the pertinent reference.
99. R. Dingle, J. Chem. Phys. 50, 545 (1969).
100. R. Dingle, P.J. McCarthy and C.J. Ballhausen, J. Chem. Phys. 50, 1957 (1969).
101. R. Dingle, J. Chem. Phys. 50, 1952 (1969).
102. H.H. Willard, L.L. Merritt, Jr. and J.A. Dean, "Instrumental Methods of Analysis," 5th Ed., D. Van Nostrand Co., New York, 1974.
103. W.W. Wendlandt, "Thermal Methods of Analysis," 2nd Ed., John Wiley and Sons, New York, 1974.
104. E.S. Watson, M.J. O'Neill, J. Justin and N. Brenner, Anal. Chem. 36, 1233 (1964).
105. M.J. O'Neill, Anal. Chem. 36, 1238 (1964).
106. A.P. Gray, in "Analytical Calorimetry," R.F. Porter and J.M. Johnson, Eds., Plenum, New York, 1968.
107. J.H. Flynn, in Thermal Anal., D.J. David, 3, 247 (1971).
108. E.A. Collins, J. Bares and F.W. Billmeyer, Jr., "Experiments in Polymer Science," John Wiley and Sons, New York, 1973.
109. R.S. Drago, "Physical Methods in Chemistry," W.B. Saunders Co., Philadelphia, 1977, p. 316.
110. B.A. Goodman and J.B. Raynor, "Advances in Inorganic Chemistry and Radiochemistry," Vol. 13, Academic Press, New York, 1970, p. 135.
111. J.E. Wertz and J.R. Bolton, "Electron Spin Resonance: Elementary Theory and Practical Applications," McGraw-Hill Inc., New York, 1972.

112. W. Low, "Paramagnetic Resonance in Solids," Academic Press, New York, 1960.
113. A. Abragam and B. Bleaney, "Electron Paramagnetic Resonance of Transition Ions," Clarendon Press, Oxford, 1970.
114. A. Carrington and H.C. Longuet-Higgins, Quart. Rev. **14**, 427 (1960).
115. J.H.M. Mooy, H.J. De Jong, M. Glasbeek and J.D.W. Van Voorst, Chem. Phys. Lett. **18**(1), 51 (1973).
116. H. Aghabozorg, G.J. Palenik, R.C. Stoufer and J.C. Summers, submitted to Inorg. Chem.
117. J.R. Fletcher, J.M. Grimshaw, A.P. Knowles and W.S. Moore, J. Phys. Chem.: Solid St. Phys. **13**, 6391 (1980).
118. G.J. Palenik and D.W. Wester, Inorg. Chem. **17**, 864 (1978).
119. D. Wester and G.J. Palenik, J. Am. Chem. Soc. **96**, 7565 (1974).
120. G.J. Palenik, D.W. Wester, U. Rychlewska and R.C. Palenik, Inorg. Chem. **15**, 1814 (1976).
121. D.D. McRitchie, R.C. Palenik and G.J. Palenik, Inorg. Chim. Acta. **20**, L27 (1976).
122. G.J. Palenik, D.W. Wester and J.H. Davis, in preparation.
123. D. Wester and G.J. Palenik, Inorg. Chem. **15**, 755 (1976).
124. T.J. Giordano, G.J. Palenik, R.C. Palenik and D.A. Sullivan, Inorg. Chem. **18**, 2445 (1979).
125. S.W. Gaines, G.J. Palenik and R.C. Palenik, Cryst. Struct. Comm. **10**, 673 (1981).
126. G.J. Palenik and J.H. Davis, in preparation.
127. A.H. White and A.C. Willis, J.C.S. Dalton 1377 (1977).
128. S.L. Lawton and G.T. Kokotailo, Inorg. Chem. **11**, 363 (1972).
129. N.W. Alcock, N. Herron and P. Moore, J.C.S. Dalton 1486 (1979).
130. M.G.B. Drew, J. De O. Cabral, M.F. Cabral, F.S. Esho and S.M. Nelson, J.C.S. Chem. Comm. 1033 (1979).
131. I.W. Nowell, Acta. Cryst. **B35**, 1891 (1979).

132. E.I. Lerner and S.J. Lippard, Inorg. Chem. **16**, 1537 (1977).
133. B. Metz and R. Weiss, Inorg. Chem. **13**, 2094 (1974).
134. J. de O. Cabral, M.F. Carbal, W.J. Cummins and M.G.B. Drew, Inorg. Chim. Acta. **30**, L313 (1978).
135. B. Metz and R. Weiss, Acta. Cryst. **B29**, 1088 (1973).
136. C.D. Garner and S.C. Wallwork, J. Chem. Soc. (A), 3092 (1970).
137. J.G. Bergman, Jr. and F.A. Cotton, Inorg. Chem. **5**, 1208 (1966).
138. C.C. Addison, N. Logan, S.C. Wallwork and C.D. Garner, Quart. Rev. **25**, 289 (1971).
139. B.E. Robertson, Inorg. Chem. **16**, 2735 (1977).
140. M.C. Favas and D.L. Kepert, "Progress in Inorganic Chemistry," Vol. 28, John Wiley and Sons, New York, 1981, p. 309.
141. A. Avdeef, K.N. Raymond, K.O. Hodgson and A. Zalkin, Inorg. Chem. **11**, 1083 (1972).
142. E.C. Baker, K.N. Raymond, T.J. Marks and W.A. Wachter, J. Am. Chem. Soc. **96**, 7586 (1974).
143. H.W. Turner, R.A. Andersen, A. Zalkin and D.H. Templeton, Inorg. Chem. **18**, 1221 (1979).
144. R.W. Broach, A.J. Schultz and J.M. Williams, Science **203**, 172 (1979).
145. J.M. Manriquez, P.J. Fagan, T.J. Marks, C.S. Day and V.W. Day, J. Am. Chem. Soc. **100**, 7112 (1978).
146. P.J. Fagan, J.M. Manriquez, T.J. Marks, V.W. Day and S.H. Vollmer, J. Am. Chem. Soc. **102**, 5393 (1980).
147. G. Johansson, Acta. Chem. Scan. **22**, 389 (1968).
148. C.S. Mancinelli, D.D. Titus and R.F. Ziolo, J. Organomet. Chem. **140**, 113 (1977).
149. G. Ferguson, F.C. March and D.R. Ridley, Acta. Cryst. **B31**, 1260 (1975).
150. D.W. Phelps, E.M. Kahn and D.J. Hodgson, Inorg. Chem. **14**, 2486 (1975).




151. A.B. Blake, F.A. Cotton and J.S. Wood, J. Am. Chem. Soc. **86**, 3024 (1964).
152. F.A. Cotton, S.M. Morehouse and J.S. Wood, Inorg. Chem. **3**, 1603 (1964).
153. E. Fleischer and S. Hawkinson, J. Am. Chem. Soc. **89**, 720 (1967).
154. C.C. Ou, R.G. Wollmann, D.N. Hendrickson, J.A. Potenza and H.J. Schugar, J. Am. Chem. Soc. **100**, 4717 (1978).
155. J.R. Knox and C.K. Prout, Chem. Comm. 1227 (1968).
156. F.A. Cotton and S.M. Morehouse, Inorg. Chem. **4**, 1377 (1965).
157. G. Ciani, A. Sironi and V.G. Albano, J.C.S. Dalton 1667 (1977).
158. A.R.E. Baikie, M.B. Hursthouse, D.B. New and P. Thornton, J.C.S. Chem. Comm. 62 (1978).
159. J.A. Bertrand, Inorg. Chem. **3**, 495 (1967).
160. R.L. Harlow and S.H. Simonsen, Acta. Cryst. **B33**, 2784 (1977).
161. J. Catterick, P. Thornton and B.W. Fitzsimmons, J.C.S. Dalton 1420 (1977).
162. K.M.A. Malik and J.W. Jeffery, Acta. Cryst. **B29**, 2687 (1973).
163. J.C. Taylor, M.H. Mueller and R.L. Hitterman, Acta. Cryst. **20**, 842 (1966).
164. N.W. Alcock, S. Esperas, K.W. Bagnall and W.H. Yun, J.C.S. Dalton 638 (1978).
165. C.E.F. Rickard and D.C. Woollard, Aust. J. Chem. **33**, 1161 (1980).
166. R.J. Hill and C.E.F. Rickard, J. Inorg. Nucl. Chem. **40**, 2029 (1978).

#### BIOGRAPHICAL SKETCH


Hossein Aghabozorg was born July 7, 1948, in Tehran, Iran. After attending elementary and junior high schools in Tehran, Iran, he graduated from Marvi High School in June, 1967. In September, 1968, he started his studies at Tehran University. In September, 1972, he received the B.S. degree in chemistry from Tehran University. While serving for eighteen months in the Iranian Army, he entered the Graduate School of Tehran University in September, 1973. In May, 1975, he received the M.S. degree in chemistry. In 1975, he was employed as an instructor at the University of Abourayhan. He was awarded a scholarship by the Iranian Government for Ph.D. studies in the United States. In March, 1978, he entered the Graduate School of the University of Florida, where he served as a teaching assistant from the Fall, 1980, to the present.

He was married to the former Fereshteh Hannany on November 1, 1974. They have one daughter, Mahsa.

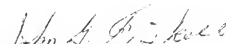
I certify that I have read this study and that in my opinion it conforms to acceptable standards of scholarly presentation and is fully adequate, in scope and quality, as a dissertation for the degree of Doctor of Philosophy.

  
Robert C. Stoufer, Chairman  
Associate Professor of Chemistry

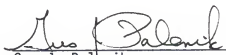
I certify that I have read this study and that in my opinion it conforms to acceptable standards of scholarly presentation and is fully adequate, in scope and quality, as a dissertation for the degree of Doctor of Philosophy.

  
Eric V. Dose  
Assistant Professor of Chemistry

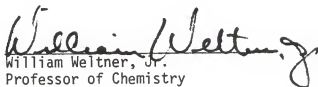
I certify that I have read this study and that in my opinion it conforms to acceptable standards of scholarly presentation and is fully adequate, in scope and quality, as a dissertation for the degree of Doctor of Philosophy.

  
John G. Fiskell  
Professor of Soil Science

I certify that I have read this study and that in my opinion it conforms to acceptable standards of scholarly presentation and is fully adequate, in scope and quality, as a dissertation for the degree of Doctor of Philosophy.

  
Gus J. Palenik  
Professor of Chemistry

I certify that I have read this study and that in my opinion it conforms to acceptable standards of scholarly presentation and is fully adequate, in scope and quality, as a dissertation for the degree of Doctor of Philosophy.

  
William Weltner, Jr.  
Professor of Chemistry

This dissertation was submitted to the Graduate Faculty of the Department of Chemistry in the College of Liberal Arts and Sciences and to the Graduate Council, and was accepted as partial fulfillment of the requirements for the degree of Doctor of Philosophy.

May, 1982

---

Dean for Graduate Studies  
and Research